Studying Tumor Induced Bone Disease using ex vivo Bone Analogue Systems to Aid Drug Prediction, Efficacy and Validation

By

Ushashi Chand Dadwal

Dissertation

Submitted to the Faculty of the

Graduate School of Vanderbilt University

In partial fulfillment of the requirements

For the degree of

DOCTOR OF PHILOSOPHY

in

Chemical Engineering

May 2016

Nashville, Tennessee

Approved:

Scott A. Guelcher, Ph.D.

Peter T. Cummings, Ph.D.

Matthew J. Lang, Ph.D.

Julie A. Sterling, Ph.D.

Copyright © 2016 by Ushashi Chand Dadwal

All rights reserved

“Let your wings soar”

To my parents for teaching me to follow my dreams,

My sister Eena, for inspiring me to be the best version of myself,

And to Patrick, for being my back up brain.

Acknowledgements

This dissertation work is a compilation of research for over five years. My advisors, Drs. Scott Guelcher and Julie Sterling have played a pivotal role in my graduate training, and I am grateful for their expertise, guidance, and excitement about our projects. Additionally, I am thankful for the support from my committee members Drs. Matthew Lang, and Peter Cummings. Their unique viewpoints helped to focus my research goals and provided interesting perspectives that we had not previously considered. I acknowledge the funding sources that have been essential for me to continue my research, including the Schlumberger Faculty for the Future Pre-doctoral fellow (UCD), VA Career Development award (JS), National Cancer Institute (JS&SG) and the Department of Chemical and Biomolecular Engineering, Vanderbilt University.

I would like to thank all of the members of the Sterling & Guelcher lab, past and present, which helped me learn important techniques, find solutions to problems, and provided guidance. Notably, Shellese Cannonier encouraged me to critically examine scientific work, ask the right questions, and approach every problem with a robust plan. Denise Buenrostro has been fundamental in introducing me to the philosophy of time management and organization, an integral skill for life. I have tremendous respect for the Guelcher lab's fantastic manager, Kasia Zienkiewicz whose knowledge about chemistry is unparalleled and without whom the lab would not run nearly as smoothly. Jonathan Page, Drew Harmata, Ruijing Guo, Elizabeth Adolph, Anne Talley, Sichang Lu, Maddi McEnery, Joe Vanderburg, Alyssa Merkel, Kristin Kwakwa, Michael Kessler, and Tommy Spoonmore all made my time in the lab very enjoyable.

Thank you to the chemical engineering staff Mary Gilleran, Rae Uson, and Julie James for all of the help during my tenure. I would like to thank Kathy Friedman (Biological Sciences, Vanderbilt University), Dan Perrien (Vanderbilt University Institute of Imaging Science), Mathilde Granke (Vanderbilt Center for Bone Biology) and Jeff Nyman (Department of Orthopedics, Vanderbilt University) for providing excellent advice and integral assistance towards this thesis work.

Finally, I would not be here if it wasn't for my family and friends. I would like to express gratitude to my parents, who supported me throughout my graduate school career and uprooting myself from India, so that I could fulfill my own goals. I could not ask for more support and love. I am forever thankful for my sister, to be the incredible inspiration she has been to me, since the day she was born. I am immensely grateful for Patrick, my fiancé, who has been my backup brain and support system throughout. It was a pleasure to find friends we have made over the years in Nashville and the wonderful memories.

TABLE OF CONTENTS

Page

LIST OF FIGURES

LIST OF TABLES

Chapter I

Introduction

Clinically, breast cancer is the second leading cause of death in the United States[1]. Moreover, breast cancer metastasizes at a higher propensity to the bone as compared to lung, prostate, and kidney[2] (**Figure 1 & Table 1**). Median survival in patients with advanced tumor cells metastasize from primary sites to the bone. Skeletal metastasis causes skeletal-related events (SRE) like hypercalcemia, bone pain, spinal instability and pathological fractures, which are the cause of considerable morbidity in patients with advanced cancer[3]. On average, a patient with metastatic disease will experience a SRE every 3 to 6 months[4]. Consequently, the standard of care during Tumor Induced Bone Disease (TIBD) consists of palliative clinical therapies like bisphosphonates and Denosumab that focus on preventing skeletal complications associated with breast cancer related bone metastasis[3,5,6].

Although previous work has contributed to significant knowledge on the molecular mechanisms that control TIBD, relatively little is known as to why tumor cells establish in the bone and the contributions of the bone microenvironment to progression of TIBD. The bone provides a distinctive microenvironment for tumor cells to establish in which its mineralized matrix and multiple cell types co-reside and interact, including hematopoietic cells - osteoclasts and immune cells, mesenchymal cells such as osteoblasts, and cells

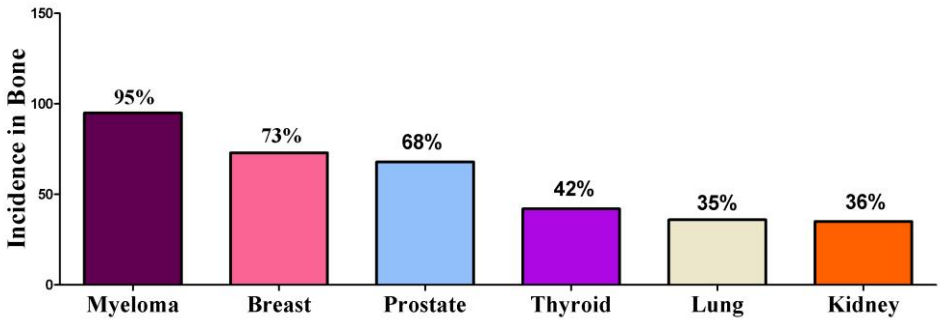

Figure 1.1 Incidence of Bone metastasis
Incidence of bone metastasis in patients that have died from metastatic disease.

Primary Tumor	Incidence to Bone	Median Survival (months)	5-year survival
Myeloma	95	20	10%
Breast	73	24	20%
Prostate	68	40	25%
Thyroid	42	<6	<5%
Kidney	35	6	10%
Lung	36	48	40%
Gastrointestinal tract	5	<6	<5%

Table 1.1 Incidence and prognosis of TIBD
Incidence and Prognosis of Bone metastasis [23,39].

forming the vasculature such as endothelial cells and pericytes. Several studies have demonstrated that Parathyroid Hormone Related Protein (PTHrP) and Gli2 (upstream transcription factor of PTHrP) are associated with tumor mediated destruction of the bone[7,8] and rigidity modulates Integrin β_3 (ITβ3) in the context of TIBD[9,10]. While previous studies have focused on 2D culture, important properties of the tumor microenvironment cannot be recapitulated in 2D. A novel approach is required to enable investigation of fundamental cell-cell and cell-matrix interactions between tumors and the complex bone microenvironment. The goal of this dissertation was to design and fabricate 3 dimensional bone analogue models to study Tumor Induced Bone Disease. Biomimetic 3D tissue engineered systems have been proposed for investigating molecular mechanisms of disease progression and for screening drugs[11].

Tissue engineering biomimetic models and subsequent technologies are increasingly being considered successful approaches to solving critical scientific problems in field of cancer biology[11]. It is well known that changes in tissue dimensionality[11-16], metabolic gradients[17], cell-extracellular matrix (ECM) interactions[1,18,19], cell to cell interactions[2,20,21], cellular response to bio physical cues[4,10,22-26]; and exogenous biomechanical cues[3,27,28] contribute to a heterogeneous microenvironment that plays a critical role in cancer pathogenesis and therapeutic resistance. Although animal studies are relevant in the tissue level context, they are limited and do not provide independent examination of the human tissue microenvironment that contribute to disease progression and metastasis[3,6,29]. Xenograft models, animals that are transplanted with human

cancer cells into mice, introduce species-dependent discrepancies in cell signaling[7,8,29] and often ignore the immune component, which is critical to cancer progression to tumors[9,10,20-22,30]. Even though traditional cell culture approaches have been widely instrumental in studying the fundamentals of tumor biology they are restricted in their ability to mimic the complexity and heterogeneity of tumor with physiological relevance integral for cancer. They offer only partial explanation as to why novel therapeutic compounds are frequently efficacious *in vitro* but disappoint in preclinical and clinical studies.

Development of new biomaterials mimicking the tumor microenvironment has been highlighted as a critical need for understanding the spatio-temporal dynamics of tumor progression, recapitulating *in vivo* conditions at distinct steps of metastasis, and understanding how tumor cells integrate mechanical and chemical signals over multiple length scales[11]. The effects of the physical component of the bone microarchitecture were examined *in vitro* in **Chapter III**. Polyurethanes, a widely used FDA approved biomaterial developed at the Guelcher lab [11,31] were used to synthesize 3D scaffold with mechanically tunable physical properties to study interactions between tumor cells and the bio-physical cues that modulate genes associated with metastasis in the bone. The mechanical properties of polyurethane are tunable by changing the crosslink density, which is easily achieved by controlling the chain length of polyol and isocyanate in the reaction [11-16,31]. Sacrificial template combined with additive Fused Deposition Modeling (FDM) developing 3D printing and melt cast method was used to generate controllable physical properties, including pore size, porosity, and elastic

modulus [17,32]. To prove its influence on tumor cells, the effects of scaffold pore size and elastic modulus in TIBD were investigated. In order to study cell-polyurethane interaction for long term, instead of utilizing lysine-derived polyurethane, Hexamethylene Diisocynate trimer (HDI) was used to synthesize polyurethane scaffolds as its hydrolytic degradation is negligible during the study time period[33]. A perfusion based 3D bioreactor model served as a platform for simulating a physiologically relevant flow in tumor-bone microenvironment. It is evident from these studies a variety of parameters can be evaluated using 3D model systems and these, in part, contribute to the disconnect between *in vitro* studies and clinical trials. Furthermore, **Chapter IV** describes the development of the 3D scaffold system *in vivo.* Athymic mice were implanted with tumor-seeded scaffolds to determine the effects of mechanotransduction in a biologically relevant model system. Host cells, specifically immune cells, are thought to promote an immunosuppressive, anti-inflammatory phenotype, and allow the tumor to escape immune detection [20,30,34]. Tumor cells can subvert the function of macrophages and take advantage of their signaling to escape from the primary tumor [35,36]. Myeloid derived suppressor cells are known to expand during breast cancer related metastasis and induce osteolytic destruction [37]. Matrix assisted laser desorption (MALDI) was used to determine protein expression of host proteins and the effects of rigidity on host-derived proteins. 3D scaffolds provide a unique advantage to study immune cell interactions with tumor cells in a biophysically relevant *in vivo* background.

Chapter V describes the use of a mathematical model of cell population dynamics based on ordinary differential equations (ODEs) developed from Ayati, et al. [38] and Komarova, et al.[39]. These models describe spatio-temporal changes in bone remodeling based on autocrine and paracrine signaling between tumor cells, osteoblasts, and osteoclasts in the context of tumor-induced bone disease caused by breast cancer. Simulating TIBD using computational modeling will add to our significant advances in knowledge of the molecular mechanisms underlying TIBD should provide therapeutic opportunities to improve overall survival rates especially. Moreover, integrating experimental findings with the power of computational modeling offers a unique opportunity to assess the impact of putative therapies on the progression of TIBD.

To conclude **Chapter VI** summarizes the results of this dissertation and discusses future work as an extrapolation of this work. Overall, this thesis dissertation bridges the gap between investigating tumor induced bone disease and the lack of robust, comprehensible *ex vivo* bone mimetic systems to study this ailment.

References

[1] American Cancer Society, *Cancer Facts & Figures 2016*, (2015)

[2] R.E. Coleman, Skeletal complications of malignancy, Cancer. (1997).

[3] R.E. Coleman, Bisphosphonates: Clinical Experience, The Oncologist. 9 (2004)

[4] R.E. Coleman, Clinical Features of Metastatic Bone Disease and Risk of Skeletal Morbidity, Clinical Cancer Research. 12 (2006)

[5] J.P. Brown, C. Roux, P.R. Ho, M.A. Bolognese, J. Hall, H.G. Bone, et al., Denosumab significantly increases bone mineral density and reduces bone turnover compared with monthly oral ibandronate and risedronate in postmenopausal women who remained at higher risk for fracture despite previous suboptimal treatment with an oral bisphosphonate, Osteoporos Int. 25 (2014)

[6] E. Prommer, Palliative Oncology: Denosumab, Am J Hosp Palliat Care. 32 (2015)

[7] J.A. Sterling, The Hedgehog Signaling Molecule Gli2 Induces Parathyroid Hormone-Related Peptide Expression and Osteolysis in Metastatic Human Breast Cancer Cells, Cancer Res. 66 (2006)

[8] R.W. Johnson, M.P. Nguyen, S.S. Padalecki, B.G. Grubbs, A.R. Merkel, B.O. Oyajobi, et al., TGF- Promotion of Gli2-Induced Expression of Parathyroid Hormone-Related Protein, an Important Osteolytic Factor in Bone Metastasis, Is Independent of Canonical Hedgehog Signaling, Cancer Res. 71 (2011)

[9] N.S. Ruppender, A.R. Merkel, T.J. Martin, G.R. Mundy, J.A. Sterling, S.A. Guelcher, Matrix rigidity induces osteolytic gene expression of metastatic breast cancer cells, PLoS ONE. 5 (2010)

[10] J.M. Page, A.R. Merkel, N.S. Ruppender, R. Guo, U.C. Dadwal, S.A. Cannonier, et al., Matrix rigidity regulates the transition of tumor cells to a bone- destructive phenotype through integrin b3 and TGF-b receptor type II. Biomaterials. 64 (2015)

[11] T.K. Schuessler, X.Y. Chan, H.J. Chen, K. Ji, K.M. Park, A. Roshan-Ghias, et al., Biomimetic tissue-engineered systems for advancing cancer research: NCI Strategic Workshop report, Cancer Res. 74 (2014)

[12] C. Fischbach, R. Chen, T. Matsumoto, T. Schmelzle, J.S. Brugge, P.J. Polverini, et al., Engineering tumors with 3D scaffolds, Nat Meth. 4 (2007)

[13] S.P. Pathi, C. Kowalczewski, R. Tadipatri, C. Fischbach, A novel 3-D mineralized tumor model to study breast cancer bone metastasis, PLoS ONE. 5 (2010)

[14] B.A. Justice, N.A. Badr, R.A. Felder, 3D cell culture opens new dimensions in cell-based assays, Drug Discovery Today. 14 (2009)

[15] L.A. Gurski, N.J. Petrelli, X. Jia, M.C. Farach-Carson, 3D matrices for anti-cancer drug testing and development, Oncology Issues. 25 (2010)
[16] E.L.S. Fong, S.-E. Lamhamedi-Cherradi, E. Burdett, V. Ramamoorthy, A.J. Lazar, F.K. Kasper, et al., Modeling Ewing sarcoma tumors in vitro with 3D scaffolds, Proc Natl Acad Sci U S A. 110 (2013)
[17] M.M. Alam, S. Lal, K.E. FitzGerald, L. Zhang, A holistic view of cancer bioenergetics: mitochondrial function and respiration play fundamental roles in the development and progression of diverse tumors, Clin Transl Med. 5 (2016)
[18] P. Friedl, S. Alexander, Cancer Invasion and the Microenvironment: Plasticity and Reciprocity, Cell. 147 (2011)
[19] D.E. Ingber, Can cancer be reversed by engineering the tumor microenvironment? Semin Cancer Biol. 18 (2008)
[20] A.D. Luster, R. Alon, U.H. von Andrian, Immune cell migration in inflammation: present and future therapeutic targets, Nat Immunol. 6 (2005)
[21] L. Yang, J. Huang, X. Ren, A.E. Gorska, A. Chytil, M. Aakre, et al., Abrogation of TGF beta signaling in mammary carcinomas recruits Gr-1+CD11b+ myeloid cells that promote metastasis, Cancer Cell. 13 (2008)
[22] J. Sceneay, B.S. Parker, M.J. Smyth, A. Möller, Hypoxia-driven immunosuppression contributes to the pre-metastatic niche, Oncoimmunology. 2 (2014)
[23] G.L. Semenza, The hypoxic tumor microenvironment: A driving force for breast cancer progression, Biochim. Biophys. Acta. 1863 (2016)
[24] A.M. Ross, Z. Jiang, M. Bastmeyer, J. Lahann, Physical aspects of cell culture substrates: topography, roughness, and elasticity, Small. 8 (2012)
[25] R.W. Tilghman, E.M. Blais, C.R. Cowan, N.E. Sherman, P.R. Grigera, E.D. Jeffery, et al., Matrix rigidity regulates cancer cell growth by modulating cellular metabolism and protein synthesis, PLoS ONE. 7 (2012).
[26] J. Schrader, T.T. Gordon-Walker, R.L. Aucott, M. van Deemter, A. Quaas, S. Walsh, et al., Matrix stiffness modulates proliferation, chemotherapeutic response, and dormancy in hepatocellular carcinoma cells, Hepatology. 53 (2011)
[27] R.D. Meng, C.C. Shelton, Y.M. Li, L.X. Qin, D. Notterman, P.B. Paty, et al., -Secretase Inhibitors Abrogate Oxaliplatin-Induced Activation of the Notch-1 Signaling Pathway in Colon Cancer Cells Resulting in Enhanced Chemosensitivity, Cancer Res. 69 (2009)
[28] A.J. Hanrahan, D.B. Solit, A Central Role for RAF->MEK->ERK Signaling in the Genesis of Pancreatic Ductal Adenocarcinoma, 2 (2012)
[29] T. Hartung, Thoughts on limitations of animal models, Parkinsonism Relat Disord. 14 Suppl 2 (2008)

[30] D. Hanahan, R.A. Weinberg, Hallmarks of cancer: the next generation, Cell. 144 (2011) 646–674. doi:10.1016/j.cell.2011.02.013.
[31] S.A. Guelcher, Biodegradable polyurethanes: synthesis and applications in regenerative medicine, Tissue Engineering Part B: Reviews. 14 (2008)
[32] R. Guo, S. Lu, J.M. Page, A.R. Merkel, S. Basu, J.A. Sterling, et al., Fabrication of 3D Scaffolds with Precisely Controlled Substrate Modulus and Pore Size by Templated-Fused Deposition Modeling to Direct Osteogenic Differentiation, Advanced Healthcare Materials. (2015)
[33] A.E. Hafeman, K.J. Zienkiewicz, A.L. Zachman, H.-J. Sung, L.B. Nanney, J.M. Davidson, et al., Characterization of the degradation mechanisms of lysine-derived aliphatic poly(ester urethane) scaffolds, 32 (2011)
[34] L. D'Amico, I. Roato, The Impact of Immune System in Regulating Bone Metastasis Formation by Osteotropic Tumors, J Immunol Res. 2015 (2015)
[35] A. Sawant, J. Deshane, J. Jules, C.M. Lee, B.A. Harris, X. Feng, et al., Myeloid-derived suppressor cells function as novel osteoclast progenitors enhancing bone loss in breast cancer, Cancer Res. 73 (2013)
[36] Y. Horimoto, U.M. Polanska, Y. Takahashi, A. Orimo, Emerging roles of the tumor-associated stroma in promoting tumor metastasis, Celladhesion. 6 (2014)
[37] S. Danilin, A. Merkel, J. Johnson, R. Johnson, J. Edwards, J. Sterling, Myeloid-derived suppressor cells expand during breast cancer progression and promote tumor-induced bone destruction, Oncoimmunology. 1 (2012)
[38] B.P. Ayati, C.M. Edwards, G.F. Webb, J.P. Wikswo, A mathematical model of bone remodeling dynamics for normal bone cell populations and myeloma bone disease, Biol Direct. 5 (2010)
[39] S.V. Komarova, R.J. Smith, S.J. Dixon, S.M. Sims, L.M. Wahl, Mathematical model predicts a critical role for osteoclast autocrine regulation in the control of bone remodeling, Bone. 33 (2003)

Chapter II

Background

Bone

The bone is an anisotropic organ, which is affected by mechanical stress in the form of fluid flow and substrate deformation. It is a dynamic; three-dimensional, highly structured tissue with an organized extracellular matrix comprised of inorganic and organic components. Its primary function is providing support and structural integrity to the body. In addition, it regulates metabolic activity is governed by interactions between the heterogeneous population of cells, the bone's physical microarchitecture, and their response to a variety of mechanical signals – fluid flow, substrate deformation, and mechanical loading.

Tissue remodeling in the bone is tightly regulated and governed by a multitude of cells and is characterized by complex mechanical and biochemical signaling cues propagated by its structural matrix. It is a highly complex process during which new bone is formed to replace old bone. Remodeling typically occurs to maintain mineral homeostasis, to adapt to mechanical changes, and to repair damage [1,2]. The key cellular players during bone homeostasis are osteoclasts, osteocytes, and osteoblasts. Although osteoclasts and osteoblasts independently govern bone resorption and bone formation respectively, they are linked metabolically under a temporary anatomical structure called basic multicellular units (BMUs)[3,4]. It is reported that the BMU has a cutting cone structure with a

peripheral front line of osteoclasts (~9 multinucleated cells). At the end of the cutting cone, several hundreds of osteoblasts (~2000 cells) form bone within the cavity[5]. The BMU exists and moves in three dimensions, excavating and refilling a tunnel through cortical bone or a trench across the surface of cancellous bone. A cortical BMU travels about 20 μm/day, taking about 200 days[5]. A cancellous BMU travels about 10 μm/day, about half the speed of a cortical BMU, taking about the same period of time (120 days)[6]. Each aspect of the BMU is controlled by direct and indirect communications among bone cells in a coupling mechanism, which includes soluble coupling factors stored in bone matrix that are released during bone resorption[7]. However, excessive resorption by osteoclasts without osteoblast activity contributes to bone loss and osteoporosis [8,9], whereas the contrary may result in osteopetrosis[10,11]. Thus, the equilibrium between bone formation and resorption is precisely dependent on microenvironment context cues.

Bone cells

Osteoblasts

Osteoblasts are single nuclei cuboidal cells that reside along the bone surface and are instrumental in laying the bone matrix during bone remodeling [12]. They are derived from the osteoprogenitor lineage of mesenchymal stem cells (MSC). Based on contextual biological cues, MSCs begin to express Runt related transcription factor 2 (Runx2), Distalless homeobox 5 (Dlx5), and osterix (Osx), which pushes these cells down the osteoblastic lineage[13-15]. The transition of pre-osteoblast to mature osteoblasts is characterized by an increase in the expression of Osx and the secretion of bone matrix proteins such as osteocalcin

(OCN), bone sialoprotein (BSP) I/II, and collagen type I as well as morphological changes (large and cuboidal cells) [13,16-18]. Osteoblasts synthesize the bone matrix by depositing organic matrix and its subsequent mineralization.

Osteoclasts

Osteoclasts are multinucleated cells that resorb the bone during bone remodeling. They are terminally differentiated cells, which originate from mononuclear cells of the hematopoietic stem cell lineage [14]. Macrophage colony-stimulating factor (M-CSF), secreted by osteoprogenitor mesenchymal cells and osteoblasts, and receptor activator of nuclear factor kappa B ligand (RANKL), secreted by osteoblasts, osteocytes, and stromal cells [8,19] promote the activation of osteoclasts and resorb the bone.

Abnormal increase in osteoclast formation and activity, where resorption exceeds formation, leads to certain bone diseases such as osteoporosis, causing decreased bone density and increased bone fractures. In some pathologic conditions including bone metastases and inflammatory arthritis, abnormal osteoclast activation results in particular erosions and painful osteolytic lesions, respectively [10,20,21]. These diseases demonstrate the importance of the normal bone remodeling process for the maintenance of bone homeostasis.

Osteocytes

Osteocytes are the most abundant cells in the bone and descend from the mesenchymal lineage via osteoblast differentiation [22]. Matrix producing osteoblasts either undergo apoptosis or osteocytogenesis (thought to be a passive process whereby a subpopulation of osteoblasts becomes encased in osteoid that

inertly mineralizes [23]). This osteoid embedded cell undergoes a dramatic transformation from a polygonal cell to a cell extending dendrites toward the mineralizing front, which is followed by cytoplasmic processes (up to 50 per each cell) extending to either the vascular space or bone surface. These dendritic extensions cross tiny tunnels across the canaliculi, forming the osteocyte lacunocanalicular system [24]. This system connects to the neighboring osteocytes and osteoblasts. The cell-cell communication can be achieved by interstitial fluid that flows between the osteocytes processes and canaliculi[14]. The lacunocanalicular system detects mechanical pressures and loads and acts as a mechanosensors[14]. Osteocytes are thought to control bone remodeling via chemotactic signaling to osteoblasts and osteoclasts.

Tumor Induced Bone Disease

Breast cancer is the most commonly diagnosed cancer in women and it metastasizes to distant organs such as the bone, liver and lung [26]. The 5-year survival rate of women with stage IV breast cancer is 22%, indicating that metastasis to distant organs remains a common and a still deadly complication associated with advanced breast cancers. Breast cancer cell metastasize at a higher propensity to the bone (83%) compared to the liver and lung (27%) [26]. Tumor establishment in the bone, or Tumor Induced Bone Disease (TIBD), causes multifaceted bone destruction that can be classified as either osteolytic or osteoblastic, with osteolytic bone destruction more commonly seen in patients with primary breast cancer disease [27,28]. Metastatic breast cancer commonly arises

months or years after treatment completion for early stage and localized breast cancer, and the risk of recurrence varies between patients, depending on the type of primary tumor, its stage at the time of initial diagnosis, and likely depending on a number of intrinsic and extrinsic factors that affect host response. Patients experience hypercalcemia, intractable bone pain, spinal instability, and skeletal events like fractures. These cause a decrease in quality of life of the patient[29]. This condition is incurable and is currently managed by palliative interventions, focused on length and quality of life.

Pathophysiology of bone metastases

The process of cancer metastasis is an organized and multistep process, which includes tumor cells metastasizing from a primary site as well as tumor cell seeding, tumor dormancy, and subsequent tumor growth and progression. Cells from the primary tumor dislodge and pass through the extracellular matrix, penetrate the basement membrane of angio-lymphatic vessels and are then transported to distant organs via the circulatory system. Circulating breast and prostate cancer cells have a particular affinity for bone [26]. Most disseminated tumor cells die, but the bone marrow microenvironment may act as a reservoir for malignant cells acting as a rich “soil” for the “seeds” [30]. Specifically, it appears dormant tumor cells preferential home to the hematopoietic stem cell niche, which results in relapse even years after the diagnosis. This concept was further expanded by elucidation the relationship between the disseminating seed (tumor) and metastatic soil (bone) through a continual supply of growth factors from the

microenvironment, loss of apoptotic signals and the recruitment of endothelial progenitor cells in the "metastatic niche" model of Psaila and Lyden [31].

Tumor cells that establish within the bone hijack the tightly regulated remodeling process. During breast cancer related bone metastasis, key mediators of the osteolytic pathway including parathyroid hormone-related peptide (PTHrP) upregulate RANKL from osteoblasts and stromal cells. This results in down regulation of osteoprotegerin, and activation of osteoclasts. The resorption of the bone releases a rich supply of bone-derived factors such as Transforming Growth Factor β (TGF-β) and Insulin Growth Factor (IGF) from the bone matrix. As a result, there is increased growth and proliferation of the tumor cell population. This in turn furthers the release of PTHrP, creating a "vicious cycle of bone metastases[32]"(**Figure.2.1**). While an improved understanding of the pathophysiology of bone metastases has ushered in and elucidated specific pathways of cancer using several experimental and animal models, experimental models that faithfully recapitulate the multiple stages of metastatic disease are still scarce and limited in delineating the molecular mechanisms underlying tumor initiation and progression in the context of the bone.

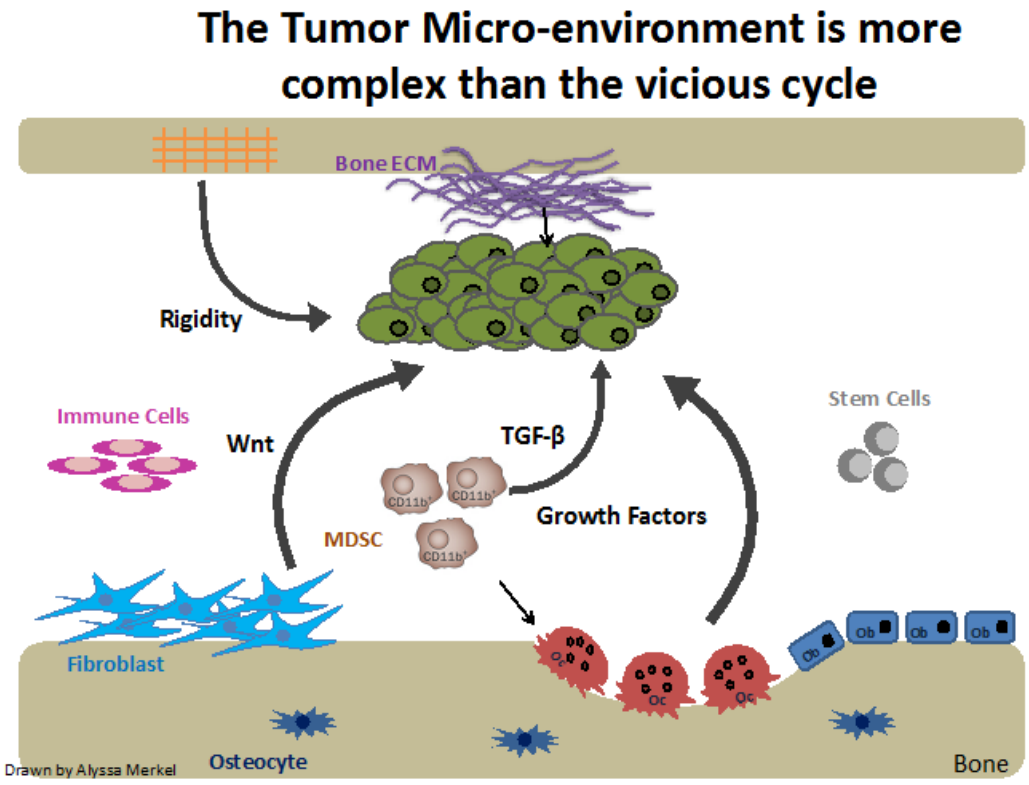

Figure 2.1 Vicious cycle

Tumors cells establish themselves in the bone and produce factors such as PTHrP that indirectly activate osteoclasts. This causes bone resorption and the release of growth factors like TGF β from the bone matrix, which increases proliferation of tumor cells, thus feeding back into the loop. Figure illustrated by A. Merkel

Palliative therapies

Currently the therapies available for patients are radiotherapy which palliate bone pain and/or prevent impending fracture, orthopedic surgery which prevent or repair fractures and increase bone stability, analgesics, and bisphosphonates, which can significantly reduce skeletal related events and delay their onset. Although radiotherapy is the conventional treatment for localized bone pain many patients have pain that is difficult to localize and several complain of bone pain after and increases fracture risk[33].

Bone targeted agents are an alternative to treat several ranges of tumor types and provide relief to bone pain[34]. Bisphosphonates are analogues of pyrophosphate, with carbon replacing the central oxygen, and primarily target active bone remodeling sites. They deposit in bone and inhibit osteolytic destruction of the bone by inhibiting the activity of bone-resorbing osteoclasts and inducing their apoptosis. Bisphosphonates decrease bone resorption and increase mineralization by specifically inhibiting osteoclast activity [35,36]. The bisphosphonates do not target tumor or repair bone directly.

A recent therapy for treating tumor related bone metastasis is Denosumab, a humananized, synthetic monoclonal antibody that binds the receptor activator of RANKL. It is thought to bind to RANKL, thus preventing the activation of pre-mature and mature osteoclasts, thereby blocking bone resorption [37,38].

Biomaterials

Tissue engineering biomimetic systems are increasingly being considered successful approaches to solving critical scientific problems in various fields of biology. The global market for Tissue Engineering has been estimated at US$23 billion in 2015 and is further expected to register a CAGR (compound annual growth rate) of about 23% between 2016 and 2022 to reach a projected US$94.2 billion by 2022 [39]. These materials are predominantly utilized for biomedical applications in the form of sutures, bone plates, joint replacements, ligaments, vascular grafts, heart valves, intraocular lenses, dental implants, and medical devices such as pacemakers and biosensors.

Tissue engineering approaches exploit classical engineering principles and modeling to allow stringent control over a multitude of physiologically relevant parameters of the physical and cellular microenvironment. The research spans the spectrum of fundamental studies to better understand the role of the biomaterial environment on cell function and the biology of tissue formation to targeted clinical applications in the design of *in situ* model systems There is a multitude of bioinspired physical science strategies suitable to address the inherent challenges of modeling and studying tumor-microenvironment interactions. However, it is essential to first define the biological and physicochemical constituents of the normal and the tumor microenvironments, and next describe engineering approaches that mimic these phenomena in a physiologically relevant manner. For the purpose of this thesis, biomaterials have been categorized as natural or synthetic

substances developed to provide a framework for support scaffolds, matrices, or constructs to study, renew or repair damaged or diseased tissue.

Natural materials

Historically natural polymeric materials such as polypeptides (for example collagens), and polysaccharides (e.g. hyaluronic acid) have been utilized extensively for the development of pancreatic replacements to cartilage repair [40]. Advantages to using natural materials include inherent cytocompatibility as well as presentation of cell adhesion sites, and ability to tailor matrix porosity, fiber structure, and stiffness via gelling conditions (e.g., temperature, concentration, gel thickness, pH, and media composition), support attachment, proliferation, and differentiation of cells [41-43]. However, the polymers are inherently variable between batches, and their complex molecular composition can complicate study reproducibility as well as any mechanistic conclusions that can be drawn from them [42,44]. Their weak mechanical strength and inability to be mechanically tunable have been long considered limitations. Recent studies have shown mechanical strength can be improved using intermolecular cross-links [45] or adjusting protein concentrations in hydrogels [46]. However, these biochemical variations are independent of the physical parameters altered and also cause additive alterations in adhesion and, subsequently, cell behavior [47]. Another important aspect of natural polymers includes the kinetics of degradation may not be easily controlled or predicted.

Synthetic materials

Synthetic polymeric scaffolds have been designed to overcome the

limitations of natural materials. They can be fabricated at large scales, and the physical properties and degradation time can be controlled. The physical and mechanical properties such as pore size, porosity, modulus, and strength can be tuned by varying the structure of the polymer. Polyurethane is a well-known example of synthetic polymer. It is porous, biodegradable, and biocompatible with applications in the development of several medical devices ranging from catheters to total artificial hearts [48]. A two step polymer process is carried out by first preparing a prepolymer iscocynate, which is then further reacted with a polyol and cured to form a solid [49]. Controlling the polyol molecular weight can modulate mechanical tunability and rigidity, allowing the study of responses based on mechanotransduction. These systems have been utilized to show that mechanical properties of the bone mineral matrix foster bone metastasis by inducing the osteolytic breast cancer phenotype [50,51].

Engineering model systems to study Tumor Induced Bone Disease

Breast cancer related metastasis causes skeletal related events, including bone pain, spinal instability and compression, as well debilitating pathological fractures that decrease the quality of life in patients[29]. Nearly, 70% of all patients with advanced metastasis related to breast cancer have osteolytic lesions upon autopsy[32]. Although, there are several treatment options available, standard of care has been predominantly palliative in nature. There are no current therapeutics that target the tumor cells present in the bone. Therefore, understanding the

pathophysiology of bone metastasis is critical in developing therapeutics to target tumor.

Over a century ago, Paget proposed the "seed and soil" hypothesis that examines preferential metastasis [30]. The process of metastasis itself is extensively complicated and dynamic: tumor cells dislodge from the primary site; they attach to the basement membrane; tumor cells secrete proteolytic enzymes to disrupt the basement membrane; they migrate through the basement membrane; attachment of tumor cells to basement membranes and to other cells is mediated through cell adhesion molecules such as laminin and E- cadherin; followed by the establishment and progression of tumor [31,35,52-56]. Inherent tumor cell motility or motility in response to chemotactic stimuli are also important factors for tumor cell invasion to the secondary site [57]. Evidently, anatomical and cytological factors such as tumor cell phenotype, suitability of the metastatic site for tumor growth, and specific gene expression contribute to the establishment to tumors in the bone. The bone, a unique organ, and its microenvironment are comprised of a mineralized extracellular matrix and specific cell types under the control of local and systemic factors all contribute into establishing a "safe haven" for tumor cells. In essence, the microenvironment of the bone to which the cancer cells metastasize serves as a fertile soil on which the cancer cells (or seeds) may grow [30,57].

Although previous work has been instrumental in elucidating the molecular mechanisms of TIBD, it has been limited from an anatomical and physiological point of view [44,58,59]. There has been a slow shift to move to 3D cell culture *in vitro* and *in silico* models to study the physiologically relevant aspect of cellular

interaction with cells, the bone and its characteristic physical microenvironment [60-64]. Cancer cells cultured in three dimensions are characterized by several factors that both differentiate them from monolayer cultures and closely resemble those of *in vivo* tumors [65]. The 3D model is a more stringent predictor of drug response than 2D monoculture [66]. These experimental studies coupled with a mathematical model that will enable screening of anti-tumor therapies, thereby reducing the numbers of drugs tested *in vivo,* and help patients make informed decisions about their treatments would be an asset to the field. To bridge the gap between *in vitro* and clinical studies, a two-fold approach has been applied - to model the physical microarchitecture using 3D scaffolds and to simulate TIBD using a population dynamics model.

Physical Model

Incorporating tissue engineering principles into *in vitro* systems that have controllable, reproducible, and functional parameters that can be designed to the study of the metastatic microenvironment is integral. Synthetic materials such as polyurethanes offer higher mechanical tenability, controllable kinetics, and are capable of mimicking tumor specific physical architecture to stimulate physiochemical cues.

2 Dimensional Model systems

Polyurethane scaffolds have wide applications as blood contacting biomaterials, such as vascular grafts, catheters, tubing, and artificial organs [48,67,68]. Molecular weight of the polyols can be modulated to reflect varying rigidity – Rigid (.86 GPa) and Compliant (10 MPa) PURs were designed to reflect

rigidity of the bone and basement membrane, respectively [50,51,69]. Previous work from the Guelcher lab has shown a correlation in the expression of osteolytic factors (PTHrP and Gli2) to mechanical rigidity using a 2 dimensional (2D) polyurethane (PUR) cell based system [51]. In the context of tumor, increasing rigidity induces increase contractility via Rho/ROCK due to activated integrins and mitogenic signaling[70,71]. Increased cell contractility further increases matrix rigidity, which drives a positive feedback loop that triggers malignant transformation in epithelial cells [70,71] and in some cases TGF β dependent epithelial mesenchymal transition (EMT) [72]. However, the extracellular matrix in bone is several orders of magnitude stiffer than soft tissue and cannot be directly remodeled by tumor cells [73]. Thus, the previously observed increase in Gli2 and PTHrP expression when metastatic tumor cells were cultured on substrates with bone-like rigidities [50] cannot be explained by this mechanical positive feedback loop associated with malignant transformation in soft tissue [46,70,71]. On matrices with rigidity equal to or exceeding that of trabecular bone, both expression of IGβ3 as well as its co-localization with TGF-β RII increased, resulting in up-regulation of TGF-b signaling through p38MAPK and Smad 2/3, and Gli2 and PTHrP expression as well (**Figure 2.2**). These data shed light on the difference in tumor types that are bone metastic or non-bone metastatic by elucidating how tumor cells respond to the rigid mineralized bone matrix.

3 Dimensional Model systems

Several decades of research have been explored in scaffold design and synthesis techniques to mimic the physiologically relevant microenvironment.

Previous work has been conducted extensively with 2D scaffolding material such as Matrigel, collagen, and laminin among other extracellular matrix proteins to study cellular responses to the environment that are closely translated to *in vivo* systems. Additionally, most 3D systems currently have moduli reflective of basement membrane or softer tissue [60,66,74]. The bone however has a moduli 1000 times that of any these substrates [75,76]. The design of new biomaterials that both mimic the bone microenvironment and facilitate studies on the spatio-temporal dynamics of cancer progression to bone have been recognized as a pressing need for 3D *in vitro* models [80]. Polyurethanes, with their mechanically tunable characteristics, are excellent candidates for studying TIBD with the biologically relevant 3D scaffolds. Specifically regarding bone, pore size is an important design consideration as it has biological effects on cell behavior [77,78]. Cell attachment, adherence, and proliferation are directly affected by this integral factor in porous biomaterials [42,60,79-81].

As a means of utilizing polyurethane to study TIBD in a biologically relevant manner, the 3D printing field can recapitulate the complex properties of the bone microenvironment. It allows precise control over many topological properties, and we have successfully incorporated templated-3D printing approaches which enable independent control of mechanical, topological, and resorptive properties [69,82]. We use a templated-Fused Deposition Mode (t-FDM) to print 3 dimensional scaffolds with interconnected pores. These 3D tFDMs act as sacrificial molds to fabricate polyurethane scaffolds with varying rigidity. This 3D model also incorporates a perfusion bioreactor to replicate *in vivo* flow

characteristics as well diffusion of nutrients and oxygen.

Theoretical Model

It is still not possible to predict which tumors will induce significant clinical complications and how these tumors will respond to therapeutics. Predicting how putative therapies will impact multiple cellular responses remains an existing challenge. Integrating key biologic findings with the power of computational modeling offers a unique opportunity to assess the impact of putative therapies on the progression of TIBD. These advances in the field could allow for earlier and more effective treatment choices, which may help improve patient survival and improve patient quality of life. Mathematical modeling and computational simulations provide a sophisticated toolset for analyzing experimental data as well as for systematic, quantitative, and multi-scale *in silico* experimentation [83].

Although several mathematical models have been developed to model normal bone homeostasis[84,85], a computational model to simulate breast cancer related metastasis to the bone and its subsequent progression has not been reported. Our model describes population dynamics and cell-cell interactions of osteoclasts, osteoblasts, and tumor cells, focusing on bone remodeling using ordinary differential equations based on Komarova *et al*.'s model of bone remodeling [84]. A mathematical model capable of simulating TIBD would provide greater insight in isolating specific elements contributing to this disease and allow a high throughput method to screen therapeutics, to predict their efficiency and efficacy.

References

[1] D.B. Burr, Targeted and nontargeted remodeling, Bone. 30 (2002)

[2] A.M. Parfitt, Targeted and nontargeted bone remodeling: relationship to basic multicellular unit origination and progression, Bone. 30 (2002)

[3] H.M. Frost, The skeletal intermediary organization, Metab Bone Dis Relat Res. 4 (1983)

[4] H.M. Frost, Intermediary organization of the skeleton, 1986.

[5] A.M. Parfitt, Osteonal and hemi-osteonal remodeling: the spatial and temporal framework for signal traffic in adult human bone, Journal of Cellular Biochemistry. (1994).

[6] A.M. Parfitt, G.R. Mundy, G.D. Roodman, D.E. Hughes, B.F. Boyce, A new model for the regulation of bone resorption, with particular reference to the effects of bisphosphonates, J Bone Miner Res. 11 (1996)

[7] G.A. Howard, B.L. Bottemiller, R.T. Turner, J.I. Rader, D.J. Baylink, Parathyroid hormone stimulates bone formation and resorption in organ culture: evidence for a coupling mechanism, Proc Natl Acad Sci U S A. 78 (1981)

[8] B.F. Boyce, D.E. Hughes, K.R. Wright, L. Xing, A. Dai, Recent advances in bone biology provide insight into the pathogenesis of bone diseases, Lab. Invest. 79 (1999)

[9] A. Klibanski, L. Adams-Campbell, Osteoporosis prevention, diagnosis, and therapy (2001).

[10] F. Lazner, M. Gowen, D. Pavasovic, I. Kola, Osteopetrosis and osteoporosis: two sides of the same coin, Human Molecular Genetics. 8 (1999)

[11] C. Sobacchi, A. Schulz, F.P. Coxon, A. Villa, M.H. Helfrich, Osteopetrosis: genetics, treatment and new insights into osteoclast function, Nat Rev Endocrinol. 9 (2013)

[12] M. Capulli, R. Paone, N. Rucci, Osteoblast and osteocyte: Games without frontiers, Archives of Biochemistry and Biophysics. (2014).

[13] P. Ducy, R. Zhang, V. Geoffroy, A.L. Ridall, G. Karsenty, Osf2/Cbfa1: a transcriptional activator of osteoblast differentiation, Cell. 89 (1997)

[14] R. Florencio-Silva, G.R. da Silva Sasso, E. Sasso-Cerri, M.J. Simões, P.S. Cerri, Biology of Bone Tissue: Structure, Function, and Factors That Influence Bone Cells, BioMed Research International. 2015

[15] T. Komori, H. Yagi, S. Nomura, A. Yamaguchi, K. Sasaki, Targeted disruption of Cbfa1results in a complete lack of bone formation owing to maturational arrest of osteoblasts, Cell. (1997).

[16] K. Nakashima, X. Zhou, G. Kunkel, Z. Zhang, J.M. Deng, The novel zinc finger-containing transcription factor osterix is required for

osteoblast differentiation and bone formation, Cell. (2002).
[17] H. Hu, M.J. Hilton, X. Tu, K. Yu, D.M. Ornitz, F. Long, Sequential roles of Hedgehog and Wnt signaling in osteoblast development, Development. 132 (2005)
[18] D.A. Glass, P. Bialek, J.D. Ahn, M. Starbuck, M.S. Patel, Canonical Wnt signaling in differentiated osteoblasts controls osteoclast differentiation, Developmental Cell. (2005).
[19] J.C. Crockett, D.J. Mellis, D.I. Scott, M.H. Helfrich, New knowledge on critical osteoclast formation and activation pathways from study of rare genetic diseases of osteoclasts: focus on the RANK/RANKL axis, Osteoporos Int. (2011).
[20] X. Feng, J.M. McDonald, Disorders of Bone Remodeling, Annu. Rev. Pathol. Mech. Dis. 6 (2011)
[21] H. Takayanagi, Osteoimmunology: shared mechanisms and crosstalk between the immune and bone systems, Nat Rev Immunol. 7 (2007)
[22] L.F. Bonewald, The amazing osteocyte, J Bone Miner Res. 26 (2011)
[23] A.M. Parfitt, Bone-forming cells in clinical conditions, Bone, 1990.
[24] S.C. Manolagas, Choreography from the tomb: an emerging role of dying osteocytes in the purposeful, and perhaps not so purposeful, targeting of bone remodeling, BoneKEy-Osteovision. (2006).
[25] American Cancer Society, *Cancer Facts & Figures 2016*, (2015)
[26] R.E. Coleman, Clinical Features of Metastatic Bone Disease and Risk of Skeletal Morbidity, Clinical Cancer Research. 12 (2006)
[27] P.K. Zysset, X.E. Guo, C.E. Hoffler, K.E. Moore, S.A. Goldstein, Elastic modulus and hardness of cortical and trabecular bone lamellae measured by nanoindentation in the human femur, J Biomech. 32 (1999)
[28] H.A. Harvey, Issues concerning the role of chemotherapy and hormonal therapy of bone metastases from breast carcinoma, Cancer. (1997).
[29] R.E. Coleman, Skeletal complications of malignancy, Cancer. (1997).
[30] S. Paget, The distribution of secondary growths in cancer of the breast. 1889, Cancer Metastasis Rev. 8 (1989)
[31] B. Psaila, D. Lyden, The metastatic niche: adapting the foreign soil, Nat Rev Cancer. 9 (2009)
[32] G.R. Mundy, Mechanisms of bone metastasis, Cancer. (1997).
[33] M.J. Wolanczyk, K. Fakhrian, I.A. Adamietz, Radiotherapy, Bisphosphonates and Surgical Stabilization of Complete or Impending Pathologic Fractures in Patients with Metastatic Bone Disease, J Cancer. 7 (2016)
[34] R. Coleman, J.J. Body, M. Aapro, P. Hadji, J. Herrstedt, Bone health in cancer patients: ESMO Clinical Practice Guidelines, Ann Oncol. 25 Suppl 3 (2014)
[35] D. Simos, C. Addison, I. Kuchuk, B. Hutton, S. Mazzarello, M. Clemons, Bone-Targeted Agents for the Management of Breast Cancer Patients with Bone Metastases, Jcm. 2 (2013)

[36] R.E. Coleman, Bisphosphonates: Clinical Experience, The Oncologist. 9 (2004)
[37] E. Prommer, Palliative Oncology: Denosumab, Am J Hosp Palliat Care. 32 (2015)
[38] U.H. Weidle, F. Birzele, G. Kollmorgen, R. Rüger, Molecular Mechanisms of Bone Metastasis, Cancer Genomics Proteomics. 13 (2016)
[39] Tissue Engineering: Technologies and Therapeutic Areas - A Global Market Overview. (2016)
[40] P.B. Malafaya, G.A. Silva, R.L. Reis, Natural-origin polymers as carriers and scaffolds for biomolecules and cell delivery in tissue engineering applications, Adv. Drug Deliv. Rev. 59 (2007)
[41] J.F. Mano, G.A. Silva, H.S. Azevedo, P.B. Malafaya, R.A. Sousa, S.S. Silva, et al., Natural origin biodegradable systems in tissue engineering and regenerative medicine: present status and some moving trends, J R Soc Interface. 4 (2007)
[42] A. Atala, F.K. Kasper, A.G. Mikos, Engineering Complex Tissues, Sci Transl Med. 4 (2012) 16012.
[43] A. Villasante, A. Marturano-Kruik, G. Vunjak-Novakovic, Bioengineered human tumor within a bone niche, Biomaterials. 35 (2014) 5785–5794. doi:10.1016/j.biomaterials.2014
[44] D.W. Infanger, M.E. Lynch, C. Fischbach, Engineered culture models for studies of tumor-microenvironment interactions, Annu. Rev. Biomed. Eng. 15 (2013)
[45] C.P. Barnes, C.W. Pemble IV, D.D. Brand, Cross-linking electrospun type II collagen tissue engineering scaffolds with carbodiimide in ethanol, Tissue (2007).
[46] M.J. Paszek, V.M. Weaver, The tension mounts: Mechanics meets morphogenesis and malignancy, J Mammary Gland Biol Neoplasia. 9 (2004)
[47] S.X. Hsiong, N. Huebsch, C. Fischbach, H.J. Kong, Integrin-adhesion ligand bond formation of preosteoblasts and stem cells in three-dimensional RGD presenting matrices (2008).
[48] R.J. Zdrahala, I.J. Zdrahala, Biomedical Applications of Polyurethanes: A Review of Past Promises, Present Realities, and a Vibrant Future, Journal of Biomaterials Applications. (1999).
[49] S.A. Guelcher, Biodegradable polyurethanes: synthesis and applications in regenerative medicine, Tissue Engineering Part B: Reviews. 14 (2008)
[50] N.S. Ruppender, A.R. Merkel, T.J. Martin, G.R. Mundy, J.A. Sterling, S.A. Guelcher, Matrix rigidity induces osteolytic gene expression of metastatic breast cancer cells, PLoS ONE. 5 (2010)
[51] J.M. Page, A.R. Merkel, N.S. Ruppender, R. Guo, U.C. Dadwal, S.A. Cannonier, et al., Matrix rigidity regulates the transition of tumor cells to a bone- destructive phenotype through integrin b3 and TGF-b receptor type II. Biomaterials. 64 (2015)

[52] H. Kennecke, R. Yerushalmi, R. Woods, M.C.U. Cheang, D. Voduc, C.H. Speers, et al., Metastatic Behavior of Breast Cancer Subtypes, J Clin Oncol. 28 (2010)
[53] C. Fontanella, V. Fanotto, K. Rihawi, G. Aprile, F. Puglisi, Skeletal metastases from breast cancer: pathogenesis of bone tropism and treatment strategy, Clin Exp Metastasis. 32 (2015)
[54] O.H. Ocaña, R. Córcoles, Á. Fabra, G. Moreno-Bueno, H. Acloque, S. Vega, et al., Metastatic Colonization Requires the Repression of the Epithelial-MesenchymalTransition Inducer Prrx1, Cancer Cell. 22 (2012)
[55] T.A. Guise, Breast cancer bone metastases: it's all about the neighborhood, Cell. 154 (2013)
[56] A.A. Voulgari, A.A. Pintzas, Epithelial–mesenchymal transition in cancer metastasis: Mechanisms, markers and strategies to overcome drug resistance in the clinic, Biochimica Et Biophysica Acta (BBA) - Reviews on Cancer. 1796 (2009)
[57] T.A. Guise, G.R. Mundy, Cancer and bone, Endocr Rev. 19 (1998)
[58] T. Hartung, Thoughts on limitations of animal models, Parkinsonism Relat Disord. 14 Suppl 2 (2008)
[59] Computational and Mathematical Methods in Medicine
[60] C. Fischbach, R. Chen, T. Matsumoto, T. Schmelzle, J.S. Brugge, P.J. Polverini, et al., Engineering tumors with 3D scaffolds, Nat Meth. 4 (2007)
[61] J.E. Moreau, K. Anderson, J.R. Mauney, T. Nguyen, D.L. Kaplan, M. Rosenblatt, Tissue-engineered bone serves as a target for metastasis of human breast cancer in a mouse model, Cancer Res. 67 (2007)
[62] B.P. Ayati, C.M. Edwards, G.F. Webb, J.P. Wikswo, A mathematical model of bone remodeling dynamics for normal bone cell populations and myeloma bone disease, Biol Direct. 5 (2010)
[63] P.R. Buenzli, P. Pivonka, B.S. Gardiner, D.W. Smith, Modelling the anabolic response of bone using a cell population model, Journal of Theoretical Biology. 307 (2012)
[64] J. Jeon, V. Quaranta, P.T. Cummings, An Off-Lattice Hybrid Discrete-Continuum Model of Tumor Growth and Invasion, Biophy (2010)
[65] D.W. Hutmacher, Biomaterials offer cancer research the third dimension, Nat Mater. 9 (2010)
[66] E.L.S. Fong, S.-E. Lamhamedi-Cherradi, E. Burdett, V. Ramamoorthy, A.J. Lazar, F.K. Kasper, et al., Modeling Ewing sarcoma tumors in vitro with 3D scaffolds, Proc Natl Acad Sci U S A. 110 (2013)
[67] S. Grad, L. Kupcsik, K. Gorna, S. Gogolewski, M. Alini, The use of biodegradable polyurethane scaffolds for cartilage tissue engineering: potential and limitations, Biomaterials. 24 (2003)
[68] Synthesis and In Vitro Biocompatibility of Injectable Polyurethane Foam Scaffolds
[69] R. Guo, S. Lu, J.M. Page, A.R. Merkel, S. Basu, J.A. Sterling, et al.,

Fabrication of 3D Scaffolds with Precisely Controlled Substrate Modulus and Pore Size by Templated-Fused Deposition Modeling to Direct Osteogenic Differentiation, Advanced Healthcare Materials. (2015)
[70] S. Huang, D.E. Ingber, Cell tension, matrix mechanics, and cancer development, Cancer Cell. 8 (2005)
[71] M.J. Paszek, N. Zahir, K.R. Johnson, J.N. Lakins, G.I. Rozenberg, A. Gefen, et al., Tensional homeostasis and the malignant phenotype, Cancer Cell. 8 (2005)
[72] A.C. Brown, V.F. Fiore, T.A. Sulchek, T.H. Barker, Physical and chemical microenvironmental cues orthogonally control the degree and duration of fibrosis-associated epithelial-to-mesenchymal transitions, J Pathol. 229 (2013)
[73] T.J. Martin, G.R. Mundy, Bone metastasis: can osteoclasts be excluded? Nature. 445 (2007)
[74] K.A. Fitzgerald, J. Guo, E.G. Tierney, C.M. Curtin, M. Malhotra, R. Darcy, et al., The use of collagen-based scaffolds to simulate prostate cancer bone metastases with potential for evaluating delivery of nanoparticulate gene therapeutics. Biomaterials. 66 (2015)
[75] J.A. Sterling, S.A. Guelcher, Bone Structural Components Regulating Sites of Tumor Metastasis, Curr Osteoporos Rep. 9 (2011)
[76] S.A. Guelcher, J.A. Sterling, Contribution of Bone Tissue Modulus to Breast Cancer Metastasis to Bone, Cancer Microenvironment. (2011)
[77] A.A. Zadpoor, Bone tissue regeneration: the role of scaffold geometry, Biomater. Sci. 3 (2015)
[78] J. Zeltinger, J.K. Sherwood, D.A. Graham, R. Müeller, L.G. Griffith, Effect of pore size and void fraction on cellular adhesion, proliferation, and matrix deposition, Tissue Eng. 7 (2001)
[79] S. Van Bael, Y.C. Chai, S. Truscello, M. Moesen, G. Kerckhofs, H. Van Oosterwyck, et al., The effect of pore geometry on the in vitro biological behavior of human periosteum-derived cells seeded on selective laser-melted Ti6Al4V bone scaffolds, Acta Biomaterialia. (2012)
[80] P. de la Puente, B. Muz, R.C. Gilson, F. Azab, M. Luderer, J. King, et al., 3D tissue-engineered bone marrow as a novel model to study pathophysiology and drug resistance in multiple myeloma, Biomaterials. 73 (2015)
[81] S.P. Pathi, C. Kowalczewski, R. Tadipatri, C. Fischbach, A novel 3-D mineralized tumor model to study breast cancer bone metastasis, PLoS ONE. 5 (2010)
[82] R. Guo, A.R. Merkel, J.A. Sterling, J.M. Davidson, S.A. Guelcher, Substrate modulus of 3D-printed scaffolds regulates the regenerative response in subcutaneous implants through the macrophage phenotype and Wnt signaling, Biomaterials. 73 (2015)
[83] T.K. Schuessler, X.Y. Chan, H.J. Chen, K. Ji, K.M. Park, A. Roshan-Ghias, et al., Biomimetic tissue-engineered systems for advancing

cancer research: NCI Strategic Workshop report, Cancer Res. 74 (2014)
[84] S.V. Komarova, R.J. Smith, S.J. Dixon, S.M. Sims, L.M. Wahl, Mathematical model predicts a critical role for osteoclast autocrine regulation in the control of bone remodeling, Bone. 33 (2003)
[85] S. Jerez, B. Chen, Stability analysis of a Komarova type model for the interactions of osteoblast and osteoclast cells during bone remodeling, Math Biosci. 264 (2015)

Chapter III

3D Bone Bioreactor Model for Studying Tumor Induced Bone Disease *in vitro* and Testing Therapeutic Drug Response

Introduction

Tumor-Induced Bone Disease (TIBD) is a common occurrence among primary breast, lung, and prostate cancer patients, with 70-90% of patients who die from the disease displaying bone metastases upon post-mortem analysis. Bone metastases lead to chronic bone pain, hypercalcemia, osteolytic lesions, pathological fractures, and bone loss, which significantly decrease patient quality of life[1]. Prior studies have demonstrated that in the primary tumor, the interactions between the tumor cells and the physical microenvironment promote integral changes in cell morphology, gene expression, cellular metabolism, protein synthesis, and response to cytotoxic therapeutics[1-3]. Bone, however, has a unique microenvironment that can affect colonization and establishment of tumor cells, such as a substrate modulus 1000 times that of the primary site, macropores between trabeculae[4], and cell populations actively participating in bone remodeling. While many research groups have studied the molecular events leading to tumor establishment and bone destruction, the specific cellular and mechanical

cues that govern these responses have not been explored in the context of the 3D bone-tumor microenvironment[1-3,5].

Several studies demonstrates that the tumor microenvironment contributes to the selection of cancer cells that are conditioned for metastasis to bone[1-3,6]. Specifically, the tumor bone microenvironment has been investigated using 2D models fabricated from materials such as hydroxyapatite[1,5,7], collagen [1-3,6,8], and PLGA[1,3,9-12] scaffolds. However, the effects of scaffold properties on expression of bone-tumor cellular interactions and metastatic genes in a tumor-bone microenvironment have not been systematically investigated. Biomimetic 3D tissue-engineered scaffolds have been proposed as alternatives to 2D culture and mouse models for investigating molecular mechanisms of disease progression and for screening drugs[13]. Previous studies have shown that cell proliferation, metabolism, gene expression, protein synthesis, and drug metabolism are substantially different in 3D scaffolds compared to 2D films. A recent study has reported that Ewing sarcoma cells cultured in electrospun poly(ε-caprolactone) 3D scaffolds showed higher resistance to anti-tumor drugs[14]. This study and others[8,15] used polymeric or collagen scaffolds to show that the 3D microenvironment substantially alters the tumor response to anti-cancer drugs compared to 2D monoculture[8,14]. However, the ability of electrospun polymeric scaffolds and hydrogels to recapitulate the mechanical and topological properties of the bone microenvironment may be limited by their low substrate modulus and nanoscale pore size. Consequently, development of new biomaterials mimicking the tumor-bone microenvironment has been highlighted as a critical need for

understanding the spatiotemporal dynamics of tumor progression, recapitulating *in vivo* conditions at distinct steps of metastasis, and understanding how tumor cells integrate mechanical and chemical signals over multiple length scales[13].

In this study, we designed 3D-printed scaffolds to investigate the effects of the bone microenvironment on progression of TIBD. We previously reported that substrate modulus of 2D films regulates tumor cell expression of the transcription factor Gli2 and parathyroid hormone-related protein (PTHrP), which have been associated with bone destruction[16,17]. Conversely, in the 3D bone microenvironment, cells are also exposed to mechanical forces resulting from surface curvature and fluid flow in addition to the substrate modulus[18], which simulates mechanosensitive tumor and bone cells[5,17]. To more accurately recapitulate the mechanical and topological properties of the bone microenvironment, we fabricated 3D scaffolds with tunable substrate moduli and pore size using a templated-Fused Deposition Modeling (t-FDM) process[17]. Substrate modulus ranged from 5 – 266 MPa, which is representative of values reported for collagen fibers (32 MPa) and trabecular bone (93 – 366 MPa). Pore sizes in the physiologically relevant range that supports bone formation and vascularization (300 – 600 μm) were also evaluated[4,17]. Scaffolds were seeded with MDA-MB-231 cells, a bone-tropic breast adenocarcinoma cell line, and cultured under static conditions or in a perfused bioreactor under flow conditions representative of the tumor-bone environment[19]. Drug efficacy was tested using 3D-printed scaffolds over a range of drugs applicable to TIBD.

Materials and Methods

Materials

Hexamethylene diisocyanate trimer (HDIt) was supplied by Bayer Materials Scientific (Pittsburgh, PA). Stannous octoate, glycerol, poly(ε-caprolactone) triol (300 Da), and ε-caprolactone were purchased from Aldrich (St. Louis, MO). Glycolide was purchased from Polysciences (Warrington, PA). Glycerol was dried at 10 mm Hg for overnight at 80°C and ε-caprolactone was dried over anhydrous magnesium sulfate prior to use. All other materials were used as received. Two-component cast poly(ester urethane)s were mixed using a Hauschild SpeedMixer^{TM} DAC 150 FVZ-K (FlackTek Inc., Landrum, SC). Fibronectin (Fn) was purchased from Life Technologies (Grand Island, NY). Dulbecco's modification of Eagle's medium (DMEM) was purchased from Invitrogen (Carlsbad, CA). Fetal bovine serum (FBS) was purchased from Hyclone Laboratories (Logan, UT). Penicillin, streptomycin, L-glutamine, trypsin, sodium pyruvate, essential and, non-essential amino acids were all acquired from Mediatech (Manassas, VA). MDA-MB-231 cells were purchased from ATCC (Manassas, VA). MDA-MB-231 cells were then selected for ability to metastasize to bone[17]. The RNeasy$^{\text{™}}$ mini kit and RNAeasy Minielute$^{\text{™}}$ clean up kit was purchased from Again (Valencia, CA). qScript cDNA synthesis kits were purchased from Quanta Biosciences (Atlanta, GA). qPCR primers for PTHrP, Gli2,

Integrin β_3 (ITGβ3) and 18S (TaqMan) were obtained from Applied Biosciences (Carlsbad, CA).

Synthesis of 2D films

2D films were synthesized by reacting a mixture of poly(ε-caprolactone-*co*-glycolide) triol (M_n=300 or 3000 g mol^{-1}), hexamethylene diisocyanate trimer (HDIt), and catalyst. The reactants were mixed in a cup for 30 seconds in a Hauschild SpeedMixer™ DAC 150 FVZ-K vortex mixer (FlackTek, Inc, Landrum, SC) and poured into 24 or 6 well plates as previously described [16,17]. To facilitate cell adhesion and ensure that the surface chemistry was comparable for all substrates tested, fibronectin (Fn) was adsorbed to the surface of the substrates by incubating them in a 4 μg/mL solution of Fn in PBS at 4°C overnight.

Fabrication of 3D scaffolds by templated-Fused Deposition Modeling (t-FDM)

A polylactic acid (PLA) template (14 mm diameter) was designed with a defined 100% connected porous architecture using Solidworks® software and printed using a MakerBot Replicator® 2 Fused Deposition Modeling (FDM) printer. The reactive liquid PUR was poured into the PLA templates and cured at 60°C overnight. The PLA template was leached with dichloromethane (DCM) and washed with a mixture of acetone:dichloromethane to yield scaffolds with interconnected pores having a channel diameter of 423 ± 34 or 557 ± 44 μm for nominal 300 or 500 μm templates, respectively (Figure 3.1)[2,3,20]. Scaffolds were sterilized under UV light for 15 minutes in 70% ethanol and incubated in a solution of 4μg mL^{-1} fibronectin overnight at 4°. The substrate modulus (E_s) of the scaffolds was controlled by the molecular weight (M_w) of the polyester triol (3000 g mol^{-1} or

300 g mol^{-1}) to attain values representative of collagen (5 MPa, Compliant (C)), trabecular bone (266 MPa, Rigid (R)), or cortical bone (871–11,500 MPa) [1-3,5,17] (**Table 3.1**).

Bioreactor

A proprietary perfusion bioreactor system from 3D Biotek consisting of four individual autoclavable polycarbonate chambers in which the PUR scaffolds seeded with cells can be placed. Cell culture medium was perfused through the open porous structure of scaffolds using a pulsatile pump feeding into a media reservoir chamber. Within each chamber there is a 1.5 mm distance separating each scaffold. Perfusion flow rate was achieved by utilizing .505 ml flow rate. The whole system, including the pump, was placed in a standard 5% CO_2 incubator at 37°C. Scaffolds seeded as described above were placed in each individual chamber (n=6), kept in dynamic cell culture for 48 hours and were harvested for gene expression studies.

Treatment Group	Nomenclature	Fluid Flow Rate ($\mu L\ s^{-1}$)	Pore Size (μm)	Substrate Modulus E_s (Mpa)
2D PUR film Compliant	2DC	0	N/A	10±3
2D PUR film Rigid	2DR	0	N/A	1800±250
3D 500μm compliant PUR scaffolds, static culture	560C-s	0	557±44	10±2.67
3D 300μm compliant PUR scaffolds, static culture	420C-s	0	423±34	10±2.67
3D 500μm rigid PUR scaffolds, static culture	560R-s	0	557±44	990±36
3D 300μm rigid PUR scaffolds, static culture	420R-s	0	423±34	990±36
3D 500μm compliant PUR scaffolds, flow condition	560C-f	9.35	557±44	10±2.67
3D 300μm compliant PUR scaffolds, flow condition	420C-f	9.35	423±34	10±2.67
3D 500μm rigid PUR scaffolds, flow condition	560R-f	9.35	557±44	990±36
3D 300μm rigid PUR scaffolds, flow condition	420R-f	9.35	423±34	990±36

Table 3.1 *In vitro* study design. Material characterization and nomenclature of 2D films and 3D scaffolds used during *in vitro* study.

In vitro cell culture

As previously described, a bone metastatic variant of MDA-MB-231 cells were transfected with a GFP overexpression plasmid was generated (MB-231-GFP) and used for all the *in vitro* experiments described below (Table 3.1). For *in vitro* studies, 0.5×10^5 MDA-MB-231 GFP cells/scaffold were seeded. For *in vivo,* studies 10^6 MDA-MB-231 cells/scaffold were seeded unless otherwise stated.

Cell viability, proliferation and metabolic activity

Trypan Blue (Sigma, St. Louis, MO) was used to measure cell viability 48 hours after seeding. Cell proliferation and metabolism were measured by total protein (BCA Protein Assay Reagent, Thermo) and MTS assay (CellTiter 96® Aqueous Non-Radioactive Cell Proliferation Assay, Promega), respectively, as per the manufacturer's protocol.

Cell motility assays

MDA-MB-231 GFP cells were plated on fibronectin-coated 2D films and 3D scaffolds. The cell-seeded films or scaffolds were then placed in a live cell chamber (LiveCell™) at 5% CO_2 and 37°C and monitored by light microscopy (Olympus CKX41). Photos of the same field were taken every hour for 48 hours, and Image J software (NIH) was used to analyze the photo series to track single cell movement. Three representative cells were selected per group.

Chemotactic migration, specifically migration towards 10% FBS was quantified as migration of cells through a filter using a 24-well plate Boyden chamber transwell assay (8μm pore size; Corning Costar, Cambridge, MA, USA).

40,000 cells were cultured on 3D scaffolds (3 mm height × 6 mm diameter) as described above, serum-starved for 4 hours, and subsequently introduced into the upper chamber of the Boyden chambers. A 30-hour assay was carried out with the chemoattractant - 10% FBS (positive control) or serum free media (negative control) in the lower chamber. The cells that were present on the upper surface of the filter were removed using a sterile cotton swab. The cells that were able to migrate through the chamber onto the lower surface of the filter were fixed and stained with Crystal Violet Dye (Sigma, St. Louis, MO). The number of migrating cells was counted in five randomly chosen fields and compared to the negative control. The experiments were performed in triplicate wells and each experiment was performed at least three times.

MDA-MB-231 GFP cells were plated on fibronectin-coated 3D scaffolds. The cell-seeded films or scaffolds were then placed in a live cell chamber at 5% CO_2 and 37°C and monitored by confocal microscopy (LSM 510 META Inverted). Photos of the pre-defined Z-stack field (500μm stack) were taken every hour for 8 hours, and IMARIS software (Bitplane) was used to analyze the photo series to track single cell movement. Analysis was carried out with IMARIS.

Drug panel studies

Tumor-seeded scaffolds were plated at a cell density of 5×10^5 cells and placed in 24-well plates 24 hours prior to treatment. 2D PUR films were plated at the same density 24 hours prior to treatment. The scaffolds were serum-starved for 8 hours. Scaffolds were then treated with either 6-TG (Sigma-Aldrich, St. Louis, MO), Celingitide (Selleck Chemicals, Huston, TX), GANT 58, SD208 (Tocris,

Minneapolis, MN) or Zoldronic acid (Sigma-Aldrich, St.Louis, MO) (**Table 3.2**). TGF-β treatments were performed at 0 (control) or 10 ng/μL alongside.

Gene expression assays

Total RNA from tumor cells was isolated using the RNeasy kits (Qiagen). Reverse transcription of the RNA template will be completed using the qScript cDNA synthesis kit (Quanta Biosciences) following DNAse I treatment. Quantitative real-time PCR (q-PCR) was performed in triplicate and normalized to 18S as per manufacturer's instructions. Gene expression was quantified using validated Taqman probes/primers as previously described [1-3,6,16,17].

Drug	Target
Bisphosphonate (ZA)	Oc inhibitor
SD 208	TGFBRI inhibitor
Cilengitide	Integrin α5
Gant 58	Gli antagonist

Table 3.2 Drug panel. Targets of drug panel relevant to TIBD

Statistical analysis

All studies were performed in triplicate with at least n=3 test substrates per replicate to ensure batch-to-batch reproducibility. ANOVA and the Bonferroni *post hoc* test were used for statistical analyses with significance set at $p<0.05$ unless otherwise stated. Cell culture data was tested for significance across time points, across materials, and interactions between time and materials with n=3 independent biological experiments.

Results

3D scaffolds support attachment and proliferation of MDA-MB-231 tumor cells.

Tumor cells are susceptible to mechanical forces modulated by the microenvironment and exhibit a more invasive and metastatic phenotype in an environment that recapitulates the *in vivo* tumor microenvironment [1-3,10-12,21]. To investigate the effects of mechanical forces on bone metastatic gene expression, we used a new templated-Fused Deposition Modeling (t-FDM) process to fabricate 3D scaffolds (**Figure 3.1**) with substrate moduli either 5 or 266 MPa, which are representative of either collagen fibers (32 Mpa[2,3,22,23]) or trabecular bone (93 – 365 MPa [1,5,16,24]), and pore sizes that support bone formation and vascularization (>300 μm).The smaller pore size (423 ± 34 μm) [1-3,8,20] simulates the optimal pore size for osteogenesis (300 – 400 μm) while the larger pore size (557±44μm) [3,9,20], mimics the diseased bone microenvironment (trabecular separation ranging from 430 – 930 μm) (**Table 3.1**).

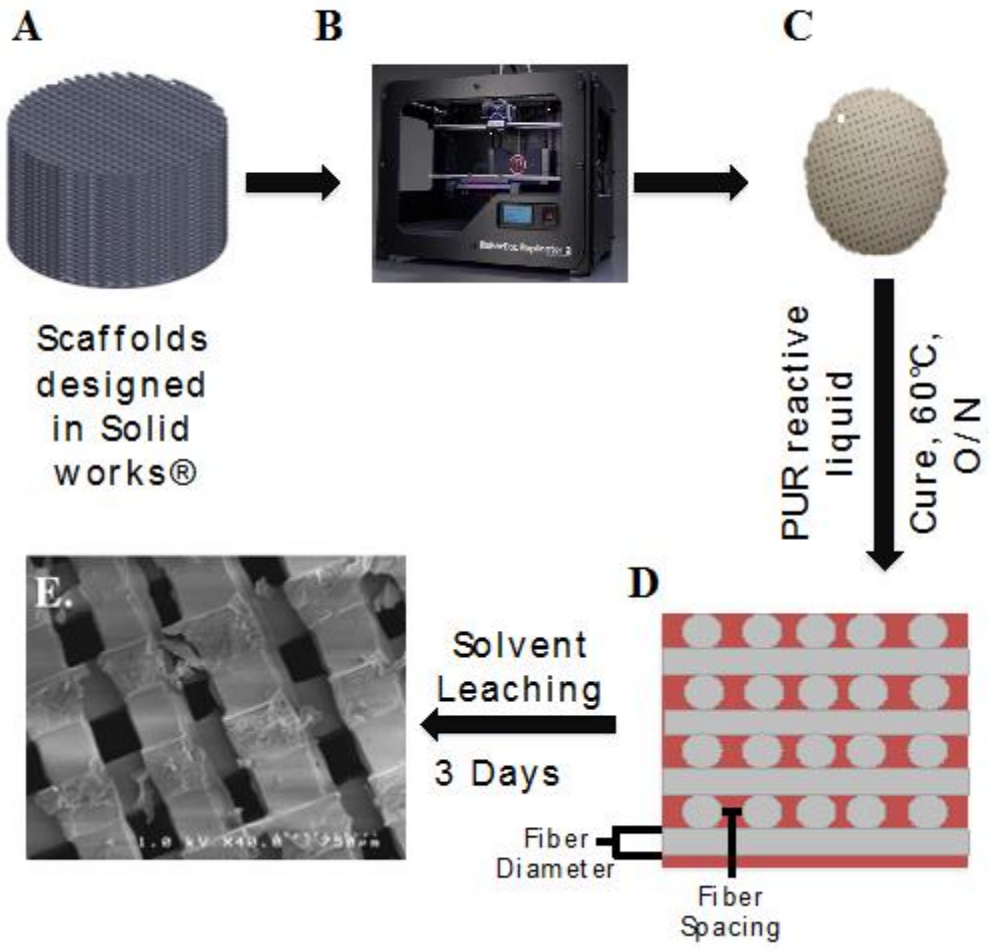

Figure 3.1 Fabrication schematic for t-FDM scaffolds. (A) Scaffold molds (inverse scaffold template) were designed in SolidWorks® software with tunable pore size and physical microarchitecture (B) Polylactic acid (PLA) templates were printed using a MakerBot Replicator® 2 Fused Deposition Modeling (FDM) printer. (C) Representative images of the designed template (left) and the scaffold mold (right) (D) Liquid polyurethane is poured into the PLA templates and cured overnight at 60°C. Scaffold molds are washed and leached using acetone-dichloromethane-acetone solution mixture. (E) Representative scanning electron microscopy (SEM) image of the 420R scaffold.

Tumor cells were seeded on scaffolds to evaluate viability, metabolic activity, and proliferation as a function of substrate rigidity and pore size. Cell viability assessed by Trypan blue staining demonstrated <5% cell death after 48 hours, suggesting that the scaffolds are not cytotoxic. Scanning electron microscopy (SEM) images show that the tumor cells spread on and adhere to the surface of all four scaffolds (**Figure 3.2.A**). We further investigated whether pore size and substrate modulus affected cell proliferation (GFP) and metabolic activity (MTT assay) from day 1 to 3. Cell proliferation and metabolic activity were not significantly affected by substrate modulus or pore size (**Figure 3.2.B&C**). Thus, the 3D scaffolds are non-cytotoxic, and their mechanical and topological properties do not influence the proliferation or metabolic activity of the tumor cells.

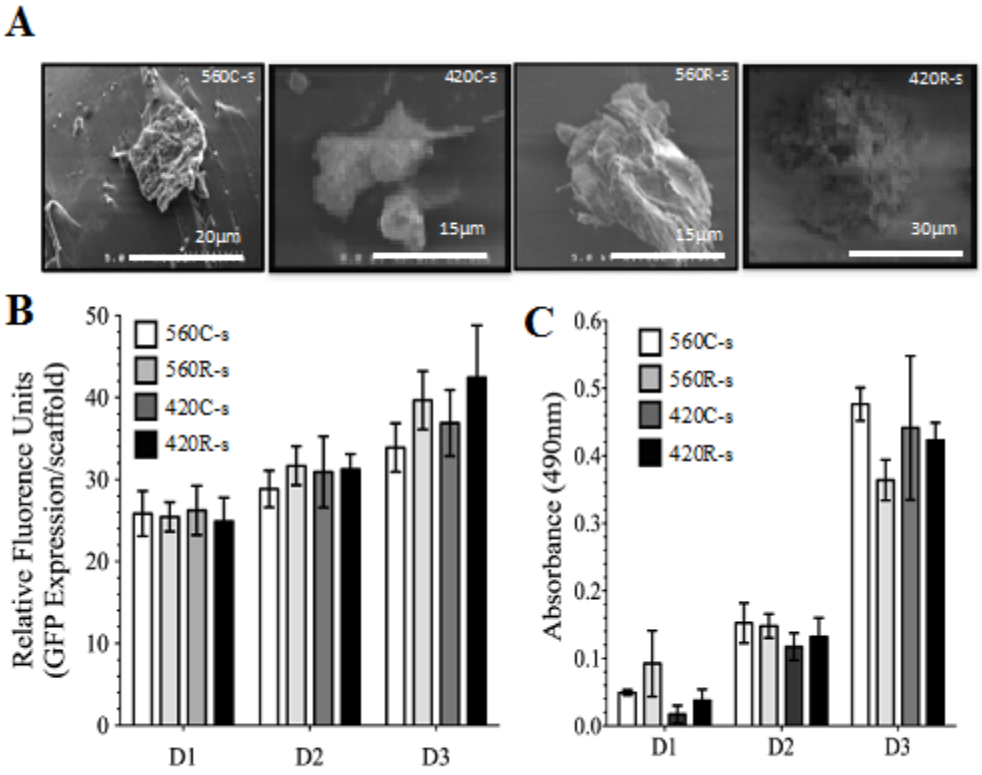

Figure 3.2. Rigidity and pore size do not affect attachment and proliferation of MDA-MB-231 tumor cells on 3D scaffolds. (A) Scanning electron microscopy (SEM) images of tumor cells attached to 500µm compliant (560C-s), 300µm compliant (420C-s), 500µm (560R-s), and 300µm (420R-s) rigid scaffolds. (B) Proliferation of MDA-MB-231 tumor cells on 3D scaffolds measured, as fluorescence expression of GFP demonstrates no statistical microscopy (SEM) images show that the tumor cells spread on and adhere to the surface of all four scaffolds (**Figure 3.2.A**). We further investigated whether pore size and substrate modulus affected cell proliferation (GFP) and metabolic activity (MTT assay) from day 1 to 3. Cell proliferation and metabolic activity were not significantly affected by substrate modulus or pore size (**Figure 3.2.B&C**). Thus, the 3D scaffolds are non-cytotoxic, and their differences between 3D scaffolds groups over a time period (days- D1, D2 and D3). (C) Metabolic activity of MDA-MB-231 tumor cells cultured on 3D scaffolds measured by the MTT assay corroborates no variation of metabolic expression over a time period (days- D1, D2 and D3).

Substrate modulus and pore size regulate the motility of tumor cells

There is increasing evidence that tumor cell motility correlates with metastasis by promoting dissemination, and clinical therapies are being pursued to target motility[13,25,26]. The microenvironment is considered to be a prominent regulator of metastatic potential and may facilitate motility by providing physical cues for metastatic cells to invade and colonize to preferred sites[6,13,14,27]. Thus, we investigated the effects of substrate modulus and pore size on motility and migration of bone metastatic MDA-MB-231-GFP tumor cells[8,15,28,29]. It is well known that there are qualitative and quantitative differences in migration between 2D and 3D substrates[8,14,30]. Using live cell image tracking, we observed random motility of tumor cells on 2D and 3D films and scaffolds. Live cell imaging found that tumor cells were significantly more motile on 3D scaffolds compared to 2D films. We observed 6- and 7-fold higher cell displacements for the 560R-s and 420R-s scaffolds compared to 2D compliant films based on random motility (**Figure 3.3.A**). These observations suggest that higher mechanical forces on the cells due to increased substrate modulus or decreased pore size resulted in higher tumor cell motility. We further tested whether substrate modulus and pore size influence cell motility using transwell assays and live cell confocal imaging.

Transwell assays are extensively used to determine cell migration using a well insert to separate the well into top and bottom chambers. Cell migration can then be studied placing cells over the insert and introducing a chemottractant solution, in our case 10% FBS, in the bottom chamber. Transwell migration assays demonstrated significantly higher migration potential of cells on 420R-s (~3 fold)

and 560R-s (~2.5 fold) scaffolds compared to 560C-s in CM media, while there were no significant changes in migration potential without a chemoattractant gradient (SFM) (**Figure 3.3.B**).

Similarly, confocal live cell imaging was utilized to observe tumor cells over the cross-section of scaffold pores. Importantly confocal imaging allowed us to discern motility of cells in x-, y-, and z-direction. When tumor cell-seeded scaffolds were placed in serum-free media for a period of 6 hours and exposed to 10% FBS media (chemoattractant, CM) and imaged using confocal imaging, cell speed increased irrespective of pore size with increasing substrate rigidity significantly ($p<0.0001$) (**Figure 3.3.C&D)**. These findings suggest that the substrate modulus has a significant effect on the motility of the cells, thereby promoting a more motile cell phenotype during early establishment of tumor cells (<48 hours) *in vitro*. When tumor cells were analyzed by live cell confocal imaging to track displacement of cells we noted tumor cell motility was modulated by rigidity only (**Figure 3.4**).

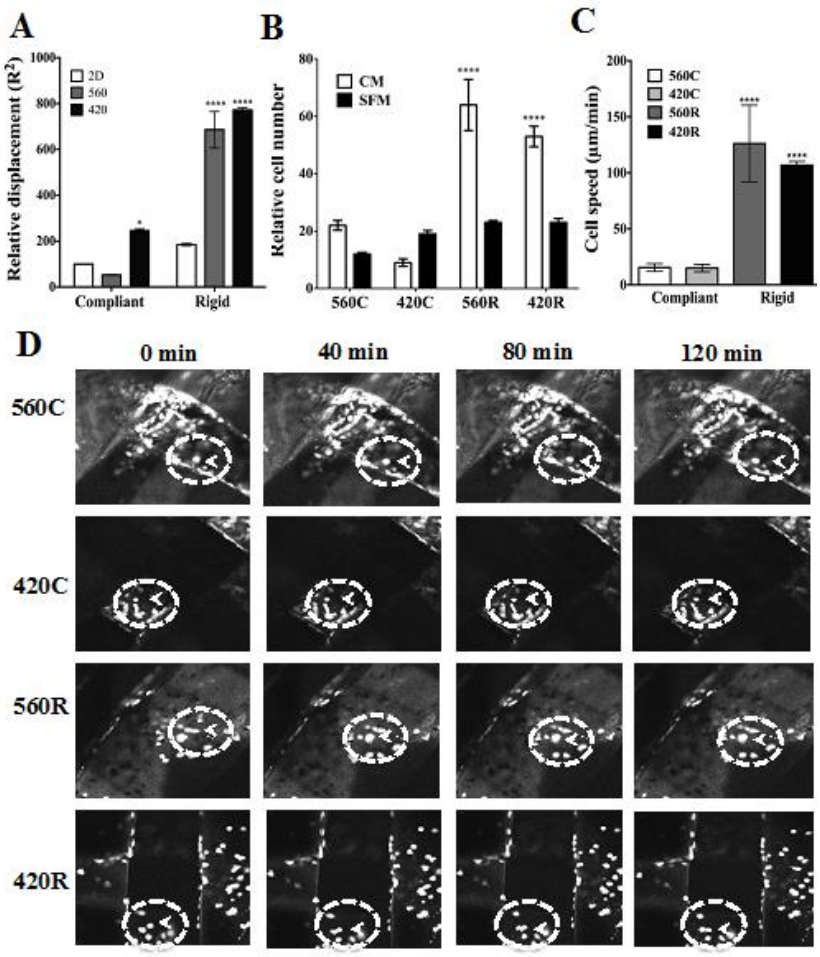

Figure 3.3. Rigidity and pore size affect migration of tumor cells on 3D scaffolds. (A) Live cell imaging using bright field microscopy demonstrates significantly higher cell motility on 560R-s (>60 fold) and 420R-s (>70 fold) substrates as compared to 2D compliant PUR film. (B) 3D migration transwell assay with either complete media (CM) or serum-free medium (SFM) determined tumor cells have higher migratory potential on 500μm and 300 μm rigid (560R-s and 420R-s) 3D scaffolds as compared to 500μm and 300μm compliant 3D scaffolds (560C-s and 420C-s). (C) Motility assay using confocal imaging shows that tumor cells have significantly increased speed on the 560R-s (12-fold) and 420R-s (10-fold) compared to 560C-s. (D) Representative confocal imaging demonstrates tumor cells (represented by area highlighted by white dotted line and white arrow following a single cell) motile over the 3D scaffolds surface. * $p < 0.05$, ****$p<0.0001$

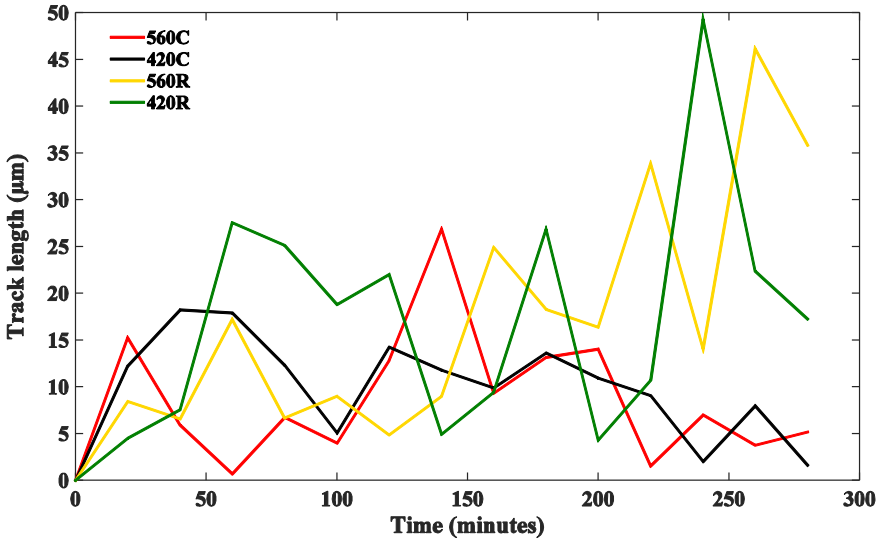

Figure 3.4 Rigidity affects displacement of tumor cells on 3D scaffolds. Live cell confocal imaging demonstrates that tumor cells have a higher displacement on rigid scaffolds (560R-s in yellow and 420R-s in green) when compared to compliant scaffolds (560C-s in red and 420C-s in black).

Expression of bone-metastatic genes is modulated by substrate rigidity and pore size in vitro

We measured the mRNA expression of genes that are correlated with tumor-induced bone destruction (Gli2, PTHrP, and, ITGβ3) and screened a panel of known bone-metastatic genes (**Table 3.3.A-B**). The effect of substrate modulus and pore size on bone-metastatic gene expression was measured at 48h by qRT-PCR. We further expanded our 3D model by mounting the scaffolds in a perfusion bioreactor to mimic the physiologically relevant interstitial flow experienced by cells (9.35 μL/s) (**Figure 3.5.A.)**. ITGβ3, Gli2, and PTHrP gene expression were 10-, 7-, and 9-fold higher on 420R-s scaffolds (**Figure 3.5.B-D.**) compared to 2D compliant films. Gene expression trended upward with decreasing pore size. Pore size effects were significant when scaffolds were perfused (9.35 μl/s) in the bioreactor, as evidenced by 40-, 25-, and 24-fold increases in ITGβ3, Gli2, and, PTHrP expression for 420R-f compared to 2D compliant films. These observations indicate that substrate modulus, pore size, and flow rate regulate expression of genes associated with bone metastasis.

Table 3.3.A. Tumor metastatic microarray in 3D scaffolds

Gene Expression	Gene ID	Fold Change
catenin (cadherin-associated protein), alpha	CTNNA1	1.271466
mannosyl (alpha-1,6-)-glycoproteinbeta-1,6-N-acetyl-glucosaminyltransferase	MGAT5	1.070686
matrix metallopeptidase 14 (membrane-inserted)	MMP14	1.186379
metastasis associated 1	MTA1	1.324846
TIMP metallopeptidase inhibitor 4	TIMP4	1.163873
tumor protein p53	TP53	1.164444

Table 3.3.B. Metastatic panel in 3D scaffolds

Gene Expression	Gene ID	Fold Change
connective tissue growth factor	CTGF	0.317
chemokine (C-X-C motif) receptor 4	CXCR4	5.570
interleukin 11	IL11	2.045
matrix metallopeptidase 9	MMP9	6.45
Secreted phosphoprotein	OPN (SPP1)	0.667

Table 3.3. Metastatic panel in 3D scaffolds.

Tumor seeded scaffolds 3D scaffolds (420R and 420C) were harvested *in vitro*. Gene expression was determined using (A)**.** tumor metastatic array and (B)**.** RT PCR array. Fold change was measured as the ratio of gene expression of tumor cells seeded on rigid and compliant 3D scaffolds (420R/420C).

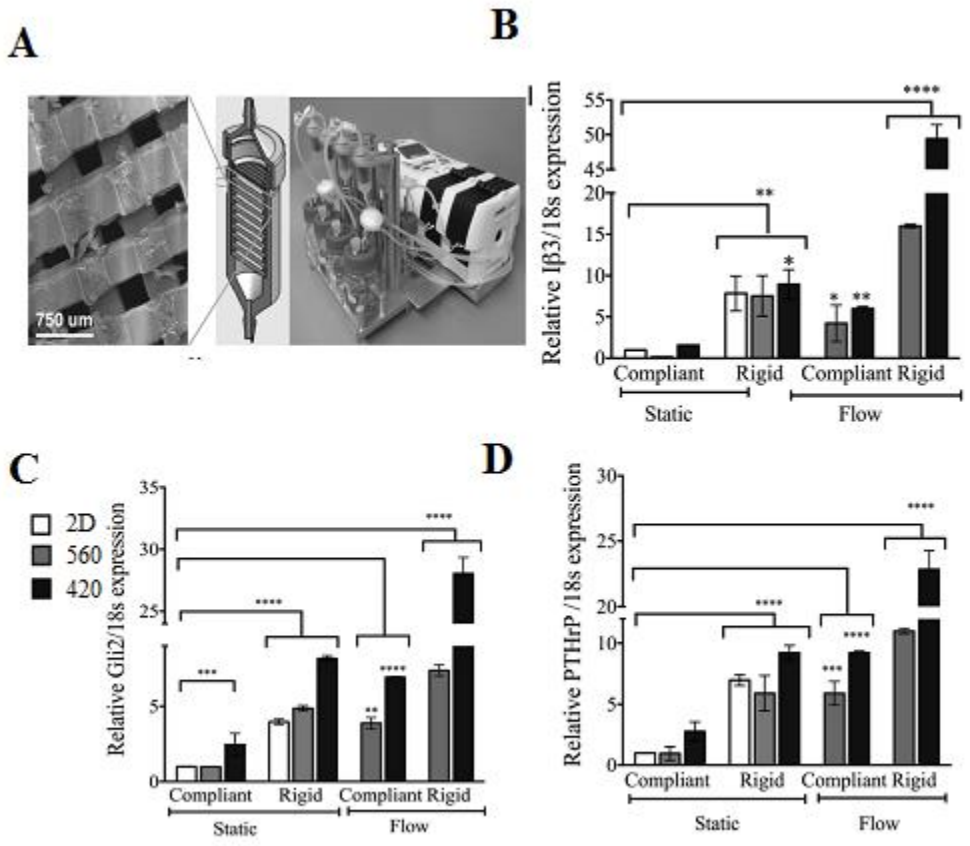

Figure 3.5 Effects of substrate modulus, pore size, and flow rate on expression by MDA-MB-231 cells. (A) Tumor cells were seeded on scaffolds and placed in individual chambers of the bioreactor and were harvested in 48 hours. Expression of (B) ITGβ3 (Iβ3) is 50 fold higher under flow conditions on 420R, (C) Gli2, is 28-fold higher on 420R-f (under flow conditions) and (D) PTHrP is upregulated 25 fold on 420R-f (under flow conditions) when compared to 2D compliant films. *p<0.05, **p<0.01, ***p<0.001, ****p<0.0001

3D scaffolds influence the response of tumor cells to therapeutics

Currently TIBD therapy includes bisphosphonate and anti-RANK ligand treatments, which are palliative and do not target the tumor present in the bone[31,32]. Previous studies have identified ROCK[13,16], TGF-β[16,17,33], ITGβ3[17,18], and Gli2[5,17,28] as promising targets for blocking the progression of TIBD. To assess the effects of the 3D bone microenvironment on tumor cell drug response, we tested four inhibitors in short-term mono-culture on 420R scaffolds. MDA-MB-231 cells were cultured on rigid 2D films or 3D scaffolds, and expression of ITGβ3, Gli2, and PTHrP was measured by qPCR at 48 h (**Figure 3.6.A)**. Drug response differed remarkably when tumors were cultured on bone-like 3D scaffolds compared to tissue culture well plates. As anticipated, treatment with zoledronic acid (ZA) did not reduce gene expression in 2D or 3D (**Figure 3.6.B-D**). While the TGF-β Receptor I kinase inhibitor (SD-208) and ITGβ3 inhibitor (Cilengitide) significantly reduced bone-metastatic gene expression in 2D by 2 – 3-fold, these drugs were not effective in 3D scaffolds (**Figure 3.6.B-D)**. In contrast, treatment with the Gli2 inhibitor GANT58 significantly reduced bone-metastatic gene expression>3-fold in both 3D and 2D. (**Figure 3.6.B-D**). GANT58 also reduced ITGβ3 expression, suggesting that the drug might also inhibit tumor cell contractility in bone [17].

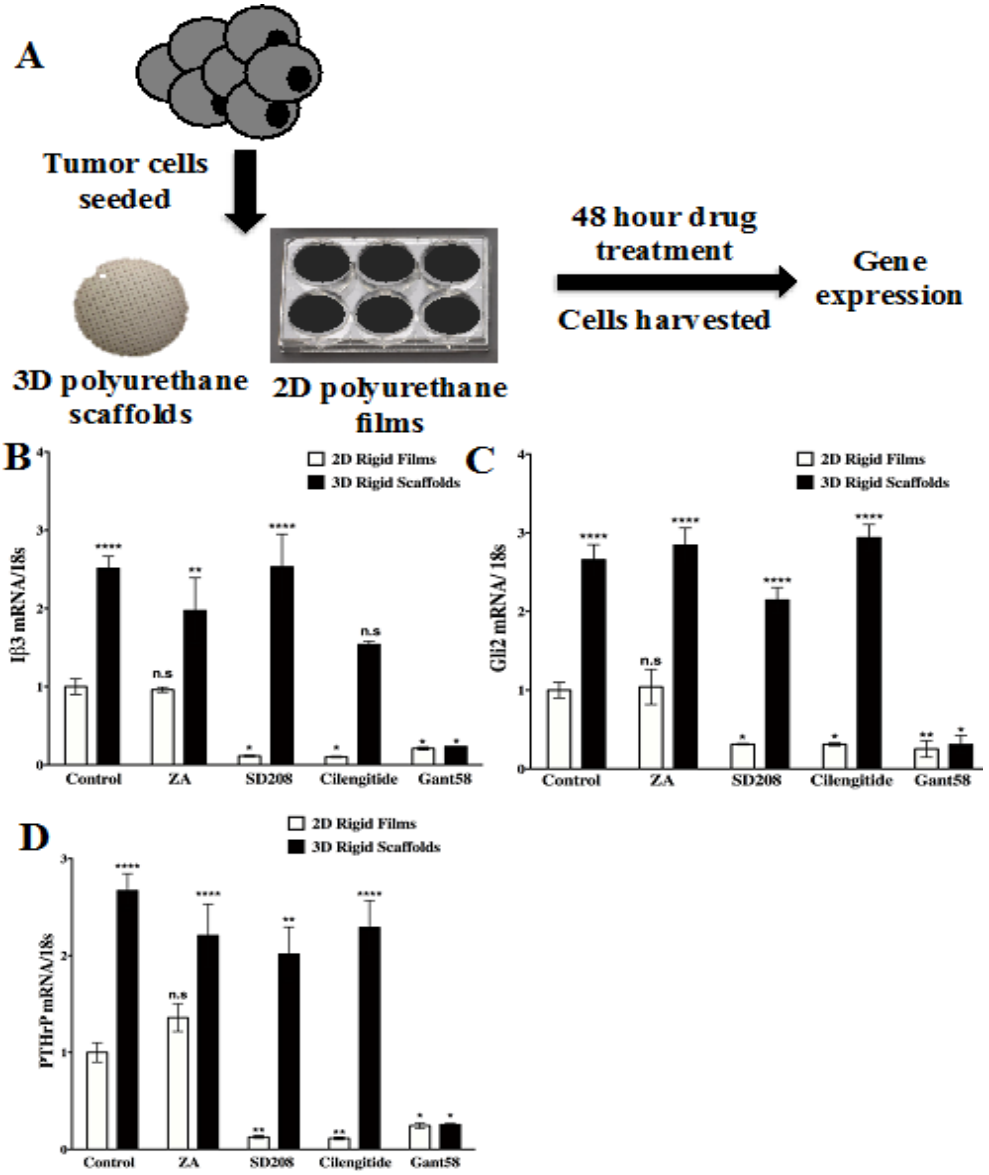

Figure 3.6 Drug treatment effects vary between 2D and 3D culture systems

(A) Schematic shows tumor cells are seeded on the 3D scaffolds or 2D films. The cells are then serum starved (12 hours) prior to a 48-hour drug treatment and harvested for gene expression. Treatment with zoledronic acid did not reduce gene expression in 2D or 3D (B-D) when compared to control 2D rigid film. (B) ITGβ3 (Iβ3), (C) Gli2 and (D) PTHrP expression is significantly reduced for SD-208, Cilengitide and Gant58 for 2D rigid films. Gant58 showed significant inhibition of (B) ITGβ3 (Iβ3), (C) Gli2 and (D) PTHrP in 3D rigid scaffolds when compared to 2D rigid films. (*p<0.05, **p<0.01, ***p<0.001, ****p<0.0001

Discussion

As cancer therapies have improved and patients are living longer with disease, bone metastatic disease continues to be a significant clinical problem, with many patients developing bone metastases years after diagnosis of primary disease [4,17,34]. While many of the interactions between cancer and bone are well known, the complexity and spatial heterogeneity of the bone microenvironment [19,23,35,36] has made it difficult to predict which tumors will colonize the bone and induce bone destruction. Trabecular bone comprises a complex mixture of rod- and plate-like trabeculae with an average spacing of 600 – 800 μm apart and substrate modulus 93 – 365 MPa, which is several orders of magnitude higher than that of soft tissue [16,17]. On rigid 2D films with substrate moduli approaching that of trabecular bone, TGF-β Receptor II (TGFβRII) physically associates with Integrin β3 sub-unit (ITGβ3), resulting in up-regulation of bone-metastatic genes and consequent bone resorption [16,17]. However, the cellular response in 3D culture is known to differ from that in 2D culture. 3D *in vitro* culture models of TIBD have recently been reported for metastatic breast cancer [15,37], Ewing sarcoma [14], and prostate cancer [8,38-40]. These studies used polymeric or collagen scaffolds to show that the 3D microenvironment substantially alters the tumor response to anti-cancer drugs compared to 2D mono-culture [8,39]. However, the ability of electrospun polymeric scaffolds and hydrogels to recapitulate the mechanical and topological properties of the bone microenvironment may be limited by their low substrate modulus and nanoscale pore size. In the present study, we investigated the effects of substrate modulus

and pore size on bone-metastatic gene expression by tumor cells *in vitro* and *in vivo*. 3D scaffolds with tunable substrate modulus (10 – 900 MPa) and pore size (423 – 557 μm) were fabricated using a templated-Fused Deposition Modeling (t-FDM) process. We found that expression of bone-metastatic genes by tumor cells increased with increasing substrate modulus, decreasing pore size, fluid flow, and in the presence of myeloid cells. Thus, 3D scaffolds that recapitulate the mechanical, topological, and cellular features of the bone microenvironment stimulate the transition to the bony-invasive phenotype, which underscores the need for new 3D systems for screening the efficacy of anti-tumor drugs.

Compared to 2D mono-culture, spheroid and gel systems more accurately mimic the effects of the 3D microenvironment on tumor cell fate [41] as cells spontaneously aggregate and create their own 3D matrix [14]. However, in TIBD, tumor cells establish in the trabecular bone [42], where they proliferate in the pores and line the surfaces of the trabeculae. Consequently, tissue-engineered 3D scaffolds have emerged as a promising technology for independently controlling the mechanical and topological properties of the 3D microenvironment [14]. Co-culture of prostate cancer cells with human osteoblasts on poly(ε-caprolactone) (PCL)-tricalcium phosphate (TCP) scaffolds exhibited up-regulation of matrix metalloproteinases (MMPs) and prostate specific antigen (PSA) compared to prostate cancer cells alone [43]. Similarly, Ewing osteosarcoma cells cultured in 3D electrospun PCL scaffolds showed higher expression and activation of insulin-like growth factor-1 receptor (IGF-1R), as well as higher expression of proteins associated with resistance to IGF-1R therapy, compared to 2D mono-culture [14].

In another study, prostate cancer cells cultured in 3D hydroxyapatite (HA)-collagen scaffolds exhibited reduced expression of MM1 and MMP9 compared to 2D culture[8]. Taken together, these studies highlight the substantial contribution of the 3D microenvironment to cell fate. However, the effects of substrate modulus and pore size were not systematically investigated.

In the present study, expression of the bone-metastatic genes Gli2 and PTHrP by tumor cells increased with the substrate modulus of the 3D scaffolds, which is consistent with our previous study using 2D substrates [17]. Our microarray (**Table 3.3.A**) and QPCR (**Table 3.3.B**) data reveal that relatively few genes related to the transition to the bone-destructive phenotype changed in response to substrate modulus. Interestingly, bone-metastatic gene expression also increased with decreasing pore size (**Figure 3.5.**). In a related study, we found that osteoblast differentiation of mesenchymal stem cells was enhanced as the pore size decreased from 557 to 423 μm [20]. Cells respond to radii of curvature larger than themselves, and the magnitude of the contractile forces and the rate of new bone formation have been suggested to increase with the degree of curvature of the surface [44,45], which in the t-FDM scaffolds utilized in this study decreases with decreasing pore size. Trabecular bone exhibits both rod- and plate-like structures, and thus the degree of curvature varies spatially within the bone[46]. Consequently, our findings suggest that tumor cells become more invasive as they migrate toward the cortical wall, where they are spatially constrained by small pores. Considering that inhibition of ITGβ3 using siRNA blocked bone resorption in a mouse tibia injection model [17], we assessed the efficacy of the ITGβ3

inhibitor Cilengitide in both the 3D and 2D tumor cell monoculture (**Fig 3.6**). While Cilengitide significantly reduced expression of ITGβ3, Gli2, and PTHrP in 2D culture, the drug did not significantly reduce bone-metastatic gene expression in 3D culture. Similar observations were made for the TGF-β Receptor I kinase inhibitor, SD-208. These findings are in agreement with several previous studies reporting that anti-tumor drugs are not as effective in the 3D bone microenvironment [8,14]. Another study utilizing oral squamous cell carcinoma (OSCC) cells cultured on 3D PLGA scaffolds reported that the PI3-kinase inhibitor LY294002 was cytotoxic to cells in 2D mono-culture but not 3D [3]. In contrast, the Gli2 inhibitor GANT58 significantly reduced bone-metastatic gene expression in both 2D and 3D mono-culture. Tumors cells established in the bone are influenced by the rigid microenvironment [17], and activate PTHrP via Gli2 downstream. GANT58, a Gli2 antagonist, is critical in inhibiting this pathway (**Figure 3.7**). Taken activate ITGβ3, which is thought to co-localize the TGFβRII receptor together, these findings suggest that downstream inhibitors of tumor-derived factors may be more effective at blocking tumor growth and bone destruction compared to upstream inhibitors that target microenvironmental factors. Testing compounds in tissue-engineered 3D cell culture models prior to pre-clinical testing may also find broad application as an effective approach for screening new drugs.

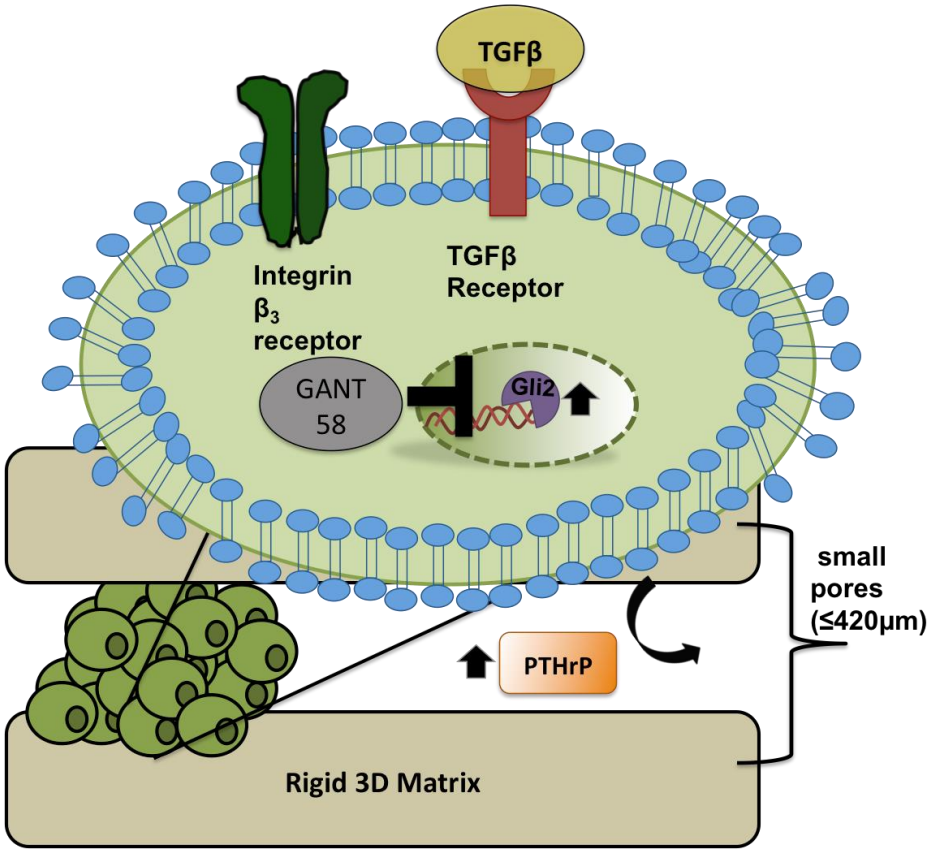

Figure 3.7 Tumor cell response to 3D scaffolds.

Schematic demonstrates tumor cells on 3D rigid scaffolds respond to physical microenvironment cues (increased mechanical rigidity and decreased pore size) to upregulate genes associated with tumor induced bone disease (Gli2 and PTHrP).

Conclusion

The substrate modulus of the surrounding tissue can dramatically effect tumor cell behavior and gene expression [16,17]. However, few studies have investigated how the mechanical and topological properties of the scaffold influence the progression of metastatic bone disease. In this study, the substrate modulus of the scaffold, pore size, and fluid flow were found to amplify the expression of genes associated with bone metastasis. Furthermore, the drug response of tumor cells in a 3D bone-like microenvironment differed remarkably from 2D mono-culture. Therefore, our model will potentially enable screening of new therapeutics in a dynamic *in vitro* system prior to pre- clinical testing and allow us to separate both the effects on the tumor cells and the microenvironment.

Acknowledgements

I thank my co-authors –Dr. Jonathan Page, Michael Kessler, Dr. Reyzer, Audra Judd, Dr. Caprioli, Dr. Sterling and Dr. Guelcher who are part of this study. We thank the VUMC Cell Imaging Shared Resource and Vanderbilt-Ingram Cancer Center. Funding sources for this publication are from the use of the VUMC Cell Imaging Shared Resource (supported by National Institutes of Health grants CA68485, DK20593, DK58404, DK59637, VICC, VA Career Development award (JS) and EY08126), Translation Pathology Shared Research Core (NCI/NIH Cancer Center Support Grant 2P30 CA068485-14), Schlumberger Faculty for the Future pre-doctoral program (UCD) and National Cancer Institute (part of the National Institutes of Health, under Award Number CA163499-01A1) (SG&JS)

References

[1] R.E. Coleman, Clinical Features of Metastatic Bone Disease and Risk of Skeletal Morbidity, Clinical Cancer Research. 12 (2006)

[2] J. Schrader, T.T. Gordon-Walker, R.L. Aucott, M. van Deemter, A. Quaas, S. Walsh, et al., Matrix stiffness modulates proliferation, chemotherapeutic response, and dormancy in hepatocellular carcinoma cells, Hepatology. 53 (2011) 1192–1205.

[3] C. Fischbach, R. Chen, T. Matsumoto, T. Schmelzle, J.S. Brugge, P.J. Polverini, et al., Engineering tumors with 3D scaffolds, Nat Meth. 4 (2007)

[4] V. Karageorgiou, D. Kaplan, Porosity of 3D biomaterial scaffolds and osteogenesis, Biomaterials. 26 (2005)

[5] M.E. Lynch, C. Fischbach, Biomechanical forces in the skeleton and their relevance to bone metastasis: biology and engineering considerations, Adv. Drug Deliv. Rev. 79-80 (2014)

[6] X.H.-F. Zhang, X. Jin, S. Malladi, Y. Zou, Y.H. Wen, E. Brogi, et al., Selection of bone metastasis seeds by mesenchymal signals in the primary tumor stroma, Cell. 154 (2013)

[7] S.P. Pathi, C. Kowalczewski, R. Tadipatri, C. Fischbach, A novel 3-D mineralized tumor model to study breast cancer bone metastasis, PLoS ONE. 5 (2010)

[8] K.A. Fitzgerald, J. Guo, E.G. Tierney, C.M. Curtin, M. Malhotra, R. Darcy, et al., The use of collagen-based scaffolds to simulate prostate cancer bone metastases with potential for evaluating delivery of nanoparticulate gene therapeutics. Biomaterials. 66 (2015)

[9] D.W. Infanger, M.E. Lynch, C. Fischbach, Engineered culture models for studies of tumor-microenvironment interactions, Annu. Rev. Biomed. Eng. 15 (2013)

[10] S.W.Z. Olechnowicz, C.M. Edwards, Contributions of the Host Microenvironment to Cancer-Induced Bone Disease, Cancer Res. 74 (2014)

[11] L. Yang, J. Huang, X. Ren, A.E. Gorska, A. Chytil, M. Aakre, et al., Abrogation of TGF beta signaling in mammary carcinomas recruits Gr-1+CD11b+ myeloid cells that promote metastasis, Cancer Cell. 13 (2008)

[12] J.A. Joyce, J.W. Pollard, Microenvironmental regulation of metastasis, Nat Rev Cancer. 9 (2008)

[13] T.K. Schuessler, X.Y. Chan, H.J. Chen, K. Ji, K.M. Park, A. Roshan-Ghias, et al., Biomimetic tissue-engineered systems for advancing cancer research: NCI Strategic Workshop report, Cancer Res. 74 (2014)

[14] E.L.S. Fong, S.-E. Lamhamedi-Cherradi, E. Burdett, V. Ramamoorthy, A.J. Lazar, F.K. Kasper, et al., Modeling Ewing sarcoma tumors in vitro with 3D scaffolds, Proc Natl Acad Sci U S A.

110 (2013)
[15] A.M. Mastro, E.A. Vogler, A Three-Dimensional Osteogenic Tissue Model for the Study of Metastatic Tumor Cell Interactions with Bone, Cancer Res. 69 (2009)
[16] N.S. Ruppender, A.R. Merkel, T.J. Martin, G.R. Mundy, J.A. Sterling, S.A. Guelcher, Matrix rigidity induces osteolytic gene expression of metastatic breast cancer cells, PLoS ONE. 5 (2010)
[17] J.M. Page, A.R. Merkel, N.S. Ruppender, R. Guo, U.C. Dadwal, S.A. Cannonier, et al., Matrix rigidity regulates the transition of tumor cells to a bone- destructive phenotype through integrin b3 and TGF-b receptor type II. Biomaterials. 64 (2015)
[18] A.A. Zadpoor, Bone tissue regeneration: the role of scaffold geometry, Biomater. Sci. 3 (2015)
[19] W.L. Grayson, S. Bhumiratana, C. Cannizzaro, P.H.G. Chao, D.P. Lennon, A.I. Caplan, et al., Effects of Initial Seeding Density and Fluid Perfusion Rate on Formation of Tissue-Engineered Bone, (2008).
[20] R. Guo, S. Lu, J.M. Page, A.R. Merkel, S. Basu, J.A. Sterling, et al., Fabrication of 3D Scaffolds with Precisely Controlled Substrate Modulus and Pore Size by Templated-Fused Deposition Modeling to Direct Osteogenic Differentiation, Advanced Healthcare Materials. (2015)
[21] S. Zustiak, R. Nossal, D.L. Sackett, Multiwell stiffness assay for the study of cell responsiveness to cytotoxic drugs, Biotechnol Bioeng. 111 (2013)
[22] J.S. Graham, A.N. Vomund, C.L. Phillips, M. Grandbois, Structural changes in human type I collagen fibrils investigated by force spectroscopy, Exp Cell Res. 299 (2004)
[23] T.A. Guise, Breast cancer bone metastases: it's all about the neighborhood, Cell. 154 (2013)
[24] S.P. Pathi, D.D.W. Lin, J.R. Dorvee, L.A. Estroff, C. Fischbach, Hydroxyapatite nanoparticle-containing scaffolds for the study of breast cancer bone metastasis, Biomaterials. 32 (2011)
[25] T.D. Palmer, W.J. Ashby, J.D. Lewis, A. Zijlstra, Targeting tumor cell motility to prevent metastasis, Adv. Drug Deliv. Rev. 63 (2011)
[26] R.Z. Carter, K.C. Micocci, A. Natoli, R.P. Redvers, S. Paquet-Fifield, A.C.B.M. Martin, et al., Tumour but not stromal expression of β3 integrin is essential, and is required early, for spontaneous dissemination of bone-metastatic breast cancer, J Pathol. (2014).
[27] P. Friedl, S. Alexander, Cancer Invasion and the Microenvironment: Plasticity and Reciprocity, Cell. 147 (2011)
[28] R.W. Johnson, M.P. Nguyen, S.S. Padalecki, B.G. Grubbs, A.R. Merkel, B.O. Oyajobi, et al., TGF- Promotion of Gli2-Induced Expression of Parathyroid Hormone-Related Protein, an Important Osteolytic Factor in Bone Metastasis, Is Independent of Canonical Hedgehog Signaling, Cancer Res. 71 (2011)
[29] J.P. Campbell, M.R. Karolak, Y. Ma, D.S. Perrien, S.K. Masood-

Campbell, N.L. Penner, et al., Stimulation of Host Bone Marrow Stromal Cells by Sympathetic Nerves Promotes Breast Cancer Bone Metastasis in Mice, PLoS Biol. 10 (2012)
[30] M.H. Zaman, L.M. Trapani, A.L. Sieminski, A. Siemeski, D. Mackellar, H. Gong, et al., Migration of tumor cells in 3D matrices is governed by matrix stiffness along with cell-matrix adhesion and proteolysis, Proc Natl Acad Sci U S A. 103 (2006)
[31] G. Gül, M.A.N. Sendur, S. Aksoy, A.R. Sever, K. Altundag, A comprehensive review of denosumab for bone metastasis in patients with solid tumors, Curr Med Res Opin. 32 (2016)
[32] R.E. Coleman, Bisphosphonates: Clinical Experience, The Oncologist. 9 (2004)
[33] J.A. Sterling, The Hedgehog Signaling Molecule Gli2 Induces Parathyroid Hormone-Related Peptide Expression and Osteolysis in Metastatic Human Breast Cancer Cells, Cancer Res. 66 (2006)
[34] F. Saad, A. Lipton, R. Cook, Y.-M. Chen, M. Smith, R. Coleman, Pathologic fractures correlate with reduced survival in patients with malignant bone disease, Cancer. 110 (2007)
[35] K.N. Weilbaecher, T.A. Guise, L.K. McCauley, Cancer to bone: a fatal attraction, Nat Rev Cancer. 11 (2011)
[36] J.A. Sterling, J.R. Edwards, T.J. Martin, G.R. Mundy, Advances in the biology of bone metastasis: How the skeleton affects tumor behavior, Bone. 48 (2011)
[37] J.E. Moreau, K. Anderson, J.R. Mauney, T. Nguyen, D.L. Kaplan, M. Rosenblatt, Tissue-engineered bone serves as a target for metastasis of human breast cancer in a mouse model, Cancer Res. 67 (2007)
[38] S.-Y. Sung, C.-L. Hsieh, A. Law, H.E. Zhau, Sen Pathak, A.S. Multani, et al., Coevolution of prostate cancer and bone stroma in three-dimensional coculture: implications for cancer growth and metastasis, Cancer Res. 68 (2008)
[39] S. Sieh, A.V. Taubenberger, M.L. Lehman, J.A. Clements, C.C. Nelson, D.W. Hutmacher, Paracrine interactions between LNCaP prostate cancer cells and bioengineered bone in 3D in vitro culture reflect molecular changes during bone metastasis, Bone. 63 (2014)
[40] S. Sieh, A.A. Lubik, J.A. Clements, C.C. Nelson, D.W. Hutmacher, Interactions between human osteoblasts and prostate cancer cells in a novel 3D in vitro model, Organogenesis. 6 (2009)
[41] H.-G. Kang, J.M. Jenabi, J. Zhang, N. Keshelava, H. Shimada, W.A. May, et al., E-cadherin cell-cell adhesion in ewing tumor cells mediates suppression of anoikis through activation of the ErbB4 tyrosine kinase, Cancer Res. 67 (2007)
[42] L.A. Kingsley, P.G.J. Fournier, J.M. Chirgwin, T.A. Guise, Molecular Biology of Bone Metastasis, Molecular Cancer Therapeutics. 6 (2007)
[43] E.R. Lawlor, C. Scheel, J. Irving, P.H.B. Sorensen, Anchorage-independent multi-cellular spheroids as an in vitro model of growth signaling in Ewing tumors, Oncogene. 21 (2002)

[44] M. Rumpler, A. Woesz, J.W.C. Dunlop, J.T. van Dongen, P. Fratzl, The effect of geometry on three-dimensional tissue growth, Journal of the Royal Society Interface. 5 (2008)

[45] J.A. Sanz-Herrera, P. Moreo, J.M. GarcIa-Aznar, M. DoblarE, On the effect of substrate curvature on cell mechanics, Biomaterials. 30 (2009)

[46] T. Hildebrand, P. Rüegsegger, Quantification of Bone Microarchitecture with the Structure Model Index, Comput Methods Biomech Biomed Engin. 1 (1997)

Chapter IV

3D Printed Scaffolds to Study *in vivo* Responses During Tumor Induced Bone Disease

Introduction

Breast cancer is the leading cause of cancer in women worldwide [1]. Patients suffer from devastating bone-related consequences, which include bone pain, spinal compression and instability and pathological fractures [2,3]. Once breast cancer related metastases are established in the bone, they are considered incurable [1,4]. The development of skeletal metastasis is based on tumor establishment in the bone, permitted by a "fertile soil" [1,4,5]. This "fertile soil" consists of a favorable physical microenvironment [6,7] rich in growth factors, chemokines, and cytokines synthesized by a multitude of cells in the bone and vascularized blood supply [8-10]. Osteoclast mediated bone destruction follows with dysregulation of the bone remodeling cycle and subsequent release of growth factors from the bone matrix that assist proliferation of the tumor cells [6,8].

Tumor cells that establish within the bone hijack the tightly regulated remodeling process. During breast cancer related bone metastasis, key mediators of the osteolytic pathway including parathyroid hormone-related protein (PTHrP), upregulate RANKL from osteoblasts and stromal cells. This results in down regulation of osteoprotegerin, and activation of osteoclasts. The resorption of the bone releases a rich supply of bone-derived factors such as Transforming Growth

Factor β (TGF-β) and Insulin Growth Factor (IGF) from the bone matrix. As a result, there is increased growth and proliferation of the tumor cell population. This in turn furthers the release of PTHrP, creating a "vicious cycle of bone metastases [11]". While an improved understanding of the pathophysiology of bone metastases using several experimental and animal models has ushered in new findings, experimental models that faithfully recapitulate the multiple stages of metastatic disease are still limited.

Primary tumors are known to modulate the host immune system by subverting immune cell populations to produce pro-tumorigenic factors that contribute to a poor prognosis [12,13]. Similarly, host bone marrow-derived cells have been implicated to work in concert with tumor cells in the primary and secondary site of metastasis [14-18]. Myeloid cells, defined by the expression of CD11b+ receptor, and macrophages, defined by the expression of F4/80+ receptor, are important contributors to tumor expansion, especially in the context of tumor in the bone [17,19-22]. It has also been postulated that tumor cells can supersede the immune cells in a tissue-specific manner to produce pro-tumorgenic factors. However, the factors mediating establishment of tumor cells in bone as they progress from the pre-osteolytic to the osteolytic phase remains an unanswered question [8,23-25].

In this study our primary goal was to address the discrepancies between 2D *in vitro* cell models and *in vivo* systems being used to study TIBD. We used novel 3D polyurethane scaffolds fabricated using template Fused Deposition Modeling (t-FDM) with tunable mechanical properties to investigate the effects of immune

cells on the expression of bone metastatic factors by tumor cells. Scaffolds were seeded with tumor cells and implanted subcutaneously in mice. Tumor cells expression of bone metastatic genes was assessed by quantitative real-time PCR (qPCR) and immune cell infiltration was determined by immunohistochemical (IHC) stainin. Matrix assisted Laser Desorption (MALDI) was used to resolve extracellular matrix deposition on the scaffolds to identify specific protein spectra from infiltrating cells. The results presented here demonstrate tumor cell gene expression is modulated by several factors – rigidity, pore size, and interaction with immune cells.

Materials and Methods

Materials

Hexamethylene diisocyanate trimer (HDIt) was supplied by Bayer Materials Scientific (Pittsburgh, PA). Stannous octoate, glycerol, poly(ε-caprolactone) triol (300 Da), and ε-caprolactone were purchased from Aldrich (St. Louis, MO). Glycolide was purchased from Polysciences (Warrington, PA). Glycerol was dried at 10 mm Hg for overnight at 80°C and ε-caprolactone was dried over anhydrous magnesium sulfate prior to use. All other materials were used as received. Two-component cast poly(ester urethane)s were mixed using a Hauschild SpeedMixer^{TM} DAC 150 FVZ-K (FlackTek Inc., Landrum, SC). Fibronectin (Fn) was purchased from Life Technologies (Grand Island, NY). Dulbecco's modification of Eagle's medium (DMEM) was purchased from

Invitrogen (Carlsbad, CA). Fetal bovine serum (FBS) was purchased from Hyclone Laboratories (Logan, UT). Penicillin, streptomycin, L-glutamine, trypsin, sodium pyruvate, essential and, non-essential amino acids were all acquired from Mediatech (Manassas, VA). MDA-MB-231 cells were purchased from ATCC (Manassas, VA). MDA-MB-231 cells were then selected for ability to metastasize to bone[26,27]. The RNeasy™ mini kit and RNAeasy Minielute™ clean up kit was purchased from Again (Valencia, CA). qScript cDNA synthesis kits were purchased from Quanta Biosciences (Atlanta, GA). qPCR primers for PTHrP, Gli2, Integrin β_3 (ITGβ3) and 18S (TaqMan) were obtained from Applied Biosciences (Carlsbad, CA).

Fabrication of 3D scaffolds by templated-Fused Deposition Modeling (t-FDM)

A polylactic acid (PLA) template (14 mm diameter) was designed with a defined 100% connected porous architecture using Solidworks® software and printed using a MakerBot Replicator® 2 Fused Deposition Modeling (FDM) printer. The reactive liquid PUR was poured into the PLA templates and cured at 60°C overnight. The PLA template was leached with dichloromethane (DCM) and washed with a mixture of acetone:dichloromethane to yield scaffolds with interconnected pores having a channel diameter of 423 ± 34 or 557 ± 44 μm for nominal 300 or 500 μm templates, respectively [24,25,28]. Scaffolds were sterilized under UV light for 15 minutes in 70% ethanol and incubated in a solution of 4μg mL^{-1} fibronectin overnight at 4°. The substrate modulus (E_s) of the scaffolds was controlled by the molecular weight (M_w) of the polyester triol (3000 g mol^{-1} or 300 g mol^{-1}) to attain values representative of collagen (5 MPa, Compliant (C)),

trabecular bone (266 MPa, Rigid (R)), or cortical bone (871–11,500 MPa) [15,24,25,27,29].

In vivo studies

All animal protocols were approved by the Vanderbilt University Institutional Animal Care and Use Committee (IACUC) and were conducted according to NIH guidelines. For mammary fat pad transplants, female 4-week-old athymic nude mice were anesthetized by continuous isoflurane and an incision made on the ventral lower abdomen. The left inguinal mammary gland between the fourth and fifth mammary fat pad was transplanted with MDA-MB-231 GFP cell-seeded scaffolds (**Table 4.1**).

Treatment Group	Nomenclature	PCR	IHC	MALDI
3D 500µm, compliant	560C	5	3	3
3D 300µm, compliant	420C	5	3	3
3D 300µm, rigid	560R	5	3	3
3D 500µm, rigid	420R	5	3	3

Table 4.1 *In vivo* study design
Athymic female mice aged 3-4 weeks were subcutaneously implanted with tumor seeded 3D scaffolds and harvested in 3.5 weeks. Animals were distributed to determine gene expression (qPCR, n=5), immunohistochemistry (IHC, n=5) and used to determine protein signal using Mass spectometery matrix assisted laser desorption/isorption (MS-MALDI, n=3) during *in vivo* study.

Mice were anesthetized using a 2%/98% isoflurane/oxygen and placed in the MAESTRO™ (CRi, Woburn, MA) imaging unit for weekly imaging. The collected images were spectrally unmixed to remove background fluorescence. Mice were sacrificed 3.5 weeks' post-tumor cell inoculation and the tumors excised and processed for gene expression and histology. Several animals were left intact for whole-body molecular imaging by matrix-assisted laser desorption/ionization imaging mass spectrometry (MALDI MS).

Gene expression assays

Total RNA from tumor cells was isolated using the RNeasy kits (Qiagen). Reverse transcription of the RNA template will be completed using the qScript cDNA synthesis kit (Quanta Biosciences) following DNAse I treatment. Quantitative real-time PCR (q-PCR) was performed in triplicate and normalized to 18S as per manufacturer's instructions. Gene expression was quantified using validated Taqman probes/primers as previously described [15,24,25,27,30,31].

Histology, histomorphometry, and immunohistochemistry

Specimens from the *in vivo* studies were dehydrated and embedded in paraffin. 4µm sections (cut using a Leica RM2255) were de-paraffinized in xylenes and stained with Hematoxylin and Eosin or CD11b, F4/80, Ly6G, Ki67/Casp3 for IHC [32]. All quantitative analysis was performed using Metamorph Analysis (Meta Imaging) or ImageJ software.

Matrix Assisted Laser Desorption/Ionization (MALDI) Imaging Mass Spectrometry

Female athymic mice were sacrificed and flash-frozen whole using liquid nitrogen, then stored at -80°C until analysis. The frozen tissue was sectioned into 12 µm thick sections on a Leica CM1900 cryostat (Leica Microsystems, Richmond, IL) in the cranial–caudal direction. Sections were thaw-mounted onto either gold-coated stainless steel MALDI target plates for imaging mass spectrometry experiments or onto glass microscope slides for staining with hematoxylin and eosin (H&E). Tissues to be imaged were washed with a series of ethanol and Carnoy's fluid solutions and dried under vacuum for 10 minutes. Matrix (2,6-dihydroxyacetophenone) was applied using a TM sprayer. Samples were analyzed on a TOF MS (Autoflex Speed, Bruker Daltonics, USA) with a 150µm raster. Images were visualized with flexImaging software (Bruker Daltonics, USA).

Protein identification

Additional sections were prepared for protein identification via hydrogel extraction [33]. Two 3 mm diameter trypsin-loaded hydrogels were placed on regions of interest (one on the rigid scaffold region, and one on the compliant scaffold region). The samples were placed in a sealed hydration chamber containing 20 mM ammonium bicarbonate for 4 hours at 50°C. After 4 hours, the hydrogels were removed from the tissue sections and placed in separate Eppendorf tubes. Peptides were extracted from the hydrogels using a series of solvent washes: 50% acetonitrile containing 5% formic acid and 100 mM ammonium bicarbonate.

100% Acetonitrile was used on the final extraction step. The pooled extracts were dried down using a vacuum concentrator (SpeedVac, ThermoScientific, USA) and reconstituted in 20 µl of 0.1% formic acid. The samples were then injected into an LTQ linear ion trap mass spectrometer (ThermoScientific, USA) and analyzed in a data-dependent manner over a 90 min HPLC run. The collected spectra were searched against a database containing both mouse and human proteins using SEQUEST and then filtered and collated at the protein level-using Scaffold.

Statistical analysis

All studies were performed in triplicate with at least n=3 test substrates per replicate to ensure batch-to-batch reproducibility. ANOVA and the Bonferroni *post hoc* test were used for statistical analyses with significance set at $p<0.05$ unless otherwise stated. Cell culture data was tested for significance across time points, across materials, and interactions between time and materials with n=3 independent biological experiments.

Results

Substrate modulus and pore size mediate expression of bone-metastatic genes in vivo

In order to recapitulate bone-metastatic gene expression in a physiologically relevant context as observed *in vitro*; we transplanted tumor-seeded scaffolds in the sub cutaneous pockets of athymic mice (**Figure 4.1.A**). Tumor burden, as measured by *in vivo* fluorescence over a period of four weeks was independent of pore size (**Figure 4.1.B**). Expression of bone-metastatic genes increased with increasing substrate modulus and decreasing pore size (**Figure 4.1.C-E**). ITGβ3, Gli2, and PTHrP mRNA significantly increased 20-, 18-, and 35-fold on 420R compared to 560C scaffolds.

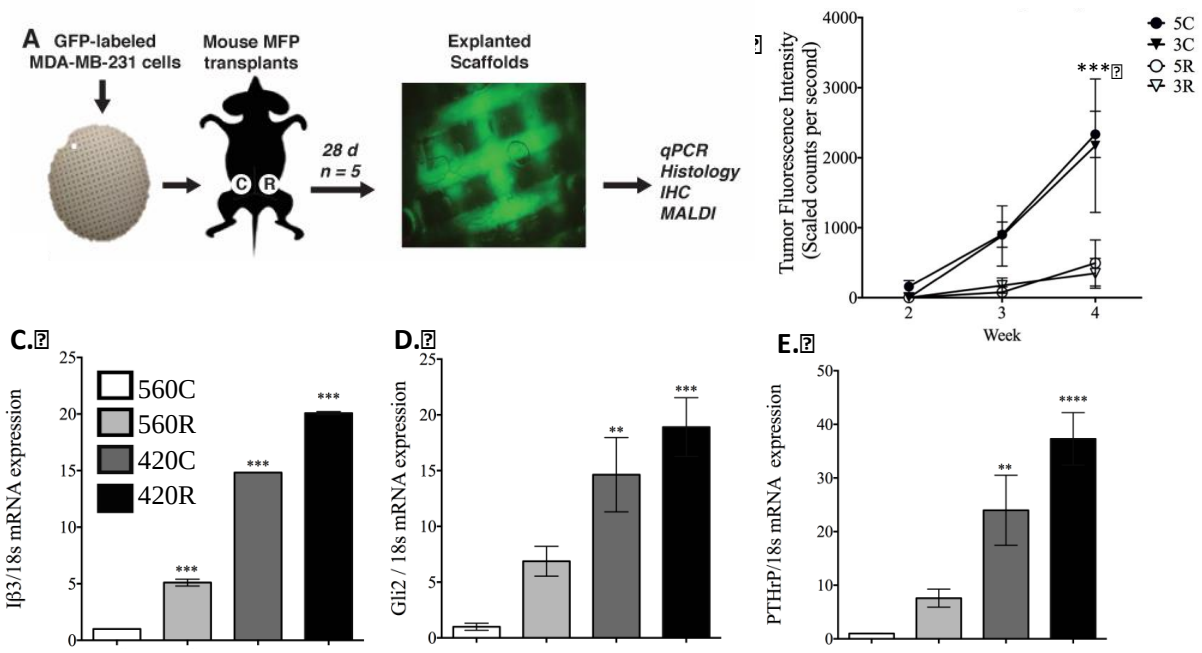

Figure 4.1 Effects of substrate modulus and pore size on bone metastatic gene expression in xenograft model

(A) Schematic of mouse xenograft transplant model. (B) Plot of tumor burden (as measured by the GFP signal, using Maestro imaging) versus time shows increased GFP expression in compliant scaffolds. Expression of (C) ITGβ3 (Iβ3), (D) Gli2, and (E) PTHrP measured by qPCR shows 20-fold, 18-fold and 35-fold upregulation on 420R respectively as compared to 560C. **p<0.01, ***p<0.001, ****p<0.0001

Substrate modulus influences extracellular matrix deposition on 3D scaffolds as visualized by MALDI MS

We further investigated the contributions of the tumor-host compartment by analyzing the extracellular matrix deposition using matrix-assisted laser desorption/ionization (MALDI) mass spectrometry (**Figure 4.2)**. An advantage of the 3D printed scaffolds is the ability to monitor these cellular and molecular interactions dynamically. Representative spectra obtained from individual pixels on the various scaffolds display show a unique peak of mass to charge ratio (10,167) for 420R compared to 420C scaffolds (**Figure 4.3.C)**. From the hydrogel digestions for each scaffold, we determined 183 proteins were present and observed an upregulation of structural proteins, such as collagen, myosin and actin actin (**Table 4.1)**. The S100 group of proteins, a group of calcium-binding proteins associated with chemoattraction of immune cells and poor patient prognosis [34,35], were also detected using MALDI (**Figure 4.2 & 4.3.C**) and protein database mining (**Table 4.1)**. The presence of this host-specific protein (mouse, s100a8) suggests the likelihood of rigidity and pore size promoting tumor mediated pro-tumorigenic activity by signaling host-immune cell infiltration.

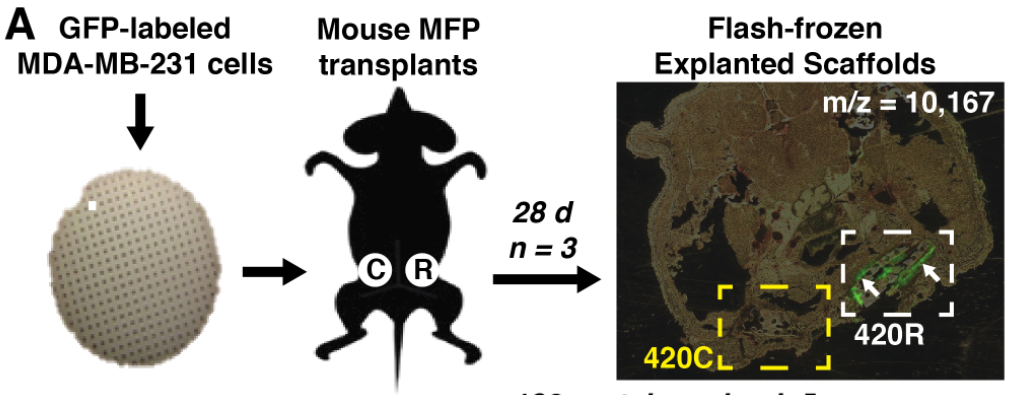

Figure 4.2 Rigidity and pore size demonstrate unique protein spectra as measured by MALDI analysis

(A) Schematic of mouse xenograft transplant model used for MALDI analysis. Tumor seeded 3D scaffolds were sub-cutaneously implanted in athymic mice. Mice were sacrificed after 4 weeks, flash frozen (-80°C) and whole mount cryosectioned. Samples were prepared and analyzed by MALDI-TOF.

Protein	Observed mass (Da)	Species
Myosin-3	223,910.5	Homo sapiens
S100a8	10,294.80	Mus musculus
Histone H1.5	22,581.5	Homo sapiens
Collagen alpha-1 (XII) chain	340,212.6	Mus musculus
Actin-related protein 2	44,761.7	Homo sapiens

Table 4.2 Proteins identified from protein database mining by MALDI-TOF present only in 3D rigid scaffolds

Tumor seeded 3D scaffolds were sub-cutaneously implanted in athymic mice. Mice were sacrificed after 4 weeks, flash frozen (-80°C) and whole mount cryosectioned. Samples were prepared and analyzed by MALDI-TOF. Protein data base mining was carried out using the Unit-prot database. Protein signals present on the 3D rigid scaffolds are reported.

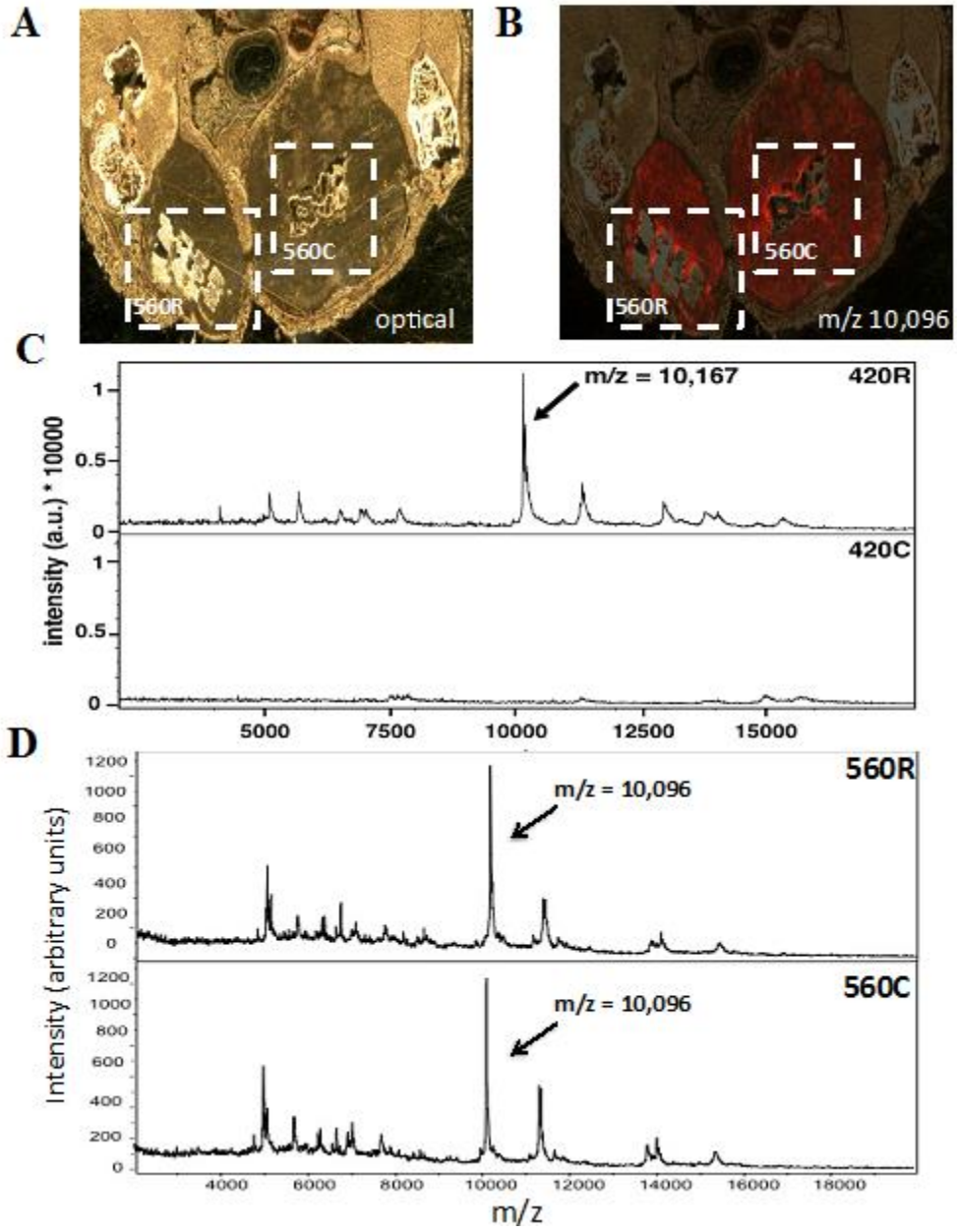

Figure 4.3 MALDI analyses for 560R and 560C t-FDM scaffolds

(A) Optical imaging of 560 t-FDM implanted whole mount crysectioned athymic mice. 560R (left) and 560C (right) (B) display no specific peak based on rigidity. Representative spectra obtained from individual pixels on the (c) 420 R and 420 C demonstrates a unique peak at 10, 167 on the 420 R t-FDM scaffolds. (D)560 R and 560 C scaffolds display show no unique peak of mass to charge ratio.

Substrate modulus influences immune cell infiltration

Previous studies have emphasized the contributions of the host microenvironment and immune response to tumor behavior during tumor establishment, proliferation, and growth [34,36,37]. We investigated whether the host immune cell populations created a pro-tumorigenic niche by infiltrating the scaffolds by examining CD11b+, F4/80+, and Ly6G+ cell populations that are known to be pro- tumorigenic [12,17,19-21,38]. We confirmed a significant ($p<0.01$) 6-fold increase in the population of CD11b+ (a myeloid cell marker) cells and a 10-fold increase in F4/80+ (a macrophage-specific marker) cells in 420R scaffolds compared to 560C scaffolds (**Figure 4.4.A-D**). Similar to the bone-metastatic gene expression data, the population of CD11b+ and F4/80+ cells increased with increasing substrate rigidity and decreasing pore size. We also detected the presence of Ly-6G+ positive population (Monocytes, Macrophages and Granulocytes marker) in all scaffolds (**Figure 4.5.A-D**). Infiltration of these immune cell types suggests the tumors cells are producing specific biomolecular signals to recruit these cells types.

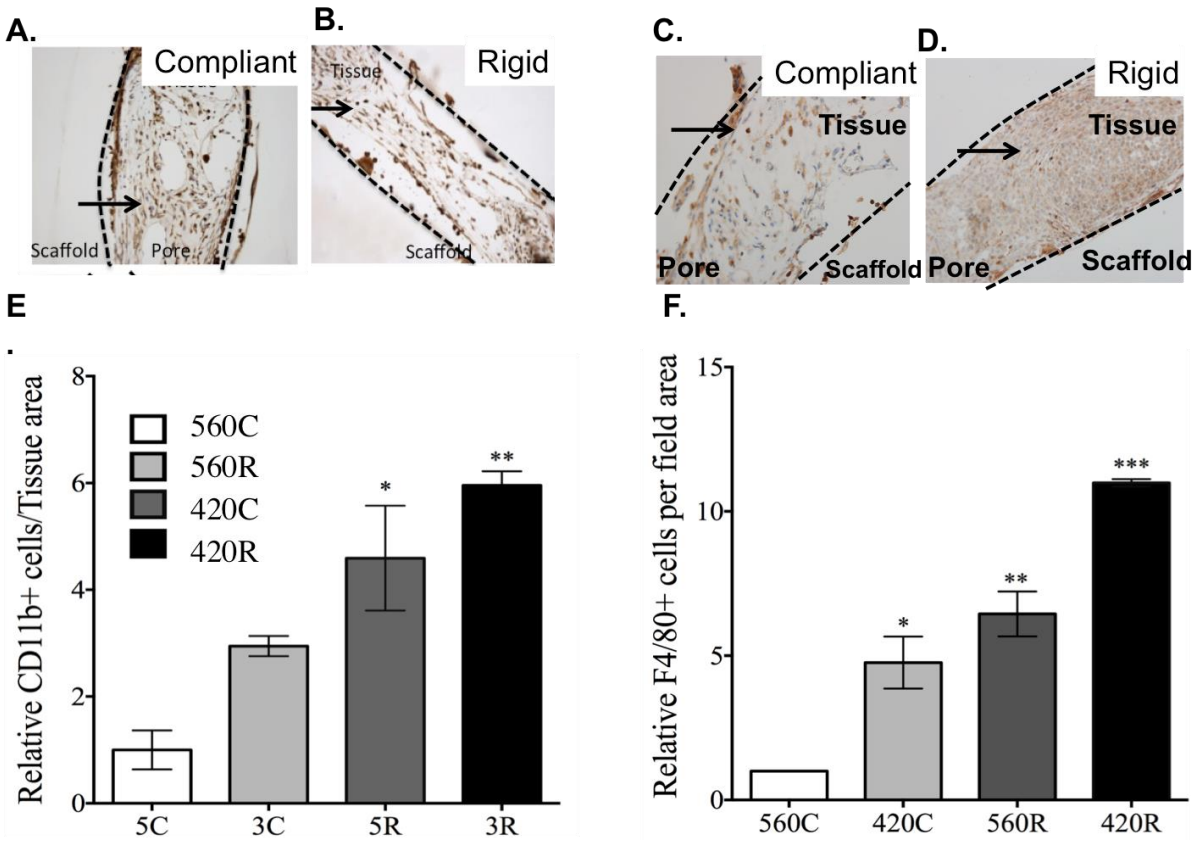

Figure 4.4 3D Scaffolds allow for infiltration of CD11b+ and F4/80+ immune cells
Representative immunohistochemistry images show scaffolds with pores outlined by dashed lines. Tissue infiltrated inside pores is shown by H&E staining. (A) Immunohistochemistry staining (20x) for CD11b+ cells (dark brown staining) in t-FDM scaffolds and (B) quantification of immunohistochemistry staining of CD11b+ cell populations in 560R (4-fold) and 420R (6-fold) shows significantly increased infiltration as compared to the 560C. (C) Immunohistochemistry staining (20x) for F4/80+ cells (dark brown staining) in t-FDM scaffolds and (D) quantification of immunohistochemistry staining. F4/80+ cell populations in 560R (7-fold) and 420R (10-fold) shows significantly increased infiltration as compared to the 560C. *$p<0.05$, **$p<0.01$, ***$p<0.001$

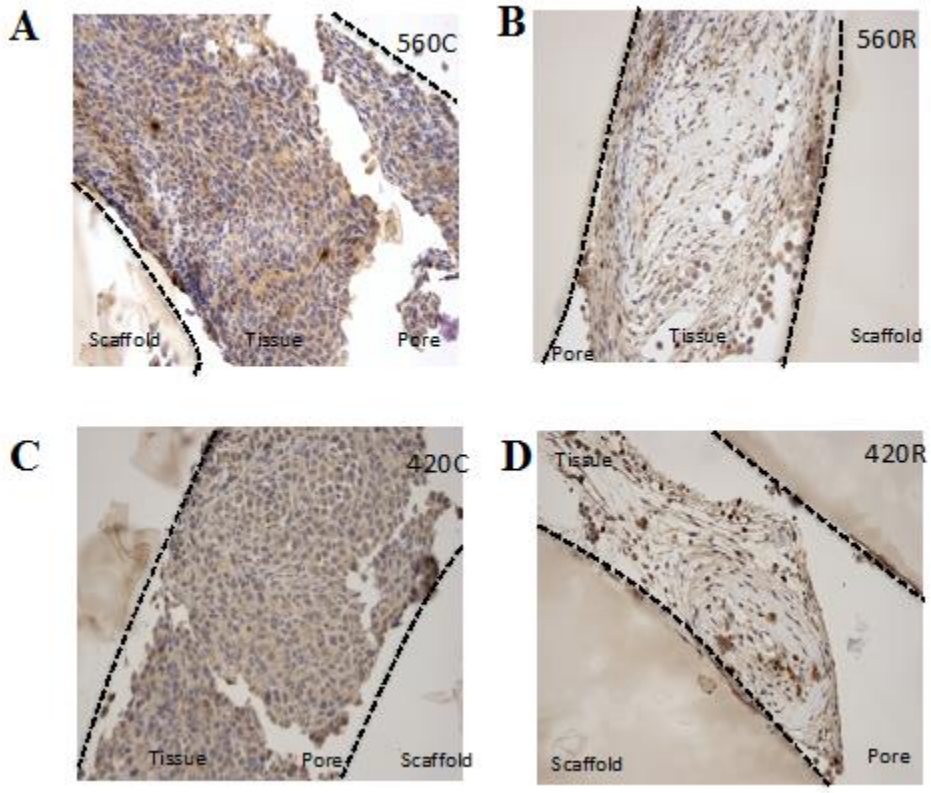

Figure 4.5 3D Scaffolds allow for infiltration of immune cells

Representative immunohistochemistry images (20X) show scaffolds with pores outlined by dashed lines. Tissue infiltrated inside pores is shown by H&E and Ly6G staining (Dark brown) in (A) 560C, (B) 560R, (C) 420C, and (D) 420R t-FDM scaffolds.

Discussion

Metastasis is a complex and dynamic multi-step process consisting of tumors cells that dislodge from the tumor site, attach to the basement membrane, secrete of proteolytic enzymes that disrupt the basement membrane, migrate through the basement membrane, mediate attachment through cell adhesion molecules such as laminin and E-cadherin to the basement membranes and to other cells, establish, and progress[39-44]. The bone provides a fertile soil[4,5] for the tumors cells, containing an endosteal and vascular niche. This leads to a highly vascularized bed of chemokines, cytokines and heterogenous cellular compartment that promote a pro-tumorgenic phenotype. While many of the interactions between cancer and bone are well known, the complexity and spatial heterogeneity of the bone microenvironment and its effects on the interaction of bone and tumor cells is still unknown[4,8,45].

In the present study, we investigated the effects of substrate modulus and pore size on bone-metastatic gene expression by tumor cells *in vivo.* 3D scaffolds with tunable substrate modulus (10 – 900 MPa) and pore size (423 – 557 μm) were fabricated using a templated-Fused Deposition Modeling (t-FDM) process. Interestingly, expression of the bone-metastatic genes Gli2 and PTHrP by tumor cells increased with the substrate modulus of the 3D scaffolds, which is consistent with our previous *in vitro* studies[27]. Interestingly, bone-metastatic gene expression also increased with decreasing pore size (**Fig. 4.1**). Consequently, our

findings suggest that tumor cells become more invasive as they migrate toward the cortical wall, where they are spatially constrained by small pores.

Bone marrow derived cells such as macrophages, monocytes, myeloid-derived suppressor cells, and osteoclasts among several other cell types are recruited to tumors and areas of hypoxia and neoangiogensis during different temporal stages of tumor progression. Consequentially, tumor progression in the bone has proved to be a challenging process to model *in vitro* and in mice. Tissue-engineered 3D scaffolds have emerged as a promising technology for independently controlling the mechanical and topological properties of the 3D microenvironment and observing dynamic process [46]. We observed in the present study a 6-fold increase in $CD11b^{+}$ cells and a 12-fold increase in F4/80+ cells in 420R compared to 560C scaffolds, which resulted in increased expression of bone-metastatic genes by tumor cells. Thus, the infiltrating immune cells created a tumor-supportive microenvironment that stimulates the transition of the tumor cells to the osteolytic phenotype.

The models currently in use are highly unstable, and selected cell lines are developed in different strains or species are inoculated into immunocompromised (or non-strain matched) animals, thus it is unclear how representative these models are of physiological bone metastases. Also, the effects of immune responses on all stages of the metastatic process are already difficult to evaluate. Future studies using 3D t-FDM scaffolds will shift to an immune-competent mouse model, which will allow us to use transgenic and knock-out models with specific pathways of interests altered in host immune-bone cell populations.

Conclusion

As previously discussed, substrate modulus can modulate bone metastatic gene expression[27,30]. Immune cell infiltration in the context of tumor is associated with a pro-tumorigenic phenotype and recruitment of cells to allow for an immune suppressive microenvironment[17,20,47]. In this study, the substrate modulus of the scaffold, pore size, and infiltration of immune cells were found to amplify the expression of genes associated with bone metastasis. This model will allow us to investigate cell specific effects induced by tumor cells and the microenvironment in a physiologically relevant model during TIBD.

Acknowledgements

I thank my co-authors –Dr. Jonathan Page, Michael Kessler, Dr. Reyzer, Audra Judd, Dr. Caprioli, Dr. Sterling and Dr. Guelcher who are part of this study. We thank the Translational Pathology Shared Research Core, VICC, and Mass Spectrometry Core. Funding sources for this publication are from the use of the Translation Pathology Shared Research Core (NCI/NIH Cancer Center Support Grant 2P30 CA068485-14), VA Career Development Award (JS) Schlumberger Faculty for the Future pre-doctoral program and National Cancer Institute (part of the National Institutes of Health, under Award Number CA163499-01A1)

References

[1] American Cancer Society, *Cancer Facts & Figures 2016*. 2015.

[2] Coleman RE. Skeletal complications of malignancy. Cancer 1997.

[3] Roodman GD. Mechanisms of Bone Metastasis. N Engl J Med 2004

[4] Weilbaecher KN, Guise TA, McCauley LK. Cancer to bone: a fatal attraction. Nat Rev Cancer 2011

[5] Paget S. The distribution of secondary growths in cancer of the breast. 1889. Cancer Metastasis Rev 1989

[6] Sterling JA, Guelcher SA. Bone Structural Components Regulating Sites of Tumor Metastasis. Curr Osteoporos Rep 2011

[7] Guelcher SA, Sterling JA. Contribution of Bone Tissue Modulus to Breast Cancer Metastasis to Bone. Cancer Microenvironment 2011

[8] Guise TA. Breast cancer bone metastases: it's all about the neighborhood. Cell 2013

[9] Kaplan RN, Rafii S, Lyden D. Preparing the "Soil": The Premetastatic Niche. Cancer Res 2006

[10] Kaplan RN, Psaila B, Lyden D. Niche-to-niche migration of bone-marrow-derived cells. Trends in Molecular Medicine 2007.

[11] Mundy GR. Mechanisms of bone metastasis. Cancer 1997.

[12] Roca H, McCauley LK. Inflammation and skeletal metastasis. Bonekey Rep 2015

[13] D'Amico L, Roato I. The Impact of Immune System in Regulating Bone Metastasis Formation by Osteotropic Tumors. J Immunol Res 2015

[14] Lutz S, Chow E. A review of recently published radiotherapy treatment guidelines for bone metastases: Contrasts or convergence? J Bone Oncol 2012

[15] Coleman RE. Clinical Features of Metastatic Bone Disease and Risk of Skeletal Morbidity. Clinical Cancer Research 2006

[16] Olechnowicz SWZ, Edwards CM. Contributions of the Host Microenvironment to Cancer-Induced Bone Disease. Cancer Res 2014

[17] Yang L, Huang J, Ren X, Gorska AE, Chytil A, Aakre M, et al. Abrogation of TGF beta signaling in mammary carcinomas recruits Gr-1+CD11b+ myeloid cells that promote metastasis. Cancer Cell 2008

[18] Joyce JA, Pollard JW. Microenvironmental regulation of metastasis. Nat Rev Cancer 2008

[19] Junankar S, Shay G, Jurczyluk J, Ali N, Down J, Pocock N, et al. Real-Time Intravital Imaging Establishes Tumor-Associated Macrophages as the Extraskeletal Target of Bisphosphonate Action in Cancer. Cancer Discovery 2015

[20] Danilin S, Merkel AR, Johnson JR, Johnson RW, Edwards JR, Sterling

JA. Myeloid-derived suppressor cells expand during breast cancer progression and promote tumor-induced bone destruction. Oncoimmunology 2012

[21] Azarin SM, Yi J, Gower RM, Aguado BA, Sullivan ME, Goodman AG, et al. In vivo capture and label-free detection of early metastatic cells. Nature Communications 2014

[22] Kaplan RN, Psaila B, Lyden D. Bone marrow cells in the "pre-metastatic niche": within bone and beyond. Cancer Metastasis Rev 2006

[23] Coleman RE. Bisphosphonates: Clinical Experience. The Oncologist 2004

[24] Schrader J, Gordon-Walker TT, Aucott RL, van Deemter M, Quaas A, Walsh S, et al. Matrix stiffness modulates proliferation, chemotherapeutic response, and dormancy in hepatocellular carcinoma cells. Hepatology 2011

[25] Fischbach C, Chen R, Matsumoto T, Schmelzle T, Brugge JS, Polverini PJ, et al. Engineering tumors with 3D scaffolds. Nat Meth 2007

[26] Prommer E. Palliative Oncology: Denosumab. Am J Hosp Palliat Care 2015

[27] Page JM, Merkel AR, Ruppender NS, Guo R, Dadwal UC, Cannonier SA, et al. Matrix rigidity regulates the transition of tumor cells to a bone- destructive phenotype through integrin b3 and TGF-b receptor type II. Biomaterials 2015

[28] Guo R, Lu S, Page JM, Merkel AR, Basu S, Sterling JA, et al. Fabrication of 3D Scaffolds with Precisely Controlled Substrate Modulus and Pore Size by Templated-Fused Deposition Modeling to Direct Osteogenic Differentiation. Advanced Healthcare Materials 2015

[29] Lynch ME, Fischbach C. Biomechanical forces in the skeleton and their relevance to bone metastasis: biology and engineering considerations. Adv Drug Deliv Rev 2014

[30] Ruppender NS, Merkel AR, Martin TJ, Mundy GR, Sterling JA, Guelcher SA. Matrix rigidity induces osteolytic gene expression of metastatic breast cancer cells. PLoS ONE 2010

[31] Zhang XH-F, Jin X, Malladi S, Zou Y, Wen YH, Brogi E, et al. Selection of bone metastasis seeds by mesenchymal signals in the primary tumor stroma. Cell 2013

[32] Johnson RW, Nguyen MP, Padalecki SS, Grubbs BG, Merkel AR, Oyajobi BO, et al. TGF- Promotion of Gli2-Induced Expression of Parathyroid Hormone-Related Protein, an Important Osteolytic Factor in Bone Metastasis, Is Independent of Canonical Hedgehog Signaling. Cancer Res 2011

[33] Harris GA, Nicklay JJ, Caprioli RM. Localized in Situ Hydrogel-Mediated Protein Digestion and Extraction Technique for on-Tissue Analysis. Anal Chem 2013

[34] Laetitia A Mauti. Myeloid-derived suppressor cells are implicated in regulating permissiveness for tumor metastasis during mouse gestation. The Journal of Clinical Investigation 2011.

[35] Seeley EH, Wilson KJ, Yankeelov TE, Johnson RW, Gore JC, Caprioli RM, et al. Co-registration of multi-modality imaging allows for comprehensive analysis of tumor-induced bone disease. Bone 2014

[36] Zaman MH, Trapani LM, Sieminski AL, Siemeski A, Mackellar D, Gong H, et al. Migration of tumor cells in 3D matrices is governed by matrix stiffness along with cell-matrix adhesion and proteolysis. Proc Natl Acad Sci U S A 2006

[37] Horimoto Y, Polanska UM, Takahashi Y, Orimo A. Emerging roles of the tumor-associated stroma in promoting tumor metastasis. Celladhesion 2014

[38] Sawant A, Deshane J, Jules J, Lee CM, Harris BA, Feng X, et al. Myeloid-derived suppressor cells function as novel osteoclast progenitors enhancing bone loss in breast cancer. Cancer Res 2013

[39] Psaila B, Lyden D. The metastatic niche: adapting the foreign soil. Nat Rev Cancer 2009

[40] Simos D, Addison C, Kuchuk I, Hutton B, Mazzarello S, Clemons M. Bone-Targeted Agents for the Management of Breast Cancer Patients with Bone Metastases. Jcm 2013

[41] Kennecke H, Yerushalmi R, Woods R, Cheang MCU, Voduc D, Speers CH, et al. Metastatic Behavior of Breast Cancer Subtypes. J Clin Oncol 2010

[42] Fontanella C, Fanotto V, Rihawi K, Aprile G, Puglisi F. Skeletal metastases from breast cancer: pathogenesis of bone tropism and treatment strategy. Clin Exp Metastasis 2015

[43] Ocaña OH, Córcoles R, Fabra Á, Moreno-Bueno G, Acloque H, Vega S, et al. Metastatic Colonization Requires the Repression of the Epithelial-MesenchymalTransition Inducer Prrx1. Cancer Cell 2012

[44] Voulgari AA, Pintzas AA. Epithelial–mesenchymal transition in cancer metastasis: Mechanisms, markers and strategies to overcome drug resistance in the clinic. Biochimica Et Biophysica Acta (BBA) - Reviews on Cancer 2009

[45] Sterling JA, Edwards JR, Martin TJ, Mundy GR. Advances in the biology of bone metastasis: How the skeleton affects tumor behavior. Bone 2011

[46] Fong ELS, Lamhamedi-Cherradi S-E, Burdett E, Ramamoorthy V, Lazar AJ, Kasper FK, et al. Modeling Ewing sarcoma tumors in vitro with 3D scaffolds. Proc Natl Acad Sci U S A 2013

[47] Gabrilovich DI, Nagaraj S. Myeloid-derived suppressor cells as regulators of the immune system. Nat Rev Immunol 2009

Chapter V

Simulating Tumor Induced Bone Disease using a Population Dynamic Model

Introduction

Breast cancer is the leading diagnosis in cancer among women in United States according to the American Cancer Society[1]. Bone is a frequent site of metastasis[2] and many cancer patients develop Tumor Induced Bone Disease (TIBD), often years after successful treatment for the primary disease. Once metastatic tumors establish in bone, patients develop increased fractures and bone pain associated with a reduction in mobility[2]. Despite the importance of bone metastatic disease, it is still not possible to predict which tumors will induce significant clinical complications and how these tumors will respond to therapeutics. Statistically, 2-4 skeletal-related events occur every 12 months[3,4], and can be reduced by only about 50% with the use of the most effective drugs currently available for managing the bone remodeling alone, namely – bisphosphonates (zoledronic acid (ZA)) and Denosamaub (RANKL inhibitor). To date, there are no therapeutics that target the cancer present in the bone.

Bone is a complex and dynamic model with a multitude of factors influencing establishment and progression of tumors – physical microarchitecture, the vasculature, and bone marrow cells. An integrated effort is required to further elucidate the molecular and biomechanical aspects affecting TIBD. Computational modeling provides sophisticated tools to analyze experimental as well as systemic

data to shed light on TIBD and allow single parameters to be investigated. Several mathematical models have been published detailing bone remodeling[5-13] as well as, prostate and multiple myeloma tumors metastasizing to the bone[14-16] . To the best of our knowledge there are no models that quantify the influence breast cancer related bone metastatic cells on bone remodeling to predict progression of TIBD.

We report a mathematical model of cell population dynamics based on ordinary differential equations (ODEs) developed from the Ayati, et al.[14] model and Komarova, et al.[5] model to describe spatiotemporal changes in bone remodeling based on autocrine and paracrine signaling between tumor cells, osteoblasts, and osteoclasts in the context of tumor-induced bone disease caused by breast cancer. Experimental data from a time course study using tumor cells intratibialy injected into athymic mice was analyzed using histopathology and micro CT (μCT) imaging to quantify the influence of tumor cells on bone remodeling. This data was then fit to the computational model to provide a robust *in silico* populations dynamic methodology to study TIBD. Advances in our knowledge of the molecular mechanisms underlying TIBD should provide therapeutic opportunities to improve overall survival rates. Moreover, integrating experimental findings with the power of computational modeling offers a unique opportunity to assess the impact of potential therapies on the progression of TIBD.

Materials and Methods

Animals

All animal protocols were approved by Vanderbilt University Institutional Animal Care and Use Committee and were conducted according to NIH guidelines. Female, 4- week-old athymic nude mice were anesthetized by continuous isoflurane and inoculated with 10,00 MDA MB 231 cells as previously described[17]. Mice were imaged weekly and were anesthetized using a 2%/98% isoflurane/oxygen and placed in the MAESTRO™ (CRi, Woburn, MA) imaging unit for weekly imaging. The collected images were spectrally unmixed to remove background fluorescence. Mice were sacrificed weekly post-tumor cell inoculation and the tumors excised, processed for μCT imaging and histology (**Table. 5.1**).

Day	Mice (n)	Treatment
7	5	Intratibial injections (PBS= Right hind limb; Tumor= Left hind limb)
14	5	Intratibial injections (PBS= Right hind limb; Tumor= Left hind limb)
21	9	Intratibial injections (PBS= Right hind limb; Tumor= Left hind limb)

Table 5.1. Description of *in vivo* experiments used to populate computational model

Microcomputed tomography (µCT)

Tibiae from each animal were dissected, cleaned, and fixed for 48 h in 10% formalin/PBS, transferred to 70% EtOH, then loaded into 12.3-mm-diameter scanning tubes, and imaged using the Scanco µCT 40 (Scanco Medical, Brüttisellen, Switzerland). A Gaussian filter (sigma=0.8, support=1) was used to reduce signal noise, and a threshold of 300 was applied to all analyzed scans. One hundred transverse slices from the proximal tibia (taken from the growth plate and extended distally) were scanned at an isotropic voxel size of 12-µm. Images were analyzed using the Scanco Medical Imaging software to determine the bone volume/total volume (BV/TV), trabecular number (Tb.N), thickness (Tb.Th), and connectivity density (ConnD).

Histology/histomorphometry

Hind-limb specimens (tibiae and femora) were removed during autopsy and fixed in 10% neutral-buffered formalin (Fisher Scientific) for 48 hours at 4°C. Bone specimens were decalcified in 10% EDTA for 4 days at room temperature and embedded in paraffin. Specimens from the *in vivo* studies were dehydrated and embedded in paraffin. 4µm sections (cut using a Leica RM2255) were de-paraffinized in xylenes and stained with hematoxylin & eosin (H&E)[18]. Malignant cells were characterized by a large nucleus, having an irregular size and shape, prominent nucleoli, and a scarce and pale cytoplasm. All quantitative analysis was performed using Fiji software[19].

Computational model

Key model parameters include co-efficient of cell recruitment (α_i), co-efficient of removal of each cell population (β_i), and net effective autocrine or paracrine signaling for cell pairs (g_{ij}). The model considers three tumor-bone cell interaction parameters: (1) osteoclast-tumor interactions resulting from release of TGF-β from the resorbing bone matrix, (2) tumor-osteoblast interactions resulting from secretion of PTHrP by tumor cells and (3) osteoclast-osteoblast interactions resulting from secretion of RANKL by osteoblast cells. Autocrine signaling represents the feedback from osteoclasts and osteoblasts to regulate their respective formation. Paracrine signaling represents the factors produced by osteoclasts that regulate osteoblast formation, and vice versa. Net effective autocrine or paracrine signaling for cell pairs (g_{ij}) have been reported for osteoclasts (C) and osteoblasts (B)[12]. The tumor (T) alters subsequent osteoblast-osteoclast (r_{ij}), which are represented by autocrine promotion of osteoclasts is increased (r_{11}), autocrine promotion of osteoblast regulation(r_{22}), paracrine promotion of osteoblasts is reduced(r_{12}), and paracrine inhibition of osteoclasts is reduced(r_{21}) in the context of tumor.

Normalized activity of bone formation (k_2) or resorption (k_1) was used as previously reported[5]. Another parameter required is z(t) for the bone mass is obtained in[5-9] by assuming bone mass is determined by the extent to which normalized values of osteoclasts and osteoblasts exceed nontrivial steady state levels. Experimentally, this data was collected after autopsy using μCT imaging of tumor laden bone weekly. This data was then normalized to percentage change in

bone resorption. Bone mass values were calculated by dividing by the early time point bone (Day 0), i.e with respect to the early time point bone. Total % change in bone mass (*z*) will be calculated from the model using these parameters and compared to the values measured in the mouse time-course study to test the predictive capability of the model. **Table 5.2 and 5.3** describes the above parameters mentioned the numerical values assigned to the parameters. All parameters reported are dimensionless. The equations from [14-16]are described -

$$\frac{d}{dt}C(t) = \alpha_1 C(t)^{g_{11}(1+r_{11}\frac{T(t)}{L_T})} B(t)^{g_{21}(1+r_{21}\frac{T(t)}{L_T})} - \beta_1 C(t) \quad (1)$$

$$\frac{d}{dt}B(t) = \alpha_2 C(t)^{\frac{g_{12}}{1+r_{12}\frac{T(t)}{L_T}}} B(t)^{g_{22}-r_{22}\frac{T(t)}{L_T})} - \beta_2 B(t) \quad (2)$$

$$\frac{d}{dt}z(t) = -k_1 max[0, C(t) - \bar{C}] + -k_2 max[0, B(t) - \bar{B}] \quad (3)$$

$$\frac{d}{dt}T(t) = \gamma_T T(t) \log\frac{L_T}{T(t)} \quad (4)$$

Model variables are as mentioned above and in **Table 5.2 & 3**. Briefly, density of osteoclasts C(t) and the density of osteoblasts B(t) at time t. The equations of the model **(Equations 1-4**) have initial conditions – $C(0) = C_O$, $B(0) = B_O$ and initial condition $z(0) = z_o$. The power law approximations in **(Equation 1**) and (**Equation 2**) are for the interactions of osteoblasts and osteoclast populations in the proliferation terms of the equations as previously described[14].

We model the influence of tumor growth on bone remodeling, and in particular how the tumor influences autocrine and paracrine signaling in the osteoclast and osteoblast cell populations (**Equation 4 & Figure. 5.1**).

Parameter	Description
C	Number of OC
B	Number of OB
T	Density of tumor (T) cells
L_T	Maximum tumor size
α_1	Specific reaction rate for OC growth
α_2	Specific reaction rate for OC growth
β_1	Specific reaction rate for OC death
β_2	Specific reaction rate for OB death
g_{11}	Net effectiveness of OC-OC autocrine signaling
g_{12}	Net effectiveness of OC-OB paracrine signaling
g_{21}	Net effectiveness of OB-OC paracrine signaling
g_{22}	Net effectiveness of OB-OB autocrine signaling
r_{11}	Tumor modification of osteoclast autocrine signaling
r_{21}	Tumor modification of osteoblast-osteoclast signaling
r_{12}	Tumor modification of osteoclast-osteoblast paracrine signaling
r_{22}	Tumor modification of osteoblast autocrine signaling
k_1	Bone loss co-efficient due to osteoclast resorption
k_2	Bone formation co-efficient due to osteoblast formation
z	Total bone mass

Table 5.2. Cell population dynamics model parameters are described.

Parameter	Value	Reference
α_1	3	Komarova, et al.
α_2	4	Komarova, et al.
β_1	0.2	Komarova, et al.
β_2	0.002	Komarova, et al.
g_{11}	0.5	Komarova, et al.
g_{12}	0.5	Komarova, et al.
g_{21}	0	Komarova, et al.
g_{22}	-0.5	Komarova, et al.
r_{11}	0.005	Ayati, et al.
r_{12}	0	Ayati, et al.
r_{22}	0.2	Ayati, et al.
r_{21}	-0.9	Fitting parameter
k_1	0.24	Komarova, et al.
k_2	0.0017	Komarova, et al.

Table 5.3. Values for parameters

We use the underlying model of bone remodeling in the absence of tumor presented in[5] and explored it further in[14,17]. This model is a dynamical system with zero explicit space dimensions that describes temporal changes as a dependent variable that records bone mass as a function of time. If we interpret the bone mass equation as one for localized trabecular mass (spongy bone found within the bone marrow) underneath a point on the surface of the bone, we obtain a representation of one spatial dimension. We then present a spatial model that suggests how we may incorporate additional spatial dimensions. Computations were conducted using MATLAB.

Statistical analyses

All statistical analyses were performed using InStat version 3.03 software (GraphPad Software, Inc.). Values are presented as mean SEM, and P values determined using unpaired t test, where *, $P < 0.05$; **, $P < 0.01$; ***, $P < 0.001$ unless otherwise stated.

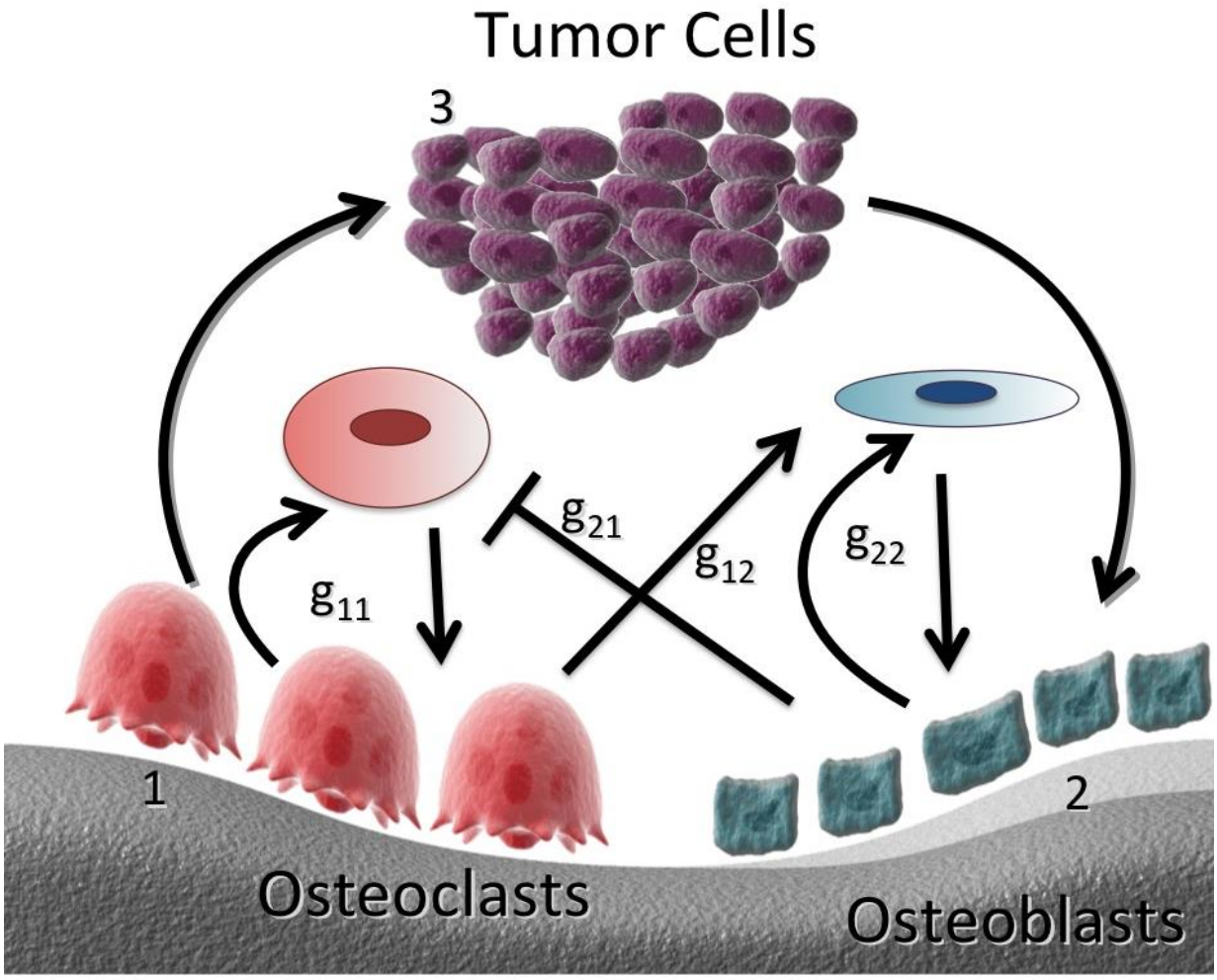

Figure 5.1. Schematic of features of the mathematical model

Schematic from showing the (1) osteoclasts (C), (2) osteoblasts (B), and (3) tumor cells (T) with during TIBD with its corresponding parameters[5] including g11 (osteoclast autocrine signaling), g12 (osteoclast stimulation of osteoblast production), g21 (osteoblast inhibition of osteoclast production), and g22 (osteoblast autocrine signaling). The tumor cells alter these interactions through modifications of the parameters – autocrine signaling of osteoclasts (r_{11}), osteoblast autocrine regulation (r_{22}), paracrine interactions of the osteoclasts on the osteoblasts (r_{12}), and osteoblast-osteoclast paracrine interactions (r_{21}). This model ignores the role of the structural as well as cellular components such as osteocytes and stromal cells in the breast cancer related bone metastasis.

Results

We developed our model to simulate the influences of tumor cells during breast cancer related bone metastasis on bone remodeling based on parameters reported in Komarova, et al.[5] and Ayati, et. al [14]. The model consists of a system of ordinary differential equations describing temporal effects of bone loss dependent on the bone cell populations in a Basic Multicellular Unit (BMU) in the context of tumor. These bone cell populations are the osteoclasts, which resorb bone, and osteoblasts, which form bone. The variables of the model are the density of osteoclasts C(t) and the density of osteoblasts B(t) at time t (**Table 5.2**).

During TIBD, tumor cells establish themselves in the bone, and stimulate osteoblast mediated activation of osteoclast via Receptor Activator of nuclear factor kapp-B ligand (RANKL)[20]. This results in a dysregulation in the remodeling of the bone and increased resorption. Growth factors such as Transforming growth factor β (TGF β) are subsequently released from the bone matrix and increase proliferation of tumors cells thus feeding into the same cycle of proliferation of tumor cells and bone destruction[20-22] (**Figure 5.1**).

Experimental data

We hypothesized that including an experimental component to the previously published mathematical models will allow us to develop stringent and robust simulation to study TIBD. As previously described, we used an intratibial model of tumor progression in athymic mice [17,18] to collect experimental data. Tumor cells present in the bone demonstrate prolific increase in number measured via histomorphometery (**Figure 5.2**). We also used μCT imaging to quantify bone

loss (BV/TV) over a course of 21 days. μCT data reveals significant bone loss over time as previously reported in literature[18,21,23,24] (**Figure 5.3**)

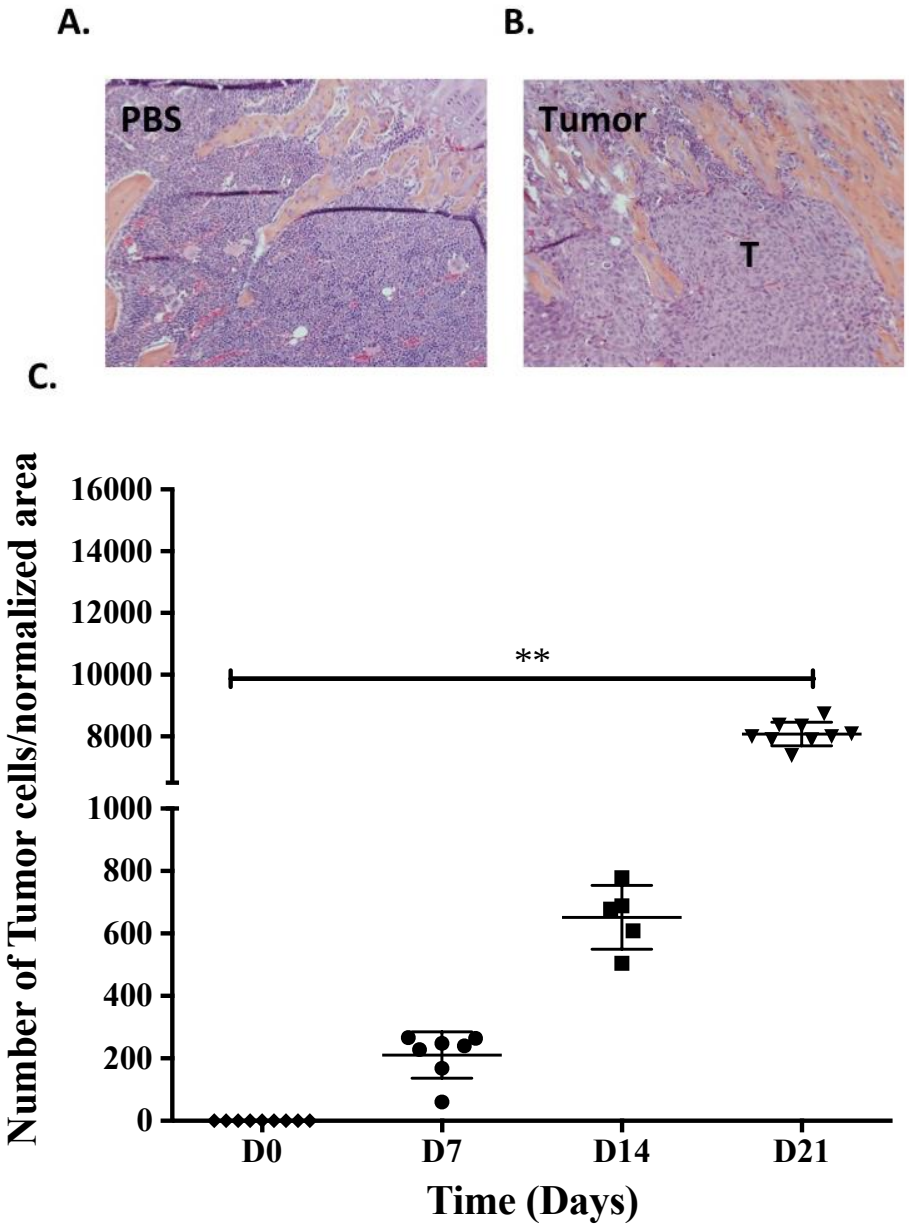

Figure 5.2. Histopathological assessment of tumor data.

Athymic mice were intratibialy injected with tumor cells (MDA MB 231 GFP) cells and sacrificed weekly. Histomorphometric analysis is shown here. (**A**) PBS (control) and (**B**) tumor laden tibial section is shown. H&E staining was used to (**C**) measure the number of tumor cells with respect to time in days. ***p<0.001

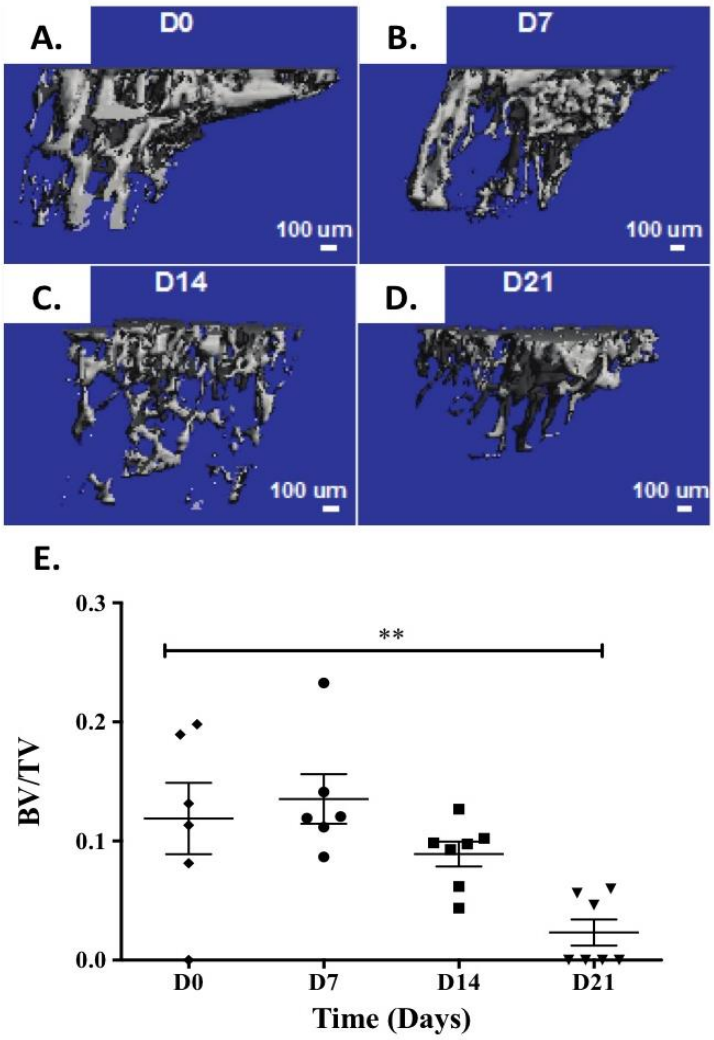

Figure 5.3: Progression of tumor-induced bone disease in a mouse model. (**A**) 3D reconstructions of the same section of the tibial plateau taken weekly for up to 21 days show progressive bone resorption. (**B**) BV/TV (measured by μCT) decreased with time.

Ayati model with tumor

The Ayati model discusses an ordinary differential equation model that replicates bone remodeling at a specific Bone Multicellular Unit (BMU) [25,26] during multiple myeloma related metastasis to the bone. The model consists of a system of ordinary differential equations describing the bone cell populations in a BMU and subsequent tumor influence on bone remodeling (**Equations 1-4**). The recruitment of these cell types to a location is interdependent. It is widely accepted that normal bone remodeling will exhibit regular periodicity of all model components[5,14]. During dysregulation of the bone remodeling cycle due to tumor cells we anticipate an initial oscillatory increase in osteoclasts and decrease in osteoblasts. As the tumor cell density increases, the entire bone remodeling system becomes damped and there should be an oscillatory decrease in both osteoclasts and osteoblast numbers, as well as bone mass. This is reported previously [14]. Interestingly, the Ayati model does not recapitulate our experimental data (data not shown). We subsequently reevaluated the Ayati model to better fit with experimental data.

Zero dimensional model with experimental data

In this section we report tumor parameters that effectively recapitulate experimental data (**Figure 5.4&5.5**). The value of the bone remodeling parameters and tumor interaction parameters are kept as previously reported[5,14] except for r_{21}.

Bone resorption is accelerated in TIBD and Osteoclast autocrine regulation effects bone remodeling during TIBD

Biologically, dysregulation of the bone remodeling cycle has been consistently shown to be characteristically osteoclast mediated[2,23,27,28] in TIBD. **Figure 5.4** reflects our simulation of TIBD with respect to tumor growth from experimental data. The parameters that are changed for this simulation were r_{21}, the interaction parameter that recapitulates paracrine inhibition of osteoclasts by osteoblasts as well as α_1 = 6 cells/day. Osteoclast cell production rate was determined to increase based on previous work [29]. **Figure 5.5** demonstrates that bone loss converges to 0.0 based on fitting parameter, r_{21} (r_{21}=-0.9). This realistic replication of biologically relevant data in an *in silico* model provides a robust method in studying specific parameters of TIBD.

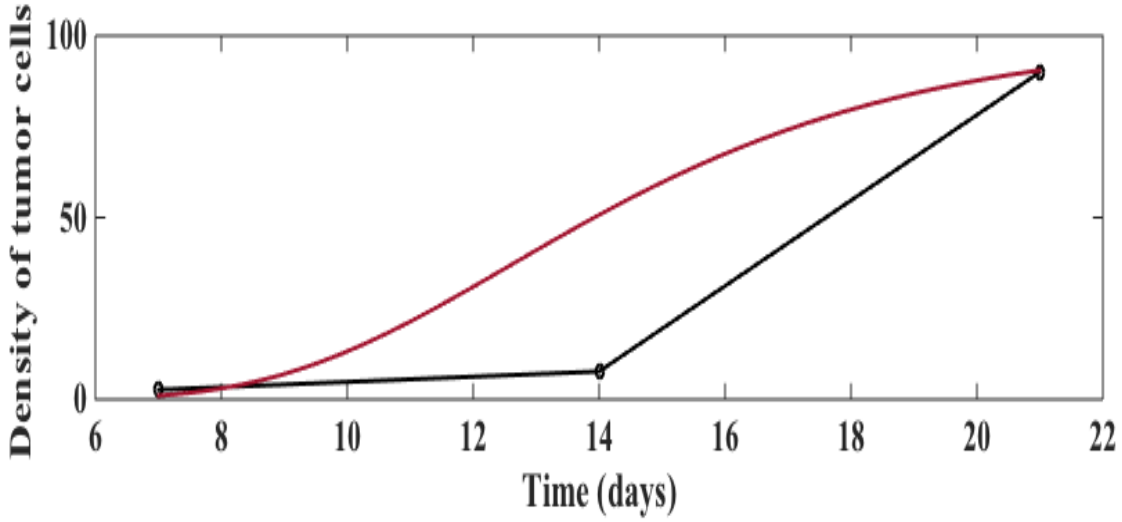

Figure 5.4. Experimental tumor data fits model

The bone mass (maroon line) converges to 0.0 along with experimental data (black line with circles). The parameters are given below. The solutions converge to the nontrivial steady state = 1.1586 and = 231.7238 with damped oscillations. The parameters are α_1 = 6.0, α_2 = 4.0, β_1 = 0.2, β_2 = .002, g_{11} = 1.1, g_{22} = 0.0, g_{12} = 1.0, g_{21} = -0.5, γ_T = .63, L_T = 100, r_{11} = .005, r_{21} = -0.9, r_{12} = 0.0, r_{22} = 0.2, k_1=0.24 and k_2=0.0017.3

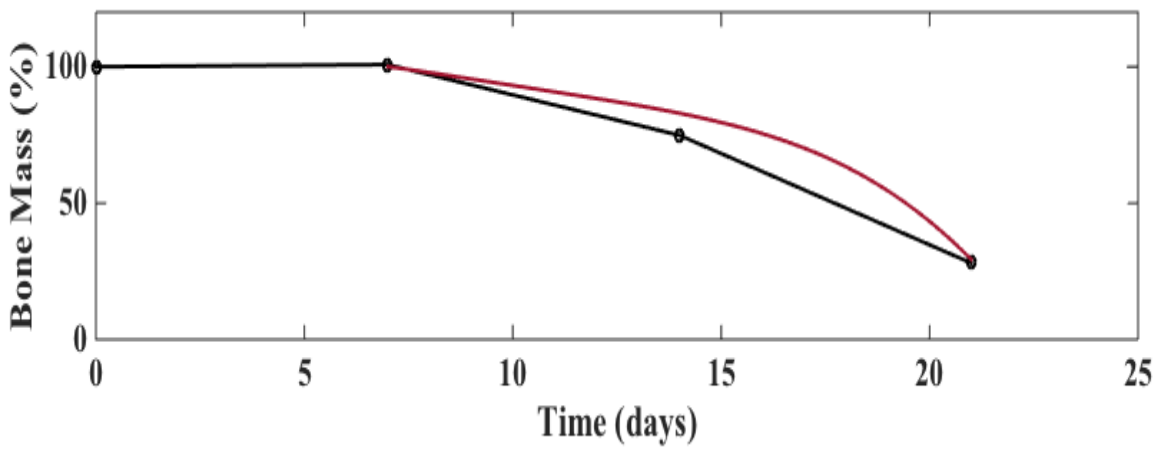

Figure 5.5. Experimental bone loss data fits model

The bone mass (maroon line) converges to maximum capacity along with experimental data (black line with circles) for a period of 21 days. The parameters are given below. The solutions converge to the nontrivial steady state = 1.1586 and = 231.7238 with damped oscillations. The parameters are $\alpha_1 = 6.0$, $\alpha_2 = 4.0$, $\beta_1 = 0.2$, $\beta_2 = .002$, $g_{11} = 1.1$, $g_{22} = 0.0$, $g_{12} = 1.0$, $g_{21} = -0.5$, $\gamma_T = .63$, $L_T = 100$, $r_{11} = .005$, $r_{21} = -0.9$, $r_{12} = 0.0$, $r_{22} = 0.2$, k_1=0.24 and k_2=0.0017.3

Discussion

As cancer therapies have improved and patients are living longer, bone metastatic disease continues to be a significant clinical problem, with many patients developing bone metastases years after diagnosis of primary disease[3,30]. Unfortunately, few successful treatments for tumor-induced bone disease are available, and none of the successful treatments cures tumor-induced bone disease. While many of the interactions between cancer and bone are well known, the complexity and heterogeneity of the bone microenvironment has made it difficult to predict which tumors will colonize the bone and induce bone destruction[31-33]. There are currently no *in vitro* experimental or *in silico* models to predict colonization or progression of breast cancer related tumor-induced bone disease. Mathematical models can better predict how interactions of tumor cells with the cellular component in the bone microenvironment drive disease progression.

In this paper we have shown the feasibility of using a population dynamics model to capture the interactions between the key players during osteolytic bone disease – osteoclasts, osteoblasts and tumor cells. We used a simplified model of the local "microenvironment" interactions that captures the bone remodeling cycle, and embedded it into Ordinary Differential equations that can predict tumor progression using bone loss as a readout. Interestingly, we note that our experimental data does not robustly fit the original Ayati model. Although the Ayati model is a dynamic model that simulates bone remodeling at the BMU, it has not been tested using experimental data. There are also few mechanistic differences between multiple myeloma metastasis to the bone and breast cancer related skeletal

metastasis[34]. In our system r_{21} does not equal 0, since the presence of tumor cells increases RANKL production in osteoblasts. This subsequently increases osteoclast differentiation, which in turn increases bone resorption [20,35] (**Figure 5.1**).

For our experimentally driven model, we subsequently fit an r_{21} value (-0.9) while keeping other parameters constant. r_{21} consolidates all paracrine signaling that is inhibitory to osteoclast. Importantly, the negative value for the tumor interaction parameter can be interpreted as stimulation of osteoclast production during TIBD. We show that changing r_{21} (paracrine regulation of osteoclasts) alone converges bone mass to zero. This suggests osteoclast related paracrine signaling is integral to skeletal metastasis, an integral aspect of breast cancer related metastasis[20,22]. Furthermore, myeloid cells are osteoclast precursors and several studies have demonstrated that myeloid cells are recruited to tumor sites in the bone[29,36,37]. This subsequently increases the rate of cell production activity for osteoclasts. This is a very exciting area of research with several groups stating that the myeloid cell populations contribute to bone destruction during TIBD[29,36,38]

The model is driven by system of ordinary differential equations for osteoclast-osteoblast interactions driven by autocrine-paracrine signaling they allow for interpretation of the corresponding spatial changes in bone mass and tumor growth. We show that in the case of breast cancer related skeletal metastasis; we can focus in on single parameters and study individual effects on tumor related bone resorption. Overall, in our experimentally driven model, bone remodeling is bone loss, and increased signaling in the osteoclasts. Importantly, these features are telling of breast cancer related metastasis to the bone[30,31,39]. This model

supported by our experimental data consistently demonstrates its ability to recapitulate skeletal metastasis due to tumors.

The model we have developed is spatially distinctive to a single BMU. Future work should consider adding palliative therapies to an *in vitro* model and feeding in parameters to the model to determine the effect of a drug, the optimal dose, treatment regimen or combination, and relative timing of the delivery of drug combinations. Since the model is sensitive to changes in bone mass, it would be interesting to see how TIBD would progress if introduced to a resorption inhibitor. Such insights into potential cellular mechanisms cannot easily be gained is an integral parameter from simulations. This finding is supported by overwhelming work in the field[23,36,37]. Ultimately, this model is being developed to understand the mechanism of TIBD and incorporate advances from the biological field to allow for a earlier and more effective treatment choice, which may help improve patient survival and improve patient quality of life.

Conclusions

We have shown an experimentally driven math model system that simulates bone loss based on interactions between osteoclasts, osteoblasts and tumor cells. The model demonstrates incredible robustness and recapitulates many characteristics of TIBD. We demonstrated the importance of paracrine osteoclast interactions and their subsequent effect on bone loss. The model is the first ever demonstration of an accurate representation of TIBD based on experimental data in breast cancer related TIBD. Since, *in vitro* models recapitulating TIBD are few and

far in between this model will be extremely useful in studying single parameters that interact during TIBD as well as the mechanism and disease progression of TIBD. This *in silico* technique will prove to be extremely useful in the context of therapeutic testing for efficacy, efficiency and effectiveness.

Acknowledgments

I thank my co-authors – Dr. Mathilde Granke, Alyssa Merkel, Dr. Jeon Junwahn, Dr. Jeffery Nyman, Dr. Peter Cummings, Dr. Julie Sterling, and Dr. Scott Guelcher. Funding sources for this work include VA Career Development Award (JS), Schlumberger Faculty for the Future pre-doctoral program, and National Cancer Institute (part of the national Institutes of Health, under the Award Number CA163499-01A1).

References

[1] American Cancer Society, *Cancer Facts & Figures 2016*. 2015

[2] Coleman RE. Clinical Features of Metastatic Bone Disease and Risk of Skeletal Morbidity. Clinical Cancer Research 2006.

[3] Coleman R, Body JJ, Aapro M, Hadji P, Herrstedt J. Bone health in cancer patients: ESMO Clinical Practice Guidelines. Ann Oncol 2014.

[4] Coleman RE, Rubens R. The clinical course of bone metastases from breast cancer. Br J Cancer 2007.

[5] Komarova SV, Smith RJ, Dixon SJ, Sims SM, Wahl LM. Mathematical model predicts a critical role for osteoclast autocrine regulation in the control of bone remodeling. Bone 2003.

[6] Buenzli PR, Pivonka P, Gardiner BS, Smith DW. Modelling the anabolic response of bone using a cell population model. Journal of Theoretical Biology 2012.

[7] Buenzli PR, Jeon J, Pivonka P, Smith DW, Cummings PT. Investigation of bone resorption within a cortical basic multicellular unit using a lattice-based computational model. Bone 2012.

[8] Jerez S, Chen B. Stability analysis of a Komarova type model for the interactions of osteoblast and osteoclast cells during bone remodeling. Math Biosci 2015.

[9] Colloca M, Blanchard R, Hellmich C, Ito K, van Rietbergen B. A multiscale analytical approach for bone remodeling simulations: linking scales from collagen to trabeculae. Bone 2014.

[10] Peinado H, Alečković M, Lavotshkin S, Matei I, Costa-Silva B, Moreno-Bueno G, et al. Melanoma exosomes educate bone marrow progenitor cells toward a pro-metastatic phenotype through MET. Nat Med 2012.

[11] Komarova SV, Safranek L, Gopalakrishnan J, Ou M-JY, McKee MD, Murshed M, et al. Mathematical model for bone mineralization. Front Cell Dev Biol 2015.

[12] Komarova SV. Bone remodeling in health and disease: lessons from mathematical modeling. Ann N Y Acad Sci 2006.

[13] Graham JM, Ayati BP, Ramakrishnan PS, Martin JA. Towards a new spatial representation of bone remodeling. Math Biosci Eng 2012.

[14] Ayati BP, Edwards CM, Webb GF, Wikswo JP. A mathematical model of bone remodeling dynamics for normal bone cell populations and myeloma bone disease. Biol Direct 2010.

[15] Araujo A, Cook LM, Lynch CC, Basanta D. An Integrated Computational Model of the Bone Microenvironment in Bone-Metastatic Prostate Cancer. Cancer Res 2014.

[16] Altrock PM, Liu LL, Michor F. The mathematics of cancer: integrating quantitative models. Nat Rev Cancer 2015.

[17] Campbell JP, Merkel AR, Masood-Campbell SK, Elefteriou F, Sterling JA. Models of bone metastasis. J Vis Exp 2012.

[18] Johnson RW, Nguyen MP, Padalecki SS, Grubbs BG, Merkel AR, Oyajobi BO, et al. TGF- Promotion of Gli2-Induced Expression of Parathyroid Hormone-

Related Protein, an Important Osteolytic Factor in Bone Metastasis, Is Independent of Canonical Hedgehog Signaling. Cancer Res 2011.
[19] Schindelin J, Arganda-Carreras I, Frise E, Kaynig V, Longair M, Pietzsch T, et al. Fiji: an open-source platform for biological-image analysis. Nat Meth 2012.
[20] Mundy GR. Mechanisms of bone metastasis. Cancer 1997.
[21] Sterling JA, Guelcher SA. Bone Structural Components Regulating Sites of Tumor Metastasis. Curr Osteoporos Rep 2011.
[22] Guise TA, Mundy GR. Cancer and bone. Endocr Rev 1998.
[23] Martin TJ, Mundy GR. Bone metastasis: can osteoclasts be excluded? Nature 2007.
[24] Johnson LC, Johnson RW, Munoz SA, Mundy GR, Peterson TE, Sterling JA. Longitudinal live animal micro-CT allows for quantitative analysis of tumor-induced bone destruction. Bone 2011.
[25] Frost HM. Intermediary organization of the skeleton. 1986.
[26] Frost HM. The skeletal intermediary organization. Metab Bone Dis Relat Res 1983.
[27] Guise TA, Yin JJ, Taylor SD, Kumagai Y, Dallas M, Boyce BF, et al. Evidence for a causal role of parathyroid hormone-related protein in the pathogenesis of human breast cancer-mediated osteolysis. J Clin Invest 1996.
[28] Kang Y, Siegel PM, Shu W, Drobnjak M, Kakonen SM, Cordón-Cardo C, et al. A multigenic program mediating breast cancer metastasis to bone. Cancer Cell 2003.
[29] Danilin S, Merkel AR, Johnson JR, Johnson RW, Edwards JR, Sterling JA. Myeloid-derived suppressor cells expand during breast cancer progression and promote tumor-induced bone destruction. Oncoimmunology 2012.
[30] Coleman RE, Smith P, Rubens RD. Clinical course and prognostic factors following bone recurrence from breast cancer. Br J Cancer 1997.
[31] Weilbaecher KN, Guise TA, McCauley LK. Cancer to bone: a fatal attraction. Nat Rev Cancer 2011.
[32] Guise TA. Breast cancer bone metastases: it's all about the neighborhood. Cell 2013.
[33] Sterling JA, Edwards JR, Martin TJ, Mundy GR. Advances in the biology of bone metastasis: How the skeleton affects tumor behavior. Bone 2011.
[34] Weidle UH, Birzele F, Kollmorgen G, Rüger R. Molecular Mechanisms of Bone Metastasis. Cancer Genomics Proteomics 2016.
[35] Suva LJ, Griffin RJ, Makhoul I. Mechanisms of bone metastases of breast cancer. Endocrine Related Cancer 2009.
[36] Roca H, McCauley LK. Inflammation and skeletal metastasis. Bonekey Rep 2015.
[37] Takayanagi H. Osteoimmunology: shared mechanisms and crosstalk between the immune and bone systems. Nat Rev Immunol 2007.
[38] Sawant A, Deshane J, Jules J, Lee CM, Harris BA, Feng X, et al. Myeloid-derived suppressor cells function as novel osteoclast progenitors enhancing bone loss in breast cancer. Cancer Res 2013.
[39] Coleman RE. Skeletal complications of malignancy. Cancer 1997.

Chapter VI

Conclusions and Future Work

Summary of Dissertation

This dissertation addresses the gap in studying the bone-tumor microenvironment in the context of tumor-induced bone disease (TIBD) and lack of model systems that replicate the disease. Cumulatively, this work demonstrates the development and characterization of two model systems to study specific cellular, molecular, and structural interactions taking place during bone metastatic disease. These novel systems provide an insight into the complex and dynamic processes of tumor-mediated osteolytic destruction of the bone and are a potential tool to decipher therapeutic efficiency, efficacy, and effectiveness.

First, a physical 3D model system is devised that can examine specific cell populations and their contributions to TIBD along with micro architectural variations. In **Chapter III**, the design and development of 3 dimensional t-FDM printed polyurethane scaffolds with tunable mechanical properties that have the potential to recapitulate the bone structural identity are discussed. Data demonstrate that tumor cells can be viably incorporated on the polyurethane scaffolds and prompt gene expression changes associated with metastatic disease. Additionally, the bone microenvironment is spatially heterogeneous, characterized by increasing trabecular separation (Tb.Sp., a morphometric parameter characterizing pore size)

encapsulated by the cortical bone. Since pathologic fractures result when tumors break through the cortical bone where Tb.Sp. is small [1,2], it is important to understand how Tb.Sp. regulates tumor cell gene expression. Results demonstrate gene expression of the seeded tumor cells is modulated by the mechanical properties (rigidity and pore size) of the scaffolds. Moreover, a perfusion bioreactor was added to overcome the limitations of static culture and recapitulate the *in vivo* bone microenvironment [1-5]. We also report significantly varied results in drug treatments administered between 2D and 3D *in vitro* cell culture systems. This work emphasizes the importance of developing *ex vivo* culture models that actively recapitulate the disease state, are capable of separating specific physical characteristics of the bone, cell types and molecular interactions to tease a detailed aspect of TIBD. This model overcomes limitations of previously reported work and may be an attractive potential to test therapeutics.

Then, in order to develop our model further and to understand the effects of polyurethane physical properties on tumor-cell interactions *in vivo*, we implanted tumor-seeded scaffolds, subcutaneously, in athymic mice. In **Chapter IV**, we describe gene expression of tumor cells *in vivo* that is induced by rigidity and pore size, thus recapitulating *in vitro* results. The bone contains a plethora of cells as well as chemokines and cytokines that influence the Vicious Cycle in a complex multistage dynamic process. The 3D t-FDM scaffolds offer the advantage of isolating definite microarchitect features of the bone, specific cell types, and growth factors to investigate a specific axis of the Vicious Cycle. Immune cells have been implicated in the process of developing a pro-tumorgenic environment. Tumor cells

are thought to produce chemokines and cytokines to encourage their recruitment[6,7]. We investigated the host cell response to tumor cells seeded on varying rigidities, i.e mimicking soft tissue (compliant) or bone (rigid) tumor microenvironments. MALDI analysis showed protein signatures of nearly 183 proteins, of which several host-immune cell associated proteins were upregulated on the rigid scaffolds. Specifically, S100 group of proteins were found on rigid scaffolds and are constitutively expressed by myeloid cells, including granulocytes, monocytes, osteoclasts and early-differentiation cells of the myeloid lineage [8-10]. Previous studies have demonstrated the importance of immune cells infiltration in the context of TIBD. Specifically, the myeloid cell lineage (CD11b+) and macrophages (F4/80) are thought to circumvent the immune system, increase angiogenesis, vasculature, and induce production of tumor-secreted and host-secreted growth factors, thereby facilitating tumor progression[11-14]. Results demonstrated CD11b+ and F4/80 cells are influenced by tumor cells seeded on increasing rigidity.

Second, in **Chapter V**, a theoretical population dynamics model was developed to capture the interactions between the key players during osteolytic bone disease – osteoclasts, osteoblasts, and tumor cells. We used a simplified model of the local "microenvironment" interactions that recapitulates the bone remodeling cycle, and embedded it into ordinary differential equations that can predict tumor progression using bone loss as a read-out. The ability to model faithfully the skeletal metastatic effects of breast cancer related bone disease provides an insight into the pathological relationship between breast cancer cells and the bone marrow

environment. Additionally, this theoretical model will improve understanding of this disease's morbidity as well as allow prediction of efficacy of therapeutic drugs.

Future Work

In conclusion, a multi-faced approach was utilized to study Tumor Induced Bone Disease. First, the design and development of polyurethane scaffolds with controllable physical and topographical properties was discussed as a robust model system to study genes associated with bone metastatic disease, shown to have *in vitro* and *in vivo* application, and used as a tool for potential drug screenings applicable to TIBD. Second, a theoretical model set to experimental parameters was used to simulate TIBD using a population dynamic mathematical model. Future directions pertinent to this dissertation work are discussed below -

Investigate host cell response to tumors on 3D tFDM scaffolds

Immune infiltration in 3D tFDM

In **Chapter IV**, immune infiltration of the host tissue was shown. It was also suggested that the tumor cells on a rigid substrate recruit specific cell types to increase tumorgenicity by producing a pro-tumorgenic environment. It is well documented that tumors crosstalk with the heamopoietic niche, bone cells and the immune system by hijacking signaling mechanisims [7]. Previous work from the Sterling lab among others has shown that during TIBD, there is an expansion of myeloid cells and macrophages [15,16]. RANKL, produced by tumor cells upon establishment [17] is a known regulator of Macrophages and T-cells [18,19].

Finally, memory T cells have been found in skeletal lesions of mBC and literature suggests that T cells can regulate tumor growth within the bone through the RANKL-RANK interaction between T cells and BC cells [20].

An animal study was carried out using athymic nude mice implanted with tumor seeded and blank scaffolds (control). These mice were monitored weekly and imaged using Maestro imaging. Mice (n=6) were sacrificed every week and explanted scaffolds were harvested for Florescence Activated Cell Sorting (FACS) (n=3) and histology (n=3). Tumors were visible after day 14, day 21 and 28 as well as vascularization. Host cell infiltration was present in each of the scaffolds via FACS on day 21 (**Figure 6.1**). The next step would be to determine whether the immune cells are indirectly being regulated based on the rigidity of the substrate the tumor cells are seeded on. Current 3D models have limitations that include the inability to isolate specific cell types and study interactions of these cell types with the tumor. The importance of developing an *ex vivo* model of TIBD is self-evident, however, if we can mimic essential components interacting with the tumor cells such as the immune compartment, the 3D model system could be used to fully examine the molecular mechanisms of TIBD.

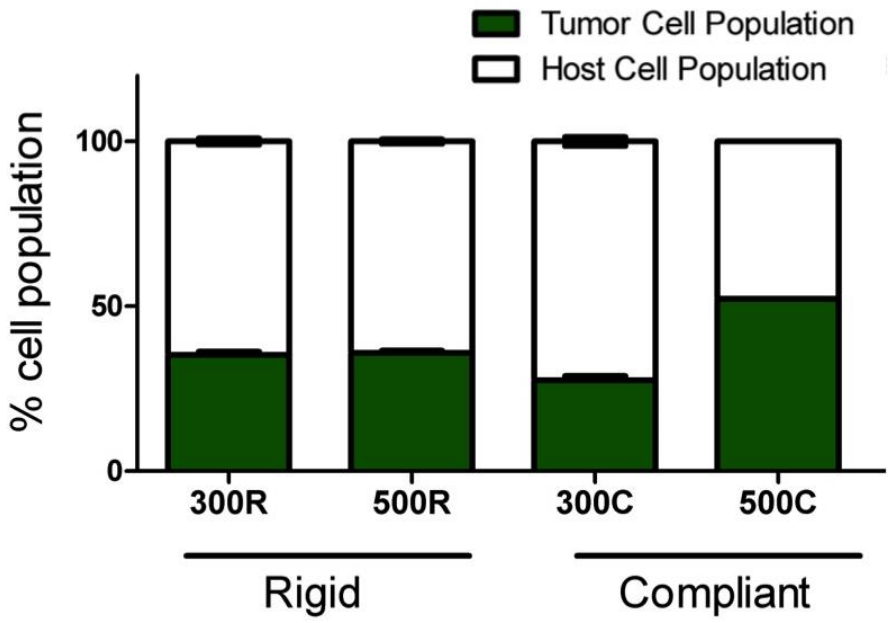

Figure 6.1 Host cell infiltration into 3D tFDM

MDA MB 231 GFP cells were seeded on 3D tFDM scaffolds and implanted in mice for 21 days. Explanted scaffolds were FACS processed and percentage of GFP positive per total population of cells in scaffold was determined using FloJo. Host cell infiltration is evident in all scaffolds

Drug response and targeting to the bone

Although there are several palliative therapies available for bone metastasis, it is still considered an incurable disease. Several reasons are responsible for this; however, an integral part is the lack of robust and reliable *in vitro* and *in silico* models available to replicate TIBD. This dissertation aims to bridge this gap. To further extrapolate on this work, therapeutics relevant to TIBD could be tested *in vitro* and *in silico*. **Chapter III** determined in a 3D environment it would be most effective to directly target the Gli2 and its PTHrP. **Figure 6.2** demonstrates two techniques used by the Sterling lab to inhibit Gli2. MDA MB 231 GFP cells were cultured on tissue culture plastic wells, serum starved and treated for 48 hours and cells were harvested to perform gene expression studies. siRNA targeting Gli2 (3 varying sequences) was used in **Figure 6.2.A** and 10μm GANT 58, is a small molecule Gli antagonist[21]was used in **Figure 6.2.B**. Separately, there are currently several natural compounds that are being used frequently in drug treatment studies[22]. These compounds are reported to inhibit Gli in the nucleus[22]. These compounds could be promising candidates for inhibiting TIBD. downstream activator,

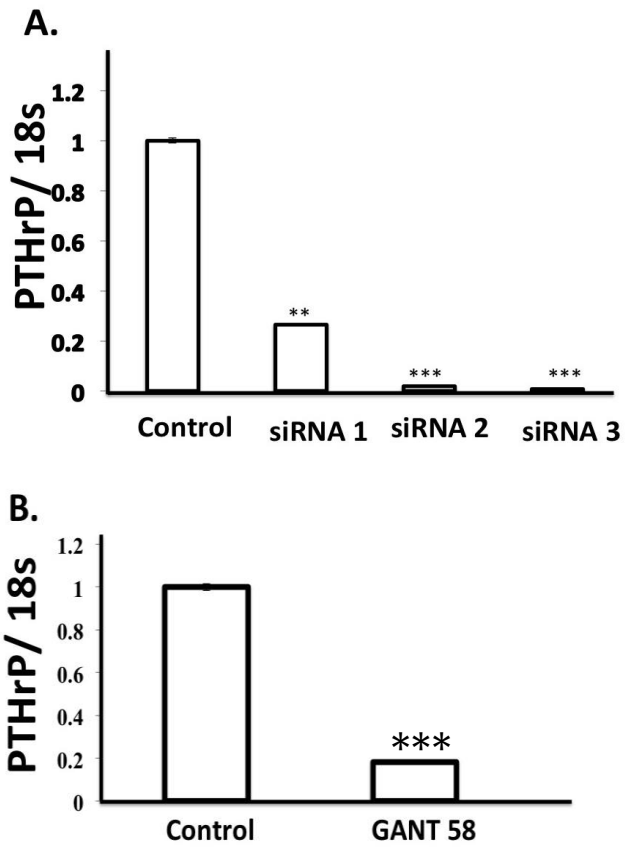

Figure 6.2 Drug response to Gli inhibitors in MDA MB 231 GFP cells. PTHrP expression from tumor cells treated with (A) Gli2 targeted siRNA and (B) GANT58 to inhibit Gli2 expression. Gene expression was quantified using qRT PCR.

Bone template scaffolds with mineral content

Although the 3D t-FDM scaffolds are mechanically tunable, precisely controlled and the scale of the designed fiber diameters are reported to enhance bone formation and vascularization[3,23], the defined microarchitecture of the scaffold is not reflective of cancellous bone[24-26]. Based on the structure of the bone, scaffold design would need to consist of gradient distribution of pore structure. Another limitation of the first generation scaffolds is its synthetic polyurethane composition and obvious lack of mineral content. This could allow incorporation of essential cell types in bones – osteoclasts and osteoblasts- to study a functional outcome during metastatic disease. Therefore, the next step for the translational application of the designed polyurethane scaffolds would be mimicking its natural state and characteristics.

A viable approach would be using SolidScale 3D ink-jet printer to fabricate scaffolds from templates printed from human bone[27]. Wax molds are printed from an μCT image of an inverted trabeculae (green) showing the distribution of Tb.Sp into which a reactive polyurethane (PUR) network with a tunable modulus[3,28,29] is casted, followed by extraction of the mold to yield a 3D scaffold (**Figure 6.3.A-D**). Relevant cell populations can be cultured on 3D scaffolds in a perfused bioreactor to investigate the effects of elastic modulus, trabecular separation (Tb.Sp.), and curvature on tumor progression in bone (**Figure 6.3.E**).

Study saptio-temporal dynamics of cancer progression in bone using Bone template scaffolds

When tumor cells establish in bone, they secrete factors (e.g., parathyroid hormone-related protein, PTHrP) that indirectly stimulate osteoclasts to resorb bone[30,31]. Secretion of PTHrP is anticipated to increase as tumor cells approach the bone cortex, resulting in pathologic fractures. Moreover, tumor cells can be seeded on osteoclast-resorbable 3D scaffolds (Nano hydroxyapatite polyurethane composite) cultured with bone cells to simulate bone resorption that occurs at the late stages of metastasis. Furthermore, the osteoblast and osteoclast precursor cell populations can be added to tune the model to *in vivo* measurements of cell populations, bone resorption, and tumor burden. These expression parameters can be measured in a dynamic fashion in the perfusion bioreactor. If successful, this validated 3D bioreactor model could be further modified to use patient-derived cells and serve as a platform for screening of new drug therapies. Future work could also include gathering specific interaction parameters between osteoclasts, osteoblasts and tumor cells and using them to form a robust computational model that is multi-dimensional. This would improve screening for drugs and allow a more refined approach to treat TIBD patients.

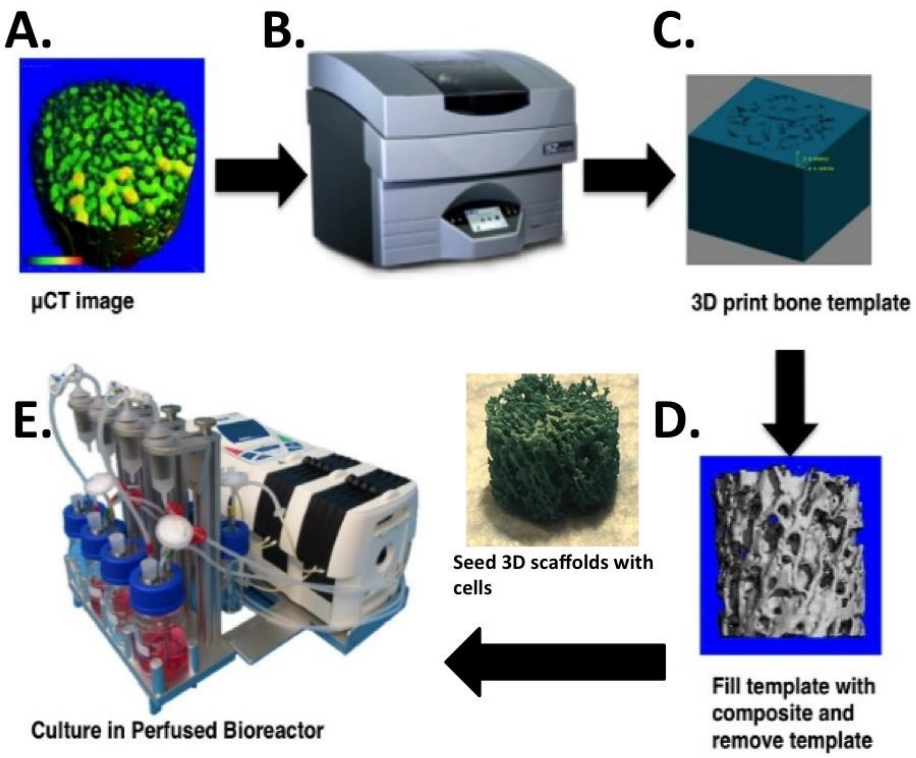

Figure 6.3 Fabrication of bone template scaffolds

(**A**) An µCT image of an inverted trabeculae (green) was used (**B**) by SolidScale 3D ink-jet printer to (**C**) print wax molds into which (**D**) a reactive polyurethane (PUR) network with a tunable modulus is casted, followed by extraction of the mold to yield a 3D scaffold (**E**) Relevant cell populations can be cultured on 3D scaffolds in a perfused bioreactor

Clinical significance of studying Tumor Induced Bone Disease using 3D bone analogue systems

Cancer is a heterogeneous disease caused by diverse genomic alterations in oncogenes and tumor suppressor genes[32]. Tumor heterogeneity, a prevalent characteristic of cancer, arises between tumors types present in different patients, and in between localized diseased state (intertumor hetrogenity). Cancer genomic studies have also categorized intratumor heterogeneity i.e. the existence of subpopulations of cells with distinct genotypes and phenotypes that may harbor divergent biological behaviors, within a primary tumor and its metastases[33]. Consequentially, genomic instability – a prominent source of this genetic variation is an important factor to consider during treatment of patients[32,34]. A systematic approach to the study of molecular heterogeneity in cancer is required, which is somewhat hindered by current trial design and funding mechanisms.

While several years of research have focused on treatment of bone metastasis they are still considered clinically incurable[35]. Bisphosphonates are currently the clinical standard of care for treating patients with bone metastases, and have been highly effective in patients to reduce fractures and improve quality of life[36]. However, they do not target tumors in the bone, are not a permanent cure, and are not without risk. Severe side effects include severe muscle pain, and osteonecrosis of the jaw and atypical subtrochanteric fractures in patients with long term high-dose treatments[37]. Similarly, Denosumab, a monoclonal antibody targeting RANKL has been demonstrated to reduce bone turnover and increase bone density

in clinical studies[38,39]. However, Denosumab presents safety risks as well, including hypocalcemia and osteonecrosis of the jaw, though the prevalence is unclear due to limited clinical data[40,41]. Despite the clinical success of these drugs, they do not target the tumor, and therefore do not address the root of the disease and are not a cure for tumors growing in the bone.

We anticipate a combination of 3D polyurethane scaffolds and the perfusion bioreactor would facilitate concurrent testing of multiple therapeutic approaches. 3D-printed scaffolds recapitulate the properties of the bone microenvironment. The design of new biomaterials that both mimic the microenvironment and facilitate studies on the spatio-temporal dynamics of cancer progression have been recognized as a pressing need for 3D *in vitro* models[42]. Advances in 3D printing have enabled more precise control over topological properties[2], and our templated-3D printing approach enables independent control of mechanical, topological, and resorptive properties[3,43]. Our novel scaffold approach will enable us to investigate how the cellular and physical components of the microenvironment regulate invasion and drug response for individual patients.

We have shown in this work; the 3D perfusion bioreactor model is a more stringent predictor of drug response than 2D mono- culture. 3D *in vitro* culture models of tumor-induced bone disease have recently been reported for metastatic breast cancer[44], Ewing sarcoma[45], and prostate cancer[46,47]. These studies used polymeric or collagen scaffolds to show that the 3D microenvironment substantially alters the tumor response to anti-cancer drugs compared to 2D monoculture[45,46]. However, the ability of electrospun polymeric scaffolds and

hydrogels to recapitulate the mechanical and topological properties of the bone microenvironment may be limited by their low substrate modulus and nanoscale pore size. Considering our findings that 3D scaffolds with bone-like mechanical and topological properties alter gene expression in bone and tumor cells[3,43,45], we anticipate that scaffolds will more accurately predict drug response than 2D culture and 3D hydrogel models. Patient samples can be obtained, incubated in the 3D bone model and the lead-candidate drug that targets the tumor could then be selected for patient therapy. Furthermore, this bone analogue model based on molecular markers and/or imaging data could help prioritize patients for therapy. These advances to the field could allow for earlier and more effective treatment choices, which may help, improve patient survival and improve patient quality of life.

References

[1] Y. Kang, P.M. Siegel, W. Shu, M. Drobnjak, S.M. Kakonen, C. Cordón-Cardo, et al., A multigenic program mediating breast cancer metastasis to bone, Cancer Cell. 3 (2003)

[2] S. Van Bael, Y.C. Chai, S. Truscello, M. Moesen, G. Kerckhofs, H. Van Oosterwyck, et al., The effect of pore geometry on the in vitro biological behavior of human periosteum-derived cells seeded on selective laser-melted Ti6Al4V bone scaffolds, Acta Biomaterialia. 8 (2012)

[3] R. Guo, S. Lu, J.M. Page, A.R. Merkel, S. Basu, J.A. Sterling, et al., Fabrication of 3D Scaffolds with Precisely Controlled Substrate Modulus and Pore Size by Templated-Fused Deposition Modeling to Direct Osteogenic Differentiation, Advanced Healthcare Materials. (2015)

[4] D.A. Gaspar, V. Gomide, F.J. Monteiro, The role of perfusion bioreactors in bone tissue engineering, Biomatter. 2 (2012)

[5] K. Suck, S. Roeker, S. Diederichs, F. Anton, J.A. Sanz-Herrera, I. Ochoa, et al., A rotating bed system bioreactor enables cultivation of primary osteoblasts on well-characterized Sponceram regarding structural and flow properties, Biotechnol Progress. 26 (2010)

[6] A.D. Luster, R. Alon, U.H. von Andrian, Immune cell migration in inflammation: present and future therapeutic targets, Nat Immunol. 6 (2005)

[7] L. D'Amico, I. Roato, The Impact of Immune System in Regulating Bone Metastasis Formation by Osteotropic Tumors, J Immunol Res. 2015 (2015)

[8] J. Roth, T. Vogl, C. Sorg, C. Sunderkötter, Phagocyte-specific S100 proteins: a novel group of proinflammatory molecules, Trends Immunol. 24 (2003)

[9] M. Ichikawa, R. Williams, L. Wang, T. Vogl, G. Srikrishna, S100A8/A9 Activate Key Genes and Pathways in Colon Tumor Progression, Molecular Cancer Research. 9 (2011)

[10] G. Srikrishna, S100A8 and S100A9: New Insights into Their Roles in Malignancy, J Innate Immun. 4 (2012)

[11] D.I. Gabrilovich, S. Ostrand-Rosenberg, V. Bronte, Coordinated regulation of myeloid cells by tumours, Nat Rev Immunol. 12 (2012) 2

[12] D.I. Gabrilovich, S. Nagaraj, Myeloid-derived suppressor cells as regulators of the immune system, Nat Rev Immunol. 9 (2009)

[13] S. Kusmartsev, D.I. Gabrilovich, Role of immature myeloid cells in mechanisms of immune evasion in cancer, Cancer Immunology. (2006).

[14] S.Y. Yang, A. Miah, A. Pabari, Growth Factors and their receptors in cancer metastases, Frontiers in Bioscience (2011).

[15] S. Danilin, A.R. Merkel, J.R. Johnson, R.W. Johnson, J.R. Edwards,

J.A. Sterling, Myeloid-derived suppressor cells expand during breast cancer progression and promote tumor-induced bone destruction, Oncoimmunology. 1 (2012)
[16] J. Wang, K. De Veirman, N. De Beule, K. Maes, E. De Bruyne, E. Van Valckenborgh, et al., The bone marrow microenvironment enhances multiple myeloma progression by exosome-mediated activation of myeloid-derived suppressor cells, Oncotarget. 6 (2015)
[17] H. Azim, H.A. Azim Jr, Targeting RANKL in breast cancer: bone metastasis and beyond, Expert Rev Anticancer Ther. 13 (2013)
[18] S. Ferrari-Lacraz, S. Ferrari, Do RANKL inhibitors (denosumab) affect inflammation and immunity? Osteoporos Int. 22 (2011)
[19] U.H. Weidle, F. Birzele, G. Kollmorgen, R. Rüger, Molecular Mechanisms of Bone Metastasis, Cancer Genomics Proteomics. 13 (2016)
[20] F. Arai, A. Hirao, M. Ohmura, H. Sato, S. Matsuoka, K. Takubo, et al., Tie2/Angiopoietin-1 Signaling Regulates Hematopoietic Stem Cell Quiescence in the Bone Marrow Niche, Cell. 118 (2004)
[21] J.M. Hyman, A.J. Firestone, V.M. Heine, Y. Zhao, C.A. Ocasio, K. Han, et al., Small-molecule inhibitors reveal multiple strategies for Hedgehog pathway blockade, Proceedings of the National Academy of Sciences. 106 (2009)
[22] Y. Rifai, M.A. Arai, S.K. Sadhu, F. Ahmed, M. Ishibashi, Bioorganic & Medicinal Chemistry Letters, Bioorganic & Medicinal Chemistry Letters. 21 (2011)
[23] F. Rossi, M. Santoro, G. Perale, Polymeric scaffolds as stem cell carriers in bone repair, J Tissue Eng Regen Med. (2013)
[24] R. Florencio-Silva, G.R. da Silva Sasso, E. Sasso-Cerri, M.J. Simões, P.S. Cerri, Biology of Bone Tissue: Structure, Function, and Factors That Influence Bone Cells, BioMed Research International. 2015
[25] D.B. Burr, Targeted and nontargeted remodeling, Bone. 30 (2002)
[26] T.A. Guise, G.R. Mundy, Cancer and bone, Endocr Rev. 19 (1998)
[27] H. Huang, M.-F. Hsieh, G. Zhang, H. Ouyang, C. Zeng, B. Yan, et al., Improved accuracy of 3D-printed navigational template during complicated tibial plateau fracture surgery, Australas Phys Eng Sci Med. 38 (2015)
[28] J.M. Page, A.R. Merkel, N.S. Ruppender, R. Guo, U.C. Dadwal, S.A. Cannonier, et al., Matrix rigidity regulates the transition of tumor cells to a bone- destructive phenotype through integrin b3 and TGF-b receptor type II. Biomaterials. 64 (2015)
[29] N.S. Ruppender, A.R. Merkel, T.J. Martin, G.R. Mundy, J.A. Sterling, S.A. Guelcher, Matrix rigidity induces osteolytic gene expression of metastatic breast cancer cells, PLoS ONE. 5 (2010)
[30] T.A. Guise, J.J. Yin, S.D. Taylor, Y. Kumagai, M. Dallas, B.F. Boyce, et al., Evidence for a causal role of parathyroid hormone-related protein in the pathogenesis of human breast cancer-mediated osteolysis, J. Clin. Invest. 98 (1996)

[31] T.J. Martin, J.M. Moseley, Mechanisms in the skeletal complications of breast cancer, Endocrine Related Cancer. 7 (2000)
[32] P.L. Bedard, A.R. Hansen, M.J. Ratain, L.L. Siu, Tumour heterogeneity in the clinic, Nature. 501 (2013)
[33] R.A. Burrell, N. McGranahan, J. Bartek, C. Swanton, The causes and consequences of genetic heterogeneity in cancer evolution, Nature. 501 (2013)
[34] R. Fisher, L. Pusztai, C. Swanton, Cancer heterogeneity: implications for targeted therapeutics, Br J Cancer. 108 (2013)
[35] G.R. Mundy, Mechanisms of bone metastasis, Cancer. (1997).
[36] R.E. Coleman, Bisphosphonates: Clinical Experience, The Oncologist. 9 (2004)
[37] A.A. Khan, A. Morrison, D.A. Hanley, D. Felsenberg, L.K. McCauley, F. O'Ryan, et al., Diagnosis and Management of Osteonecrosis of the Jaw: A Systematic Review and International Consensus, J Bone Miner Res. (2014)
[38] E. Prommer, Palliative Oncology: Denosumab, Am J Hosp Palliat Care. 32 (2015)
[39] J.P. Brown, C. Roux, P.R. Ho, M.A. Bolognese, J. Hall, H.G. Bone, et al., Denosumab significantly increases bone mineral density and reduces bone turnover compared with monthly oral ibandronate and risedronate in postmenopausal women who remained at higher risk for fracture despite previous suboptimal treatment with an oral bisphosphonate, Osteoporos Int. 25 (2014)
[40] B. Smyth, S. Ong, Severe hypocalcaemia and hypophosphataemia following intravenous iron and denosumab: a novel drug interaction, Intern Med J. 46 (2016)
[41] A.A. Owosho, A. Blanchard, L. Levi, A. Kadempour, H. Rosenberg, S.K. Yom, et al., Osteonecrosis of the jaw in patients treated with denosumab for metastatic tumors to the bone: A series of thirteen patients, J Craniomaxillofac Surg. 44 (2016)
[42] T.K. Schuessler, X.Y. Chan, H.J. Chen, K. Ji, K.M. Park, A. Roshan-Ghias, et al., Biomimetic tissue-engineered systems for advancing cancer research: NCI Strategic Workshop report, Cancer Res. 74 (2014)
[43] R. Guo, A.R. Merkel, J.A. Sterling, J.M. Davidson, S.A. Guelcher, Substrate modulus of 3D-printed scaffolds regulates the regenerative response in subcutaneous implants through the macrophage phenotype and Wnt signaling, Biomaterials. 73 (2015)
[44] A.M. Mastro, E.A. Vogler, A Three-Dimensional Osteogenic Tissue Model for the Study of Metastatic Tumor Cell Interactions with Bone, Cancer Res. 69 (2009)
[45] E.L.S. Fong, S.-E. Lamhamedi-Cherradi, E. Burdett, V. Ramamoorthy, A.J. Lazar, F.K. Kasper, et al., Modeling Ewing sarcoma tumors in vitro with 3D scaffolds, Proc Natl Acad Sci U S A. 110 (2013)

[46] K.A. Fitzgerald, J. Guo, E.G. Tierney, C.M. Curtin, M. Malhotra, R. Darcy, et al., The use of collagen-based scaffolds to simulate prostate cancer bone metastases with potential for evaluating delivery of nanoparticulate gene therapeutics. Biomaterials. 66 (2015)

[47] S. Sieh, A.V. Taubenberger, M.L. Lehman, J.A. Clements, C.C. Nelson, D.W. Hutmacher, Paracrine interactions between LNCaP prostate cancer cells and bioengineered bone in 3D in vitro culture reflect molecular changes during bone metastasis, Bone. 63 (2014)

APPENDIX

```
%%file for osteoblast, osteoclast, and tumor cell counts.
function dxdt = tumor_solvediff2(t,x)

global alpha1 alpha2
global beta1 beta2
global g11 g12 g21 g22
global r11 r22 r12 r21
global gamma L
global k1 k2
global y1 y2
global ssx

dx1dt = alpha1*x(1)^(g11*(1+r11*x(3)/L))*x(2)^(g21*(1+r21*x(3)/L)) - beta1*x(1);
dx2dt = alpha2*x(1)^(g12/(1+r12*x(3)/L))*x(2)^(g22-r22*x(3)/L) - beta2*x(2);
dx3dt = gamma*x(3)*log10(L/x(3));

%%alternative equations
% dx1dt = alpha1*x(1)^g11 *x(2)^(g21+r21*x(3)/L) - beta1*x(1);
% dx2dt = alpha2*x(1)^g12*x(2)^(g22-r22*x(3)/L) - beta2*x(2);


if x(1) > ssx(1)
    y1 = x(1) - ssx(1);
else
    y1 = 0.0;
end

if x(2) > ssx(2)
    y2 = x(2) - ssx(2);
else
    y2 = 0.0;
end

dzdt = -k1*y1 + k2*y2;

dxdt = [dx1dt; dx2dt; dx3dt; dzdt];
```

Contents


```
%%%%%%%%%%%%%%%%%%%%%%%%%%%%%%%%%%%%%%%%%%%%%%%%%%%%%%%%%%%%%%%%%%%%%%%%%%%%
% A model of vicious cycle based on Komarova's model
% 1. Komarova SV, Smith RJ, Dixon SJ, Sims SM, and Wahl LM, Bone 33 (2003) 206-215
% 2. Komarova SV, Endocrinology 146 (2005) 3589-3595

% Edited: M Granke 02/22/2016
%editted UCD 030816
% edited 030916
% EDITED UCD 031316
%%%%%%%%%%%%%%%%%%%%%%%%%%%%%%%%%%%%%%%%%%%%%%%%%%%%%%%%%%%%%%%%%%%%%%%%%%%%
warning('off')
clear all
clc

set(0,'defaultFigureColor','w')
set(0,'defaultaxesfontname','Times New Roman');
set(0,'defaultaxesfontweight','bold')
set(0,'defaultaxesfontsize',20);
set(0,'defaulttextfontsize',20);
set(0,'defaultaxesfontname','Times New Roman');
set(0,'defaultaxesfontweight','bold')
set(0,'DefaultAxesXGrid','on','DefaultAxesYGrid','on')

global alpha1 alpha2
global beta1 beta2
global g11 g12 g22 g21
global r11 r22 r12 r21
global gamma L
global k1 k2
global y1 y
global ssx
```

Define parameters

```
% Rate of overall production = net effect of recruitment of precursors and formation of mat
ure cells
% Note: chosen so that steadystate(OC)~1 and steady-state(OB)~200
% alpha1 = 3.0;   % # of 3 OC / day  komarova
% % Data used to simulate tumor experimental data
alpha1 = 6;   % # of 6 OB / day based on myeloid cell data from 3D immune infiltration scaf
folds
alpha2 = 4;   % # of 4 OB / day Komarova


% Rate of cell removal = cell death, differentiation of OB into osteocytes or lining cells
```

```
% erosion by OC achieved in 9-14 days
% cavity filling by OB: 3 to 5 months (90 - 150 days)
% beta1 and beta2 chosen so that OC and OB returns to steady state after these respective t
ime ranges
% beta1 = 0.16;   %# of 0.1 / day for ayati model and new alpha value
% beta2 = 0.2;   %# of .002 OB / day for new k values
% % Data used to simulate tumor experimental data (Komarova data)
beta1 = 0.2;    %# of .2 OC / day
beta2 = 0.02;   %# of .002 OB / day

% Effects of autocrine and paracrine regulators on the rates of OC, OB, and cancer cells fo
rmation
% g11 = 1.1; %ayati original (beyond this you encounter unstable oscillations)

g11 = 0.5; % OC autocrine regulation (factors produced by OC that regulate OC formation)
g12 = 1; % factors produced by OC that regulate OB formation (e.g. OC releases TGF-beta fro
m the matrix => affects OB formation)
g22 = 0.0; % OB autocimr signaling (e.g. IGF): can be neglected
g21 = -0.5; % factors produced by OB that regulate OC formation (e.g. OB release RANKL/OPG
=> affects OC differentiation)

%Ayati model based tumor interaction paramets
%  r11 = .005; r21 =0.0; r12 = 0; r22 = 0.2;
%Use these values to fit experimental data
r11 = .005; r21 =-.90; r12 = 0; r22 = 0.2; %ayti r with komarova k 031016

%Tumor data from Ayati
gamma = 0.63; %Fit tumor cell population by varrying gamma
L = 100;

% Normalized activities of bone resorption and formation
% dz/dt = -k1y.1 + k2.y2
% from Komorova et al. 2005 "the rates of bone resorption and formation wer
% assumed to be proportional to the numbers of OC and OB exceeding initial
% steady-state levels
k1 = 0.24;     % percent /cell /day    (in Komorova k1 = 0.24)
k2 = 0.0017;% percent /cell /day    (in Komorova k2 = 0.0017)
```

Steady-state solution (analytical)

Other method for obtaining steady-state solution

```
ssx0 =  [11.06 212.13 1.0];
options = optimoptions('fsolve','Display','off');
[ssx, fval] = fsolve(@tumor_steadystate2,ssx0,options);
```

Solving differential equation

```
% ode45: solve nonstiff differential equations
% [T,Y] = ode45(odefun, tspan, y0)
% T: column vector of time points
% Y: Solution array. Ech row in Y corresponds to the solution at a time returned in the cor
responding row of T
% odefun: a function handle that evaluates the right side of the differential equations.
```

```
% tspan: a vector specifying the interval of integration [t0,tf]
% y0: vector of initial conditions

tspan = [7 21]; % 0 to 150 days
[t, X] = ode45('tumor_solvediff2', tspan, [10 10 1 100]);
X = real(X);
```

Graphs

```
% Tumor cell
% subplot(2,2,3)
 subplot(2,1,1)
days = [7 14 21];
Tper = [2.642529466 7.670147943 90];
hold on, plot(days,Tper,'o-k','linewidth',2)
hold on, plot(t,X(:,3),'r','LineWidth',2)
xlabel('Time (days)')
ylabel('Density of tumor cells')
grid minor


% Bone loss
% subplot(2,2,4)
subplot(2,1,2)
days = [0 7 14 21];
Boneloss = [100 100.7612108 74.85586163 27.99887892];
hold on, plot(days,Boneloss,'o-k', 'linewidth',2)
hold on, plot(t,X(:,4),'r','LineWidth',2)
xlabel('Time (days)')
ylabel('Bone Mass (%)')
ylim([0 120])
grid minor



% Stability of solution
phi = beta1*(g11*(1+r11)-1) + beta2*(g22-r22-1);
disp(['Phi = ',num2str(phi)])
```

```
Phi = -0.1235
```

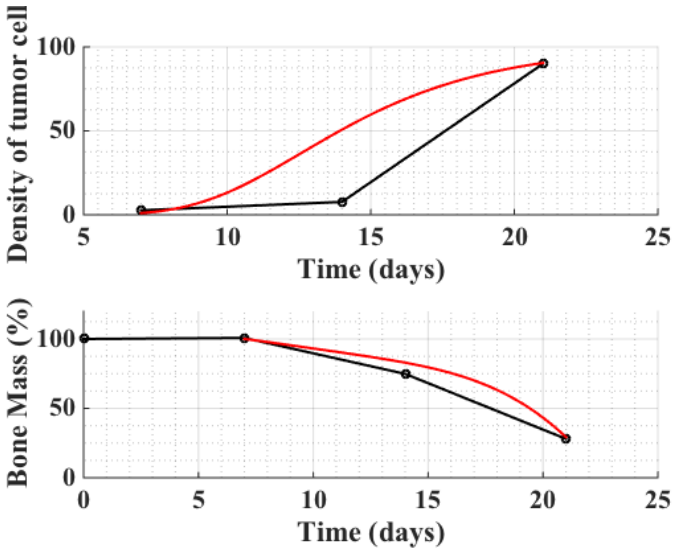

Published with MATLAB® R2014b